INTERNATIONAL ATOMIC ENERGY AGENCY
UNITED NATIONS EDUCATIONAL, SCIENTIFIC AND CULTURAL ORGANIZATION

INTERNATIONAL CENTRE FOR THEORETICAL PHYSICS
34100 TRIESTE (ITALY) - P.O.B. 586 - MIRAMARE - STRADA COSTIERA 11 - TELEPHONE: 2240-1
CABLE: CENTRATOM - TELEX 460892 - I

SMR/389 - 7

WORKING PARTY ON MODELLING THERMOMECHANICAL BEHAVIOUR OF MATERIALS (29 May - 16 June 1989)

Lecture 1 : Simple microstructural models for deformation and radiation damage

Lecture 2 : Internal interfaces

Lecture 3 : Thermo-elasticity

Lecture 4 : Plasticity and creep

Lecture 5 : Failure of structures

J.R. MATTHEWS
Aere Harwell
Theoretical Physics Division
Oxon OX11 ORA
Didcot
United Kingdom

Lecture 1 Simple Microstructural Models for Deformation and Radiation Damage

1.1 Introduction

The strength of crystalline solids is almost completely determined by the movement and interaction of defects in the perfection of the crystal lattice. The strength of perfect crystals is inherently large and is estimated to be of the order of $^1/_{10}$ of the shear modulus (Kelly and MacMillan 1986). The production of single crystal whiskers, that are essentially defect free, enables such strength limits to be approached, but although whisker re-enforced composites are useful large perfect crystal structures are not attainable. Reducing defect concentrations is the route chosen in the optimisation of fabrication techniques for ceramics but metal alloys for engineering applications are cocktails of components with several phases and complex microstructure.

Defects form a hierarchy of types: (i) point defects which include lattice *vacancies*, self *interstitial* atoms (which we will refer to simply as interstitials), substitutional foreign atoms and interstitial foreign atoms; (ii) *dislocations* which are line defects in character; (iii) two dimensional defects which include *stacking faults*, *grain boundaries*, *twin boundaries* and we may also include free surface, cracks and interfaces with other phases; and (iv) three dimensional defects such as cavities, bubbles and precipitates. In the second lecture of this course we will consider defects in class (iv) in some detail, but there is no space to draw attention to more than a few important aspects of the behaviour of the other defect types. A general text book on physical metallurgy will provide any background if required (e.g. Cahn and Haasen 1983 or at a more elementary level Wulf 1964). The properties of dislocations are particularly rich in detail and as the motion of dislocations generates the plastic strain in crystals, under most circumstances, some understanding of their nature is needed here (e.g. see Nabarro 1967). Before we discuss microstructural modelling we will briefly review some of the main features of dislocations.

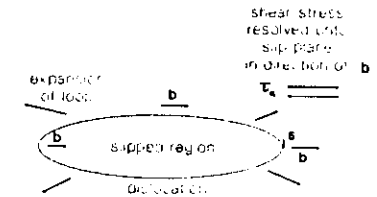

Fig.1.1

Fig. 1.1 shows a dislocation glide loop, i.e. a closed dislocation loop where the *Burgers* vector lies in the *slip* plane. An arbitrary stress in the material will produce a force per unit on the dislocation of (Peach and Koehler, 1950)

$$F = b \sigma x s. \tag{1.1}$$

A shear stress τ_a lying in the same plane as **b** and **s** and in the direction of **b** will produce a glide force of magnitude $b \tau_a$ that will expand the loop propagating slip. A glide loop will have some parts which are predominantly *edge* in character and some parts predominantly *screw*. Edge dislocations are constrained to glide within the glide plane and any motion away from the glide plane requires emission or absorption of point defects, i.e. *climb*. Screw dislocations may move on glide planes other than the principal one, which is termed *cross slip*. The force on the dislocation is a virtual force that comes from the work done in displacing the material about the slip plane by a distance b.

Dislocations have an associated elastic field that is dependent on the orientation of the Burgers vector to the dislocation line. Both the stress and strain fields are inversely proportional to the distance from the dislocation line. The stress field can be expressed generally as:

$$\sigma_{ij} = \frac{\mu b f_{ij}(\theta)}{2\pi r} . \tag{1.2}$$

For an edge dislocation the stress field has dilational and compressive parts below and above the dislocation line, see Fig. 1.2. The components of stress are given by:

$$f_{rr}(\theta) = f_{\theta\theta}(\theta) = \sin\theta/(1-\nu),\ f_{r\theta}(\theta) = \cos\theta/(1-\nu)$$
$$\text{and} \quad f_{zz} = -\nu \sin\theta/(1-\nu), \tag{1.3}$$

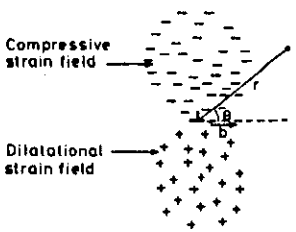

Fig. 1.2

where z is the direction along the dislocation line. The stress field around a screw dislocation is purely shear in character, where:

$$f_{r\theta}(\theta) = 1 . \tag{1.4}$$

The self elastic energy of a dislocation is complicated by the stress singularity at the core. If it is assumed that the core energy is small and a cut off is made at a distance of 1 atomic spacing then the elastic energy is approximately:

$$E_s \equiv \frac{\mu b^2}{4\pi K_1} [\ln (R/a) - 1] , \tag{1.5}$$

where R is the dimension of the body containing the dislocation, $K_1 = 1$ for screw dislocations and $K_1 = (1-\nu)$ for edge dislocations. This energy is large and dislocations are thermodynamically unstable as the configurational entropy is too small to provide an offset. The dependence of the dislocation energy on the square of the Burgers vector means that normally dislocations have Burgers' vectors corresponding to the smallest *lattice vectors*, i.e. in the closest packed directions. Occasionally dislocations are formed, from dislocations or point defect reactions, with other lattice vectors but they tend to be unstable, although some materials are found with several types of stable dislocation. Super dislocations are also unstable unless they are forced together by an applied stress against an obstacle. In some materials the dislocation may split into *partial dislocations* which are separated by a stacking fault. If the dislocation has an initial Burgers vector **b** and splits into two partials $\mathbf{b}_1$ and $\mathbf{b}_2$ (determined by the lattice structure) then the separation is given approximately by:

$$d_p \equiv \mu\, \mathbf{b}_1 \mathbf{b}_2 / 2\pi K_1 \Gamma \tag{1.6}$$

where Γ is the stacking fault energy. For Al and bcc iron there is no energetic advantage in such splitting, but it is an important phenomenon in austenitic stainless steels where the dislocations can separate by up to 50 atomic spacings.

A useful concept in developing microstructural models is the dislocation density, ρ_d. This is defined as the number of dislocations per unit area intersecting a random cut made in the material. In real materials after deformation the dislocation density will be an anisotropic property but for many purposes we can assume that it is isotropic. The concept of dislocation density also has some assumption of a balance between dislocations of opposite signs. If this is the case the material will have no long range elastic field as statistically the fields of the various dislocations will cancel. If dislocations of a particular sign predominate one of two things can happen. If the material is constrained, e.g. if a region of high dislocation density is buried in dislocation free crystal, there will be a large self elastic energy and a long range elastic

field as if the material contained a super-dislocation. If the material can relax the crystal will exhibit a curvature of the lattice (Kroener 1958).

The motion of a population of dislocations of a particular type (but they could be of both signs) with a density ρ_d are related to a strain ε by the Orowan relation:

$$\varepsilon = \rho_d \, bL, \tag{1.7}$$

where ε is the shear strain in the glide plane and L is the average distance each dislocation moved (dislocation of opposite sign moving in opposite directions).

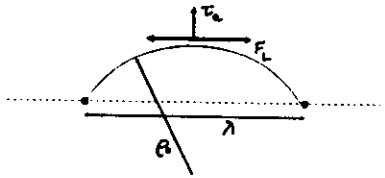

Fig. 1.3

A frequent configuration, that is encountered in the theory of solute and strain hardening, in dislocation multiplication and in climb interactions, is the pinning of a dislocation between a pair of obstacles. A dislocation has a line tension which is related to the curvature of the dislocation line (Friedel 1964):

$$F_L = \frac{\mu b^2}{4\pi K_1} \ln (\rho_o / 2b) \tag{1.8}$$

where ρ_o is the local radius of curvature. The loop shown in Fig. 1.1 will therefore tend to collapse under its line tension and stress from eq. (1.1) a stress of magnitude:

$$\tau_a = F_L/(\rho_o b) \tag{1.9}$$

is required to maintain the loop in equilibrium. When a dislocation is pinned between obstacles, spaced by a distance λ, the line tension will keep the dislocation strain unless a stress is applied when it will bow out in the manner in Fig. 1.3. For most applications the logarithmic term may be replaced and we can approximate the radius of curvature by:

$$\rho_o \equiv \mu b/\tau_a \, . \tag{1.10}$$

The force on the pinning points is given by:

$$\tau_a = \frac{\mu b}{\lambda} \cos(\phi/2) = \frac{F_p}{b\lambda} \, . \tag{1.11}$$

1.2 Low Temperature Deformation

Before going further some definition is required as to what are low temperatures and high temperatures with respect to deformation and radiation damage. A convenient split is given by the temperature at which lattice self-diffusion becomes important. For most materials this is approximately at 0.4 Tm where Tm is the absolute melting point. Below this temperature some thermally activated processes may occur during deformation, but creep strains are not significant and dislocation motion is dominated by *glide*.

The main features we are interested in this section are the material *flow stress* and *work hardening*.

From the point of view of mechanical behaviour of materials the most imortant property of dislocations is that they can move under applied stresses that are much smaller than the theoretical strength of the material. In a material with a low dislocation density and without the complicating effects of soluble impurities and precipitates, the dislocation flow stress is determined by the energy barrier to move the dislocation through the lattice. This stress is usually referred to as the Peierls stress after the first simple model that was used to describe the process (Peierls 1940). Simple estimates of the Peierls stress are not useful and even detailed atomistic models are as yet inaccurate. The following points are worth noting from experimental observation. Edge dislocations generally have a lower flow stress than screw dislocations; this is particularly marked in bcc metals, where the edge components of loops move preferentially leaving long arrays of screw dislocations. The Peierls stress in close packed metals is low and usually below $10^{-4}\mu$, which is the value for most bcc metals. The Peierls stress is much higher for covalent and ionic crystals with values of around $10^{-3}\mu$ and $10^{-2}\mu$ respectively. The motion of dislocations with a high Peierls stress often has to be achieved by the nucleation and motion of ***kinks*** on the dislocation. Dislocations that split into partials generally have a lower Peierls stress. However split dislocations are less likely to exhibit cross slip as there is an energy penalty in having to

restore the perfect dislocation before it can move into a new glide plane. Cross slip is easier for screw dislocations in bcc metals and this is seen in characteristic wavy slip lines.

Adding other types of atoms to materials in most cases increases the dislocation flow stress. This may be a small effect in solid solution binary alloys but much larger in ordered alloys where passage of the dislocation destroys the order on the slip plane. *Interstitial solutes* or *substitutional solutes* with large atomic size differences from the host materials can increase the flow stress of the material even at low concentrations. This is an important means of strengthening engineering materials. For lower temperatures the effect of solutes arises mainly from the interaction between the strain field around the dislocation and the strain field around the solute atom. There are three main sources of this interaction. The easiest of these to understand is the 'size' interaction which is proportional to the mismatch volume e_s, which is the ratio of the solute atomic volume to the host atomic volume for interstitial solutes or this ratio minus one for substitutional solutes. This type of interaction is only valid for the edge components of dislocations where there is a volume strain field. There is also a 'shape' interaction where the solute distorts the surrounding lattice in a non-spherically symmetric way. This occurs naturally in anisotropic crystal lattices but interstitial solutes can break the symmetry of the lattice in isotropic crystal structure. This type of interaction couples with shear stresses and thus affects both edge and screw dislocations. Where such effects occur they usually dominate. The third type of interaction is called the 'inhomogeneity' effect and arises because of the effect of the solute on the elastic modulus of the lattice (Eshelby, 1951). This type of interaction is usually less strong than the size and shape effect. Where the bulk modulus is affected the interaction is only with edge dislocations, but if the shear modulus is affected screw dislocation components are also involved.

If we characterise the dislocation solute interaction by f_s, which could be identified with e_s for the size effect, a simple model can be constructed for the effect of solutes on the dislocation flow stress (Friedel 1964). For a dilute concentration of solute atoms lying near the slip plane, which is shown schematically in Fig. 1.4, from eq. (1.11) the stress required to break away from pinning solute atoms spaced λ apart is given by:

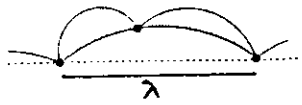

Fig. 1.4

$$\tau_o = \mu f_s b/2\lambda \quad (1.12)$$

As the dislocation bows out between solute atoms it may encounter a third solute atom and in this way the pinning distance λ will decrease with increasing applied stress (Nabarro 1985):

$$\lambda = (\mu\Omega/\tau_o C_s)^{1/3} \quad (1.13)$$

where C_s is the atomic concentration of solute. The flow stress then becomes on replacing λ in eq. (1.12):

$$\tau_o \equiv \mu (f_s/2)^{3/2} C_s^{1/2} \quad (1.14)$$

This type of expression for solute hardening is useful for dilute concentrations of weakly interacting atoms and is termed the Friedel limit. The other extreme is for high concentration where the size of the solute atoms is comparable to their spacing this is termed the Labusch limit (Labusch 1970). In this case the flow stress is given approximately by:

$$\tau_o \equiv \mu (f_s^4 c_s^2 r_s/2b)^{1/3} . \quad (1.15)$$

The effective flow stress from the lattice resistance or solute hardening is strongly temperature dependent even at low temperatures. This is because the interaction energies are usually much lower than those for lattice diffusion, although this is often not the case for covalent or ionic crystals. A general expression for the velocity of a dislocation is:

$$v_g = v_o b \exp\left[-\frac{(E_m - \tau_e V_m}{kT}\right] \quad (1.16)$$

where E_m is the energy barrier for migration and V_m is the activation volume of the reaction. From eq. (1.7) we get the strain rate from the moving dislocations:

$$\dot{\varepsilon} = b \rho_d v_g \,. \tag{1.17}$$

Combining (1.16) and (1.17) and inverting we can express $\tau_f(T)$ as:

$$\tau_f = \frac{1}{V_m}\left[E_m - \frac{kT}{\ln(\rho_d b^2 v_o/\dot{\varepsilon})}\right] \tag{1.18}$$

which because of the log term is only weakly dependent on the strain rate. For flow limited by Peierls force we can re-express eq. (1.18) as:

$$\tau_f = \tau_o (1 - T/T_o) \,. \tag{1.19}$$

When flow is enabled by kink motion E_m is identified with the sum of the kink migration energy and the formation energy of a kink pair. When solute hardening is important the temperature dependence is more complex and there are often several temperature regions with different controlling parameters (Nabarro 1985). For the simplest material, as we have already seen, the activation volume is stress dependent and there may be other temperature dependences of the parameters. The temperature dependence is frequently of the form:

$$\tau_f = \tau_o [1 - (T/T_o)^{2/3}] \,. \tag{1.20}$$

For bcc metals, and particularly iron alloys, one of the main effects of solutes is in inhibiting kink motion. This was used by Suzuki (1971) to explain the dependence of flow stress on c_s^2 and T^{-1} in this group of materials.

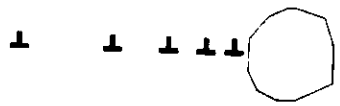

Fig. 1.5

The dislocation flow stress is not always identified with the yield stress to propagate plastic flow over a polycrystalline material. There is usually a weak dependence on grain size that was first explained by Hall (1951) and Petch (1953). This requires the concept of the dislocation pile-up, see Fig. 1.5. The dislocations are emitted from a *dislocation source* a distance L from an obstacle, in this case a grain boundary. The dislocations move out under the action of the applied stress τ_a. The first dislocation is stopped by the obstacle and its elastic field stops the second dislocation and so on. This continues until the back stress from the pile-up prevents the source emitting any further dislocations. The number of dislocations in the final pile-up is (Hirth and Lothe, 1982):

$$N_d = \pi (1 - \nu) L \tau_a / \mu b \,. \tag{1.21}$$

The stress at the head of the pile-up is:

$$\tau_p = N\tau_a = \pi (1 - \nu) L \tau_a^2 / \mu b \,. \tag{1.22}$$

In order to propagate slip into the next grain τ_p has to reach some critical level, e.g. the stress required to punch dislocation loops out of the grain boundary. If $L \sim d_b$ it can be seen that the applied stress required to propagate yield is proportional to $d_b^{-1/2}$. This leads to the Hall-Petch relation for the yield stress of

$$\tau_y = \tau_i + k_p / d_b^{1/2} \tag{1.23}$$

where k_p is a constant. This relationship is found to hold well experimentally for a wide range of materials.

In materials containing precipitates, the stress to produce extensive yield must be able to force the dislocations between the precipitates if the dislocations are not able to penetrate them. This simplest case is for hard incoherent precipitates with a low concentration, where the spacing between the precipitates, λ, is much larger than their size. The dislocations bow out between the precipitates and if the applied stress is large enough the adjacent bowed segments join (Orowan 1948). This allows the dislocation to break through leaving a small loop around the precipitate behind:

$$\tau_y \equiv \tau_i + 2\mu b/\lambda \tag{1.24}$$

where $\lambda \sim 1/c_p^{1/3}$ for a spherical precipitate, c_p being the concentration of precipitates per unit volume. This expression can be improved to take into account the radius of the precipitates (Ashby 1968):

$$\tau_y \equiv \tau_f + \frac{\mu b}{2\pi(\lambda - 2r_p)} \ln\left(\frac{2r_p}{a_o}\right). \qquad (1.25)$$

There are other types of interaction for precipitates that are coherent with associated elastic strain fields and for soft inclusions that can be sheared but there is not space to go too deeply into the subject.

We will now turn to the topic of work or strain hardening. For single crystals this occurs in several stages as the dislocation configuration becomes more complex. For polycrystalline engineering materials the hardening starts at lower strain values; the constraint of having to match strains in differently orientated crystals prevents easy slip and complex dislocation interactions build-up quickly. There are three main processes which control the hardening rate: limitations to the dislocation glide distance; direct interaction between dislocations on different slip planes; and the effect of the internal strain field of the dislocation distribution. In order to build a model of these processes we will look at strain hardening at its simplest level.

The Orowan equation (1.7) gives us the main expression to develop a work hardening theory. This is obtained by differentiating (1.7) with respect to time and gives the rise in dislocation density with strain:

$$\frac{d\rho_d}{dt} = \frac{\dot{\varepsilon}}{bL}. \qquad (1.26)$$

There are two main cases of interest. The distance moved by the dislocations may be fixed by the presence of some obstacles, such as an impenetrable array of inclusions or grain boundaries. Alternatively the obstacles may be other dislocations and the average distance moved by the dislocations will be dependent on the dislocation density. In practice we might expect L to be fixed for low stresses giving $\varepsilon \propto \rho_d$ and for higher stresses when the dislocations can bow out past the obstacles or the dislocation spacing is finer than the obstacle spacing $L \propto \rho_d^{1/2}$ and $\varepsilon \propto \rho_d^{1/2}$.

There are many types of interaction between dislocations and some examples are listed here to show the richness of the subject. Dislocation of opposite sign by lying on parallel glide planes can interact elastically and stop, forming a *dipole*. We have already encountered the concept of the dislocation pile-up, which eventually stops the emission of dislocation from sources. Screw components of dislocations can cross-

slip out of the pile-up at the expense of activating a less favourably orientated slip system but dislocations with edge components are trapped unless they can move non-conservatively. Dislocations moving on non-parallel glide planes are either pinned at the contact points and have to bow out between the pinning points or they can cut through one another which leads to the generation of jogs or kinks at the interactions. Screw dislocations that have jogs imposed on them in this way are pinned at the jogs and can only move by bowing out from the pinning points or by emitting point defects when the stresses are large. Finally the tangle of dislocations will produce a modulated elastic strain field which will in some areas attract individual dislocations and in other areas repel. This will impede dislocation motion. We will look at some of these interactions again when we investigate creep and construct a simple deformation model, but for many purposes we can envisage an internal stress that opposes dislocation motion with the form:

$$\tau_i \equiv \alpha \mu b \rho_d^{1/2} \qquad (1.27)$$

where α lies between 0.2 and 1.

We can now see from eqs. (1.26) and (1.27) that for fixed dislocation motion we would expect:

$$\tau_i \equiv \alpha \mu (\varepsilon b/L)^{1/2} \qquad (1.28)$$

which give parabolic strain hardening and for dislocation motion of distances $L = \beta/\rho^{1/2}$:

$$\tau_i = \alpha \mu \varepsilon/\beta \qquad (1.29)$$

which is linear strain hardening. Strain hardening is frequently found to lie between these two extremes. The yield stress is now given by:

$$\tau_y = \tau_f(T) + \tau_i. \qquad (1.30)$$

A special case of strain hardening occurs in precipitate hardened materials when the applied stress is larger than the Orowan stress to break through the obstacles. The remaining dislocation loops left around the particles by this process repel other

dislocations. The strain hardening law in this case is given by (Fisher, Hart and Fry 1953):

$$\tau_s = 6\mu f_p^{3/2} \varepsilon, \tag{1.31}$$

where f_p is the volume fraction of the precipitates.

Before moving on to creep deformation it is worth noting that strain hardening eventually saturates at high strain, when the applied stress produces very high dislocation densities. As the dislocation density increases random anihilation of dislocations becomes more probable, cross slip occurs freely for screw dislocations and edge components may be forced to climb by point defect emission. Stress emitted point defects can also permit limited non-conservative dislocation motion in other dislocations.

1.3 High Temperature Deformation

This section is mainly concerned with the phenomena known as *creep*, which is the term for thermally activated continuing deformation under a load. We have already seen that dislocation motion and the yield stress can be thermally activated. At the lowest temperatures where creep is seen the deformation on the application of the load decreases continuously with time and because of this is termed logarithmic creep. Often part or most of this is recoverable on removal of the load, i.e. *anelasticity*. The strains are limited to a few tenths of a % at most. These strains arise from thermally activated redistribution of the dislocation network acting against the Peirels force or solute hardening in the presence of obstacles such as precipitates or other dislocations.

Once temperatures are above 0.4 T_m creep in its proper sense is observed. This is invariably associated with the commencement of lattice self diffusion as an important process and the activtion energy for creep has long been identified with the self diffusion energy for a wide range of conditions (Dorn and Mote 1964). At these temperatures a constant creep rate or a quasi-steady creep rate is observed after some initial transient. For long times and high strains the steady creep breaks down and the creep rate rapidly increases to failure. Thus creep is often divided into three stages; primary secondary and tertiary, shown schematically in Fig. 1.6. The primary and secondary stages are frequently expressed as (Andrade 1910):

$$\varepsilon_{creep} = a t^{1/3} + \dot{\varepsilon}_s t, \tag{1.32}$$

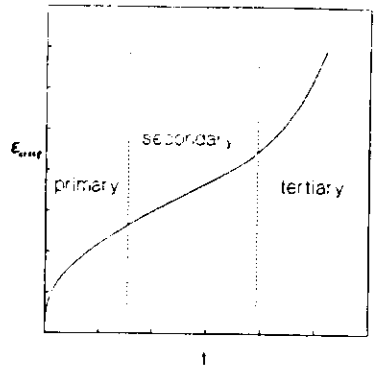

Fig. 1.6

where $\dot{\varepsilon}_s$ is the steady state creep rate and a is the primary creep coefficient, both quantities are functions of stress and temperature. Alternatively an exponential form is preferred by Garofalo (1965):

$$\varepsilon_{creep} = \dot{\varepsilon}_s \{t + (\beta/t_r)[1 - \exp(-t/t_r)]\}, \tag{1.33}$$

where β is constant for the material and t_r is a relaxation time which may be a function of stress and temperature. This pattern of three distinct stages of creep is an idealisation found mainly in pure well annealed materials. Engineering alloys and cold worked materials are subject to microstructural and microchemical changes at creep temperatures and this can sometimes result in increasing rather than decreasing initial creep rates and the failure to establish a clear steady state creep rate.

Creep for most of the range of interest results from dislocation movements, but for low stresses and very high temperatures purely diffusional creep can occur. The driving force for this is the difference in chemical potential for vacancy formation on grain boundaries with different orientation to applied stress. If vacancy transport is by lattice diffusion the mechanism is termed Nabarro-Herring creep after the first proposers (Nabarro 1948, Herring 1950). If vacancy transport is by grain boundary diffusion the mechanism is termed Coble creep (Coble 1963). The two mechanisms can be described by the simple expression:

$$\dot{\varepsilon} = \frac{C\tau_s\Omega}{d_b^2}\left(D_L + \frac{\pi\delta_b D_b}{d_b}\right) \tag{1.34}$$

where C is a constant reflecting the grain boundary geometry and has been given by various authors between 24 and 40. Diffusional creep at these rates is rarely observed. There are two reasons for this, both of which impose a threshold to this type of creep (Arzt, Ashby and Verrall 1983). Constraints are imposed on diffusional creep from the shape changes to the grains during deformation. This leads to a back-stress proportional to γ_b/d_b or for dislocation models of the boundary $\mu b/d_b$. For pure materials this back-stress is less than 5 MPa. The other constraint is an important one for engineering alloys where the boundary is prevented from being a good source of vacancies by the presence of particles or segregated solutes. In this case the magnitude of the back-stress may be very substantial (up to 50 MPa) and completely inhibit diffusional creep.

Purely diffusional creep is linear with stress but for higher stresses and lower temperatures creep is found to be very sensitive to stress. At intermediate stress levels the secondary creep strain rate is found to obey the relationship:

$$\dot{\varepsilon} = A \frac{\mu b D_L}{kT} \left(\frac{\sigma_a}{\mu}\right)^n \tag{1.35}$$

where A is a constant dependent on the material and n lies between 3 and 7 with a tendency for smaller values of n at higher temperature. For higher stresses the creep rate becomes more sensitive still to stress, in what is sometimes referred to as power law breakdown, and the strain rate is better represented by an exponential function of stress. Garofalo (1965) has tried to combine these two regimes into a single expression:

$$\dot{\varepsilon} = A'[\sin h\,(b\sigma)]^n \exp(-Q/kT), \tag{1.36}$$

with some degree of success.

In order to explain these observations a there is a rich literature of dislocation models, which are reviewed in Takeuchi and Argon (1976). Since then there is a growing concensus that simple models based on the balance between hardening and recovery can explain most of the observations and also provides a basis for models of transient deformation as well as steady state creep. A number of key observations should be noted as guides to the construction of a model:

(i) Dislocation pile-ups and other debris associated from cold work are not observed during creep;

(ii) The dislocations form a polygonal network, which nucleates subgrain boundaries if the temperature is high enough and the subgrain size is inversely proportional to the applied stress;

(iii) The dislocation density is low within the subgrains and increases with the square of the applied stress;

(iv) The creep rate for a given set of conditions is higher for a material with a high stacking fault energy;

(v) The creep activation energy is around 0.6 the lattice diffusion value for temperatures around 0.5 T_m and increases to the lattice diffusion value for slightly higher temperatures.

These observations support a creep mechanism based on the limb of dislocations into subgrain boundaries where they anihilate or have their long range strain fields cancelled. We can see how this happens by taking the dislocation density growth equation (1.26) and adding a term that controls recovery:

$$\frac{d\rho_d}{dt} = \frac{\dot{\varepsilon}}{bL} - 8\rho_d \frac{v_c}{h}, \tag{1.37}$$

where v_c is the rate of climb of the dislocations and h is the distance the dislocation has to move to be anihilated or to join the sub-grain boundary. The dislocation climb rate is determined by the elastic interaction between dislocations which provides a chemical potential difference for vacancy absorption and emission at the dislocation. For an isolated dislocation dipole separated by h the rate of climb towards one another is:

$$v_c = D_L \frac{\Omega\mu}{kT} \frac{b}{hs}, \tag{1.38}$$

where s is a scale parameter controlling the absorption of point defects by dislocations, which is equal to the spacing of jogs on the dislocation when climb is jog limited. In pure materials we expect that L and h are inversley proportional to the dislocation density. (For a discussion of this point see Matthews (1985)). For a steady-state creep

on making the rate of change of dislocation density zero in eq. (1.37) we obtain an expression for the strain rate:

$$\dot{\varepsilon} = 8\rho_d \frac{b^2 L}{h^2 s} D_L \frac{\Omega\mu}{kT} = B_1 \rho_d^{3/2} b^2 D_L \frac{\Omega\mu}{kT}, \tag{1.39}$$

where B_1 is a constant characteristic of the dislocation arrangement. The condition that dislocation motion is governed by an effective stress consisting the applied stress minus the internal stress from the other dislocations, eq. (1.27), makes the dislocation density proportional to the applied stress, provided that dislocation glide is much easier than climb. If we take $\sigma_s \propto \mu b \rho_s^{1/2}$ then eq. (1.39) is found to give a creep rate of the same form as eq. (1.35) with n=3. The dependence of creep rate on stacking fault energy is almost certainly associated with a reduction in the case of absorption of point defects on dislocations that are split into partials, as suggested by Argon and Moffat (1981).

If the dislocation climb rate is controlled by dislocation core diffusion rather than lattice diffusion eq. (1.38) is replaced by:

$$v_c = 2\pi D_p \frac{\Omega\mu}{kT} \frac{b^2}{h^3 s} \tag{1.40}$$

The creep rate will now be of the form:

$$\dot{\varepsilon} = A \mu \frac{bD_p}{kT} \left(\frac{\sigma_s}{\mu}\right)^5. \tag{1.41}$$

Typically the activation energy for core diffusion is around 0.5 to 0.75 of the activation energy for lattice diffusion which may explain the reduction in activation energy with temperature.

The breakdown of power law creep and the transition to an exponential dependence on stress is probably due to dislocation recovery becoming a dynamic process. This means that both the recovery rate and the hardening rate are proportional to the strain rate. In these circumstances the creep rate is fixed by the dislocation velocity and the dislocation density necessary to sustain dynamic recovery. As such the creep behaviour is relatively insensitive to temperature, until temperatures are well below 0.5 T_m.

These ideas are used in Fig. 1.7 to schematically illustrate the stress dependence of creep rate for a pure metal, which gives for an intermediate stress range an apparent stress power of ~4.5 which is frequently observed. A useful way of showing the relative importance of various creep mechanisms are the deformation maps introduced by Ashby (1972). An example is shown for a pure metal in Fig. 1.7. Creep rates below 10^{-10}/s are considered insignificant for engineering purposes.

So far we have concentrated on pure metals. Real engineering materials are hardened by solutes and the creep strength is improved by precipitates or dispersal particles. Let us briefly discuss solutes first. For low dislocation velocities at high temperature the solutes tend to be drawn to dislocations because of their stress field. Provided the solute does not precipitate on the dislocation core an atmosphere is formed round the dislocation imposing a back force to any movement. This solute atmosphere can move with the dislocation by diffusion fixing the dislocation velocity (Cottrell 1952). The dislocation velocity is not very important in determining the steady state creep rate unless the glide rate is inhibited to much lower levels than the climb rate. The main importance of the glide rate is in determining the timescale of transient creep, but the redistribution of microstructure such as the subgrain boundary size is also important and on a much longer timescale.

For higher stress and dislocation velocities the mobile dislocations can break free of the solute atmosphere and the glide rate will be determined by dislocation intersection rate or the drag of jogs. There will, however, be a back stress on the dislocation from the presence of the solute such as that given by eqs. (1.14) or (1.15).

The presence of precipitates is also important and alloys for high temperature applications are designed with dispersion hardened structures that inhibit creep. There are two main regimes of interest: low stresses where the effective stress on the dislocations is below the Orowan stress to break through the particles; and high stress where the dislocations can force their way through the obstacles. In the low stress regime the distance moved by the dislocation L is now fixed by the particle spacing. Recovery occurs by anihilation at the particles or by climb of the dislocations over the particles (McLean 1985). This leads to a creep rate of:

$$\dot{\varepsilon} = B_1 \rho_d^2 \lambda b^2 D_L \frac{\Omega\mu}{kT} = A(\lambda) \mu \frac{bD_L}{kT} \left(\frac{\sigma_s}{\mu}\right)^4 \tag{1.42}$$

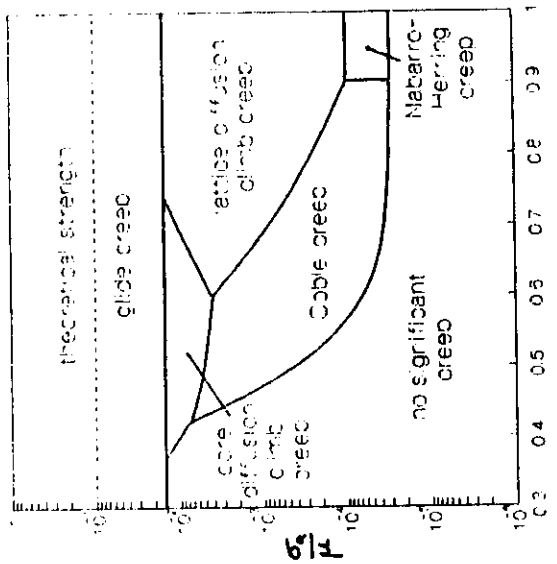

Fig. 1.8

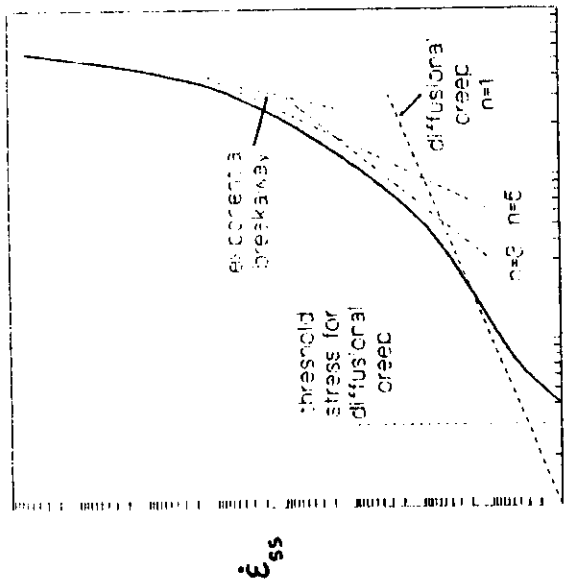

Fig.1.7

For the high stress case there is a back stress from the Orowan stress, σ_o, that gives a strain rate of the form:

$$\dot{\varepsilon} = A\frac{\mu b D_L}{kT}\left(\frac{\sigma_a - \sigma_o}{\mu}\right)^3. \qquad (1.43)$$

This gives a stress power that is apparently much higher than 3. The creep rate is fixed by the recovery of the dislocation loops left behind around the particles. An example of the stress sensitivity of a precipitate hardened material is shown in Fig. 1.9 and an equivalent deformation map in Fig. 1.10. The map is more complex because of the effect of a high threshold stress for diffusion and creep.

Two types of alloys are of particular interest for high temperature structures. Oxide dispersion hardened (ODS) alloys contain incoherent oxide particles that are particularly effective in suppressing creep. In such alloys the lower stress behaviour is inhibited almost completely for reasons which are not yet clear. Super-alloys are formed from high nickel alloys in which there are coherent intermetallic precipitates, γ' consisting of Ni_3Al. These alloys are very important in the construction of gas turbines. The coherency of the precipitates permits dislocations from one phase to pass into the other and the precipitates may be sheared. This can only happen when two dislocations in the γ structure combine and are then able to move into the γ' structure. There is threshold stress for this process that is a strong function of the volume fraction of the γ' (McLean 1985). Super-alloys frequently have 20 to 30% γ' phase.

In dealing with engineering alloys it is worth noting that the structure of most alloys is strongly temperature dependent. Stabilised steels, i.e. steel with reactive elements added that precipitate C and N, and other precipitate hardened alloys will undergo progressive coarsening of the second phases when aged at high temperatures. In most cases there is a solution temperature where the second phases disappear completely. The recovery of cold work may be inhibited by precipitation but ageing at high temperature can permit *recrystallisation* which can drastically reduce the strength of the material. At high temperature recrystallisation can also occur during deformation again reducing the strength.

1.4 Radiation Damage Processes

We are concerned here with the effects of neutron irradiation and to some extent the effect of energetic charged ions and electrons. Gamma radiation has little effect on

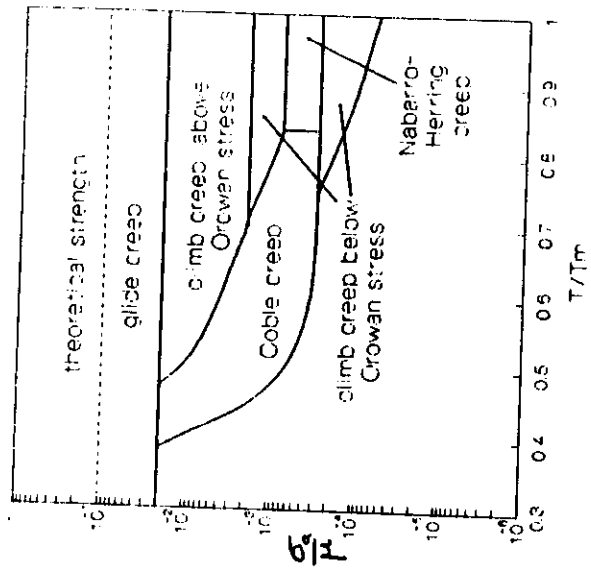

Fig. 1.10

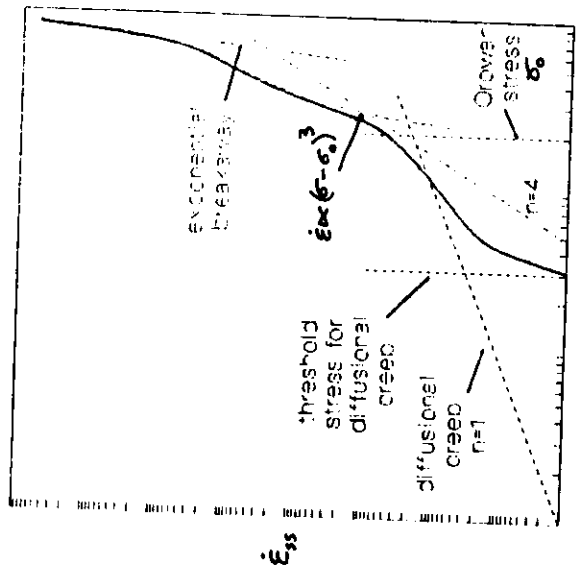

Fig.1.9

metals and the effect of ionisation in ionic and covalent solids is mainly of interest for optical and electronic effects rather than on the mechanical properties. Neutrons have two main effects on structural materials: *displacement damage* where collisions between neutrons and nucleii displace atoms from their lattice positions; and transmutation reactions where the neutron causes the nucleus to emit another particle changing its chemical nature.

Displacement damage is characterised by the *Frenkel* reaction where the displaced atom becomes a self interstitial atom and the space it once occupied becomes a vacancy. The energy required to do this in a typical metal crystal is around 30 eV but is closer to 100 eV in covalent and ionic crystals. The maximum energy transfers for a particle of mass m and kinetic energy E_o emitting a lattice atom of mass M is:

$$E_m = 4mM/(m+m)^2 E_o = \mu_m E_o. \qquad (1.44).$$

This determines the threshold energy necessary to produce displacement damage by a particular type of particle. As an example if we assume the displacement energy for iron is 25 eV the threshold energies for to displace iron atoms are:

Type of particle	μ_m	Threshold energy (eV)
^{238}U	0.617	41
^{56}Fe	1	25
^{12}C	0.518	43
^{4}He	0.249	100
n	0.069	363
e	3.92×10^{-5}	6.38×10^{5}

If substantially more energy than the displacement energy is transferred to a lattice atom it can then cause further displacements. The first ion displaced is referred to as the primary recoil ion as an energetic displacement will strip electrons from the atom. The secondary recoil ions are produced locally over a few tens of nanometers in a *cascade*. A cascade is shown schematically in Fig. 1.11. The nature of the cascade, together with a tendency for displaced atoms to channel along close packed direction, is to have a core of vacancies surrounded by a cloud of interstitials. The simplest estimate of the number of Frenkel pairs formed by a singl primary recoil can be obtained by simply dividing the recoil energy by the displacement energy. This is an overestimate as energetic ions can transmit energy to electrons. A simple rule of thumb gives the threshold energy for ionisation in keV as 1.5 times the mass of the lattice ions in atomic mass units. Above this threshold more of the energy goes into

lattice heating than displacement damage. From these considerations it can be seen that a 1 MeV electron can only produce isolated Frenkel pairs, but a 1MeV neutron or α-particle can generate cascades with around 100 displacements. Fission fragments with energies of

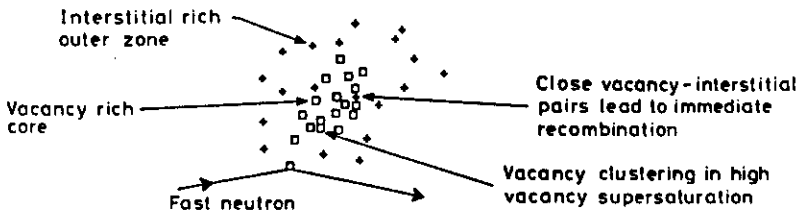

Fig. 1.11

between 60 and 140 MeV produce a large number of displacements, but the large electronic energy deposition produces a thermal spike extending over several μm which is just as important.

Displacement damage is measured in displacements per atom (dpa). Structural components in the core of a fast reactore are subjected to a displacement damage rate of around 10^{-6} dpa a^{-1} and accumulate displacement doses of 100 to 150 dpa. Core components in a water cooled thermal reactor suffer displacement damage doses about an order of magnitude lower and the pressure vessel might receive around 1 dpa.

In a displacement cascade after the initial energy deposition has dissapated, any close interstitial - vacancy pairs will recombine leaving perfect lattice. The high local concentration of vacancies also permits the vacancies to cluster and hence reduce their energy. In most materials vacancy clusters will collapse to form a vacancy loop. Such loops are unstable in the long term as they will collapse by emitting vacancies driven by the energy of the dislocation surrounding the loop and the stacking fault it usually contains. The interstitials surrounding the cascade are more widely separated and will random walk until they are absorbed by a dislocation line, combine with other

interstitials to form interstitial loops or recombine with vacancies (or a vacancy loop). Interstitials have a large elastic energy and once an interstitial is absorbed by a loop it is extremely improbable that it will be repemitted. Interstitial loops are thus very stable.

The chemical rate theory is frequently used to provide a framework to model point defect kinetics (Bullough 1985). We will use a simplified version of the rate theory of radiation damage to illustrate some of the main features of the behaviour. The rate of change of concentration of point defects is given by:

$$\dot{c}_i = K - D_i k_i^2 - \alpha c_i c_v$$

and

$$\dot{c}_v = K + K_e - D_v k_v^2 c_v - \alpha c_i c_v , \qquad (1.45)$$

where K is the displacement damage rate. The quantities k_i^2 and k_v^2 are the sum of the strengths of interstitials and vacancies for all the sinks in the material, e.g. point defect loops, dislocations, cavities and grain boundaries. The thermal emission of vacies is included with the term $K_e = \Sigma_\alpha D_v k_{v\alpha}^2 \bar{c}_{v\alpha}$ where α indicates a particular sink type and $\bar{c}_{v\alpha}^2$ is the thermal equilibrium vacancy concentration adjacent to the sink. The final term in the eqs. (1.45) is the recombination rate where the recombination rate α is generally proportional to D_i as interstitials migrate more rapidly than vacancies.

At the start of irradiation the defect fluxes are subjected to a transient which is dominated by the relative mobilities of the interstitials and vacancies. This will only last on average a few hours. Once a dynamic equilbrium is established we can easily find a steady state solution for eqs. (1.45):

$$c_i = \left[KF(\eta) - \frac{1}{2} K_e \right] / k_i^2 D_i c_i$$

and

$$c_v = \left[KF(\eta) + \frac{1}{2} K_e \right] / k_v^2 D_v c_v \qquad (1.46)$$

where

$$F(\eta) = (2/\eta) \left\{ \left[(1 + K_e \eta / 4K)^2 + \eta \right]^{1/2} - 1 \right\}$$

and

$$\eta = 4 \alpha K / D_i D_v k_i^2 k_v^2 .$$

The function F(η) gives the effect of recombination and thermal emission on the defect populations. At low temperature η and K_e are very small and $F(\eta) \rightarrow 0$. In this case the defect concentrations rise until the quadratic recombination term dominates. For high temperatures (>1/2 Tm) thermal emission become important and the vacancy concentration is large, suppressing the interstitial concentration. At intermediate temperature both vacancies and interstitials are mobile and the point defects are mainly lost to sinks. It is in this intermediate range that most of the interesting and important radiation damage effects occur. Fig. 1.12 shows the extent of the temperature zones as function of displacement dose rate. The solid lines define the zones for a high sink strength of 10^{16} m^{-2} and the dashed lines define the zones for a low sink strength of 10^{14} m^{-2}.

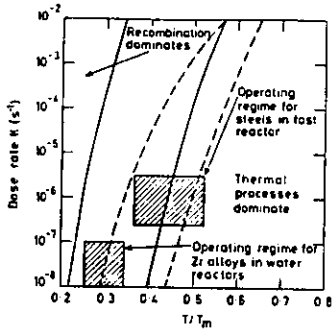

Fig. 1.12

Displacement damge produces a wide range of effects in structural materials. These include irradiation creep, irradiation growth, fast neutron induced swelling, irradiation hardening and irradiation softening. All these effects are to a large extent due to the elastic interaction between dislocations and point defects, particularly interstitials. Point defect sinks such as grain boundaries and cavities are frequently referred to as neutral sinks as they only weakly interact with point defects. The point defects mainly find these sinks by random walk and there is no large preference for a particular defect type. Dislocation, however, as we have seen, have a long range elastic field that interacts strongly with the large mismatch volume of the interstitial. The intersititials are attracted to the dilatation region of the strain field of an edge dislocation but are repelled from the compressive region. The net effect, however, is a drift of the intersitials to the dislocation and a difference in the dislocation sink strength for vacancies and interstitials. We can represent the dislocation sink strength by:

$$k_{id} = Z_i \rho_d \cong Z(1+\Delta)\rho_d$$

and

$$k_{vd} = Z_v \rho_d \cong Z\rho_d. \qquad (1.47)$$

The sink strength of point defect loops can be handled in a similar manner. For the effect of dislocation bias for interstitials over vacancies to be apparent a neutral sink must also be present. We will just consider cavities where:

$$k_{ic}^2 \cong k_{vc}^2 \cong 4\pi r_c C_c. \qquad (1.48)$$

The net flow of interstitials over vacancies to dislocation is given by:

$$\dot{q}_d = k_{id}^2 D_i c_i - k_{vd}^2 D_v c_v + k_{vd}^2 D_v \bar{c}_{vd}. \qquad (1.49)$$

Substituting the values of c_i and c_v from eq. (1.46) and using (1.47) and (1.48) we get:

$$\dot{q}_d \cong Z\rho_d \left[\frac{\Delta F(\eta)\, 4\pi r_c C_c}{(4\pi r_c C_c + Z\rho_d)^2} - \frac{K_e}{(4\pi r_c C_c + \rho_d} + D_v \bar{c}_{vd} \right]. \qquad (1.50)$$

When thermal emission can be ignored the net flux of interstitials to dislocations (or interstitial loops) is proportional to Δ. The excess vacancies will flow to the cavities and produce swelling, see section 2.4.

Swelling is a direct consequence of displacement damage provided suitable cavity nuclei are present (helium from transmutation reactions is available for this role). The other effects are slightly less direct. Radiation hardening arises from the build-up of a combination of obstacles to dislocation. The first is from point defect loops both the unstable vacancy loops and the interstitial loops. If no neutral sinks are present the effect of radiation hardening saturates on the accumulation of a dose of around 1 dpa. If neutral sinks are present the interstitial loops grow until they touch one another. This can trigger an unfaulting reaction and the resulting dislocations join the dislocation network. The net flux of interstitials to dislocations in the presence of neutral sinks can also lead to dislocation multiplication, by new dislocation line length that is generated when climbing dislocations bow out between obstacles. In well annealed material the yield stress will always increase during irradiation but thermal recovery will reduce the effect at high temperature. In heavily cold worked materials irradition may soften the material by accelerating thermal recovery. The cavities that grow in the point defect flux also increase the crystal flow stress, unless they grow large enough to weaken the material, see section 5.3. These effects can lead to a long term evolution of the properties of the material throughout the irradiation. There are also effects from radiation induced segregation where the point defects interact with solute atoms and

either accelerate the formation of equilibrium microchemical structures or even generate structures that are thermodynamically unstable.

Radiation creep is an important phenomenon in materials undergoing irradiation. A review of the mechanisms that can produce the effect can be found in Matthews and Finnis (1988). There are basically two types of creep: SIPA (stress induced preferential absorption of defects) creep that is insensitive to temperature and microstructure; and creep that is proportional to the swelling rate or relies on the presence of some other neutral sink. A number of explanations of SIPA creep have been offered. The effect may come from the inhomogeneity interaction where the effective shear modulus of an interstitial is lower than the surrounding host material. This will result in dislocations with different orientations with respect to an applied stress interacting with interstitial differently. The result is a net drift of interstitials to preferred dislocations (Heald and Speight 1974). An alternative explanation is that an applied stress constrains the diffusion of interstitials and this leads to a higher absorption by preferred dislocations (Woo 1984). For either explanation the resulting creep can be expressed as:

$$\dot{\varepsilon} = C \frac{\sigma_a}{\mu} \frac{k_S^2}{k_T^2} K F(\eta), \tag{1.51}$$

where k_N^2 is the sink strength of favourable orientated dislocations and k_s^2 is the strength of all other sinks for interstitials. The coefficient C is dependent on the material and is found to lie usually between 0.05 and 0.5. For cold worked steels where the dislocation sink strength dominates and in the temperature range where recombination and thermal emission can be neglected:

$$\dot{\varepsilon} \equiv 0.1\, \sigma_a K/\mu. \tag{1.52}$$

A variety of mechanisms can produce creep that is proportional to swelling. One example is the creep that results from preferred nucleation of interstitial loop in the presence of stress. Other mechanisms rely on interstitial driven climb interaction modifying glide creep processes. A simple example would be where dislocations held against an obstacle climb so that further glide is made possible. Such climb can also nucleate recovery by allowing favourably orientated dipoles to anihilate. This is a random process as unfavourably orientated dipoles are driven apart. Other processes rely on internal stress fluctuations that arise from random climb interactions. Some of these mechanisms are proportional to the applied stress others modify the thermal creep

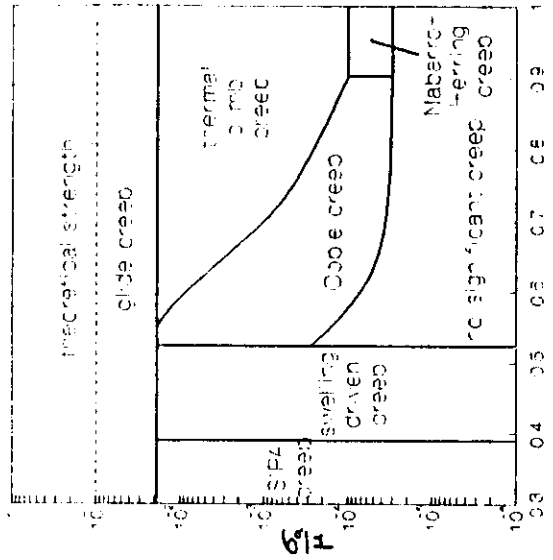

Fig. 1.14

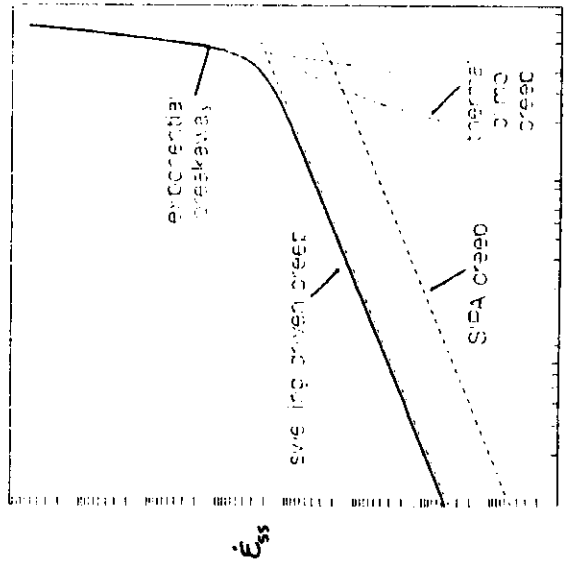

Fig.1.13

mechanism by reducing the creep stress power by one. Where swelling occurs this type of creep is substantial and usually is larger than SIPA.

In Figs. 1.13 and 1.14 we show the effect of irradiation on the deformation of a pure metal or simple alloy. Fig. 1.13 shows the stress dependence of creep at a temperature near 0.5 Tm. Fig. 1.14 shows a deformation map. The range of interactions involved in calculating the mechanical properties of a material under

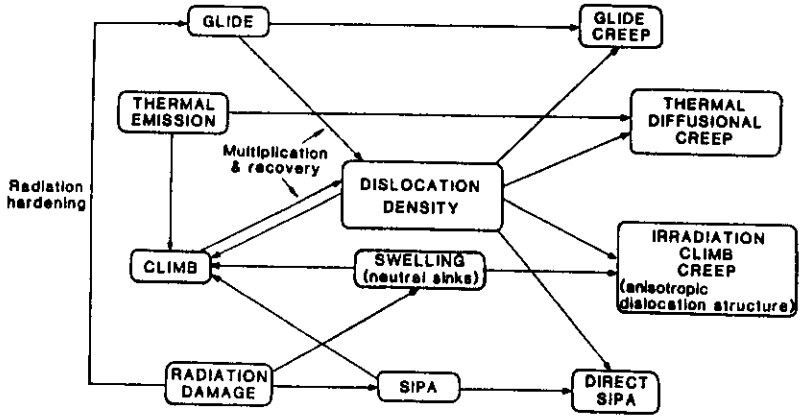

Fig. 1.15

irradiation are very large. They are summarised in Fig. 1.15. In addition to irradiation creep there are substantial effects on thermal creep, which is inhibited by radiation hardening. In real materials the presence of solutes is very important. The mismatch strain of solutes provides a binding energy with vacancies and interstitials. Undersized solutes tend to bind with interstitials while oversized and interstitial solutes tend to bind with vacancies. The trapping of point defects by impurities results in higher recomination rates and a reduction in radiation damage effects. Swelling and irradiation creep are in general lower in impure materials or complex engineering alloys.

Before closing this section it is worth mentioning irradiation growth. This is the property of some materials to change shape under irradiation, without associated volume changes. This phenomenon is most important in materials with anisotropic crystal structures, but some effects are also seen in cubic materials with anisotropic microstructure produced by cold working. In anisotropic crystals the effect is now though to be due to anisotropic diffusion leading to absorption of point defects on

particular dislocation or loop types. To be fully effective either two types of disloction or loop are required or the presence of a neutral sink such as a grain boundary. Growth is very important in the behaviour of zironium alloys used in the cladding materials of water reactor fuels. Macroscopic growth is observed if the material has a texture. Growth is also responsible for the degradation of anisotropic ceramic materials under irradiation, because of the formation of internal stresses from growth strain mismatch.

List of Symbols

(NB. some symbols may be used for other quantities, but in these cases the definition will be made in the text)

Roman

a	-	crack width for edge crack, crack half width or radius for internal crack.
a_o	-	atomic lattice spacing.
b	-	magnitude of Burgers vector.
B_L	-	creep coefficient in expression $\dot{\varepsilon}_a = B\sigma_a^n$.
c		
c_i	-	interstitial atomic concentration.
c_v	-	vacancy atomic concentration.
D_L	-	lattice diffusion coefficient.
D_a	-	solute diffusivity.
D_b	-	grain boundary diffusion coefficient.
D_i	-	interstitial diffusivity.
D_s	-	surface diffusion coefficient.
D_v	-	vacancy diffusivity, $D_L = D_v C_v$.
E	-	Young's modulus, i.e. elastic modulus relating a uniaxial load to a uniaxial strain.
f	-	packing fraction.
F	-	Force or force per unit length as appropriate.
h	-	thickness of section.
I	-	Moment of inertia.
J	-	Eshalby/Rice integral used to assess fracture toughness.
K	-	stress intensity factor.
L	-	Length of structure.
m	-	work hardening index in $\varepsilon_a = (\sigma_a/\sigma_p)^{1/m}$.
n	-	creep stress index in expression $\dot{\varepsilon}_a = B\sigma_a^n$.

N - number of cycles, N_f number cycles to failure.

r_b - grain boundary radius.

r_c - cavity radius.

t - time.

T - absolute temperature.

T_m - melting point.

W - width of structure, work.

Greek

δ - small displacement.

δ_b - effective width of grain boundary for diffusion.

δ_i - effective width of interface.

δ_s - effective width of surface for diffusion.

γ_b - grain boundary energy.

γ_i - interfacial energy.

γ_s - surface energy.

γ_f - equivalent surface energy for fracture.

ε - hydrostatic strain.

ε_a - uniaxial plastic strain.

κ - geometric curvature, sum of reciprocal principle radii of curvature.

μ - shear modulus, $\mu = E/2(1+\nu)$.

μ_a - atomic chemical potential.

ν - Poisson's ration, i.e. the ratio of strain normal to the load and parallel to the load during elastic uniaxial loading.

ν_o - lattice vibrational frequency, ~ $10^{12} s^{-1}$.

ρ_d - dislocation density.

ρ_D - density.

ρ_o - local radius of curvature.

σ - hydrostatic component of stress.

σ_a - applied uniaxial of stress.

σ_e - von Mises equivalent stress.

σ_f - failure stress (uniaxial).

σ_o - back stress from impurities or solutes.

σ_p - work hardening coefficient in $\varepsilon_a = (\sigma_a/\sigma_p)^{1/m}$.

σ_Y - yield stress (uniaxial).

τ_a - applied shear stress. $\tau_a = \sigma_a/\sqrt{3}$

τ_f - flow stress (shear).

Ω - atomic volume.

References

Adamson, M. G., Reineking, W. H., Kangiluski, M. and Vaidyanathan, (1986) Proc. Int. Conf. on Reliable Fuels for Liquid Metal Reactors, ANS, Tucson, Arizona, p4-30.

Ainsworth, R. A., (1982) Int. J. Fracture, 20, 147.

Argon, A. S. and Moffatt, W. C., (1981) Acta Met. 29, 293.

Arzt, E., Ashby, M. F. and Verrall, R. A., (1983) Acta Met. 31, 1977.

Ashby, M. F., (1968) Proc. 2nd Bolton Loading Conf. on Oxide Dispersion Strengthening, pub. Gordon and Breach, New York, p.143.

Ashby, M. F., (1972) Acta Met. 20, 887.

Atkinson, H. V., (1988) Acta Met. 36, 469.

Atkinson, H. V., (1988) Acta Met. 36, 469.

Andrade, E. N., daC., (1910) Proc. Roy. Soc. A84, 1.

Bagley, K. Q. et al, (1987) Proc. Int. Conf. on Materials for Nuclear Reactor Core Applications, BNES, Bristol, vol 2, p. 37.

Baker, C., Beere, W., Callen, V. M. and Clay, B. D., (1987) Proc. Int. Conf. on Materials for Nuclear Reactor Core Applications, BNES, Bristol, vol. 1, p.1.

Banerjee, P. K. and Butterfield, R., (1981) Boundary Element Methods in Engineering Science, McGraw Hill, London.

Beere, W., (1981) in Cavities and Cracks in Creep and Fatigue, ed. J. H. Gittus, Applied Science Publishers, London, Chaps. 1 and 2.

Birnbaum, H., (1979), Proc. Conf. on Environmentally Sensitive Fracture in Engineering Materials, AIME.

Brearley, I. R. and MacInnes, D. A., (1980) J. Nucl. Mater. 95, 239.

Brown, L. M. and Embury, J. D., (1973) Proc. 3rd Conf. on the Strength of Materials and Alloys, Inst. Metals, London, p .

Bullough, C. K. and Jenkins, J. K., (1987) Proc. Int. Conf. on Materials for Nuclear Reactor Core Applications, BNES, Bristol, vol. 1, p.9.

Bullough, R., (1985) Dislocations and the Properties of Real Materials, Proc. Conf. at Royal Society London, Metals Soc., p.283.

Burke, J. E. and Turnbull, D., (1952) Prog. Metal Phys. 3, 220.

Burke, J. E. and Turnbull, D., (1952) Prog. Metal. Phys. 3, 220.

Cahn, R.W. and Haasen, P., (1983) eds. Physical Metallurgy, 3rd edition, in 2 volumes, North-Holland, Amsterdam.

Cameron, R. F., and Temple, J. A. G., (1986) Nucl. Eng. & Design 91, 57.

Chan, K. S., (1989) Acta Met. 37, 1217.

Chang, T-J., Kagawa, K. I., Rice, J. R. and Sills, L. B., (1979) Acta Met. 27, 265.

Christensen, R. M., (1979) Mechanics of Composite Materials, John Wiley and Sones, New York.

Chuang, T-J., Kagawa, I. I., Rice, J. R. and Sills, L. B., (1979) Acta Met. 27, 265.

Clemm, P. J. and Fisher, J. C., (1955) Acta Met. 3, 70.

Coble, R. L., J. Appl. Phys. 34, 1679.

Coffin, L. F., (1954) Trans. ASME 76, 931.

Cottrell, A. H., (1952) Prog. Metall. Physics 1, 77.

Cottrell, A. H., (1958) Trans. Met. Soc. AIME 212, 192.

Cowen, H. C.and Thorley, A. W., (1983) Proc. Conf. on Ferritic Alloys for use in Nuclear Energy Technologies, AIME, Snowbird, Utah, p.51.

Crendall, S. H., Dahl, N. C. and Lardner, T. J., (1978) An Introduction to the Mechanics of solids, 2nd Edition revised, McGrear-Hill, New York.

Dimelfi, R. J. and Nix, W. D., (1977) Int. J. Fracture. 13, 341.

Dorn, J. E. and Mote, J. D., (1964) in High Temperature Structure and Materials, ed. A. M. Freundenthal, B. A. Boley and H. Liebowitz, Pergamon Press, Oxford, p.95.

Edwards, G. H. and Ashby, M. F., (1979) Acta Met. 27, 1505.

Eshalby, J. D., (1956) in Solid State Physics, ed. F. Seitz and D Turnbull, Academic Press, New York, 397.

Eshelby, J. D., (1951) Phil. Trans. Roy. Soc. A244, 87.

Evans, J. H. and Mazey, D. J., (1985) J. Phys. F-Met. Phys. 15, L1.

Fish, R. L. and Hunter, C. W., (1976) ASTM Spec. Techn. Pub. 611, p.119.

Fisher, J. C., Hart, E. W. and Pry, R. H., (1953) Acta Met. 1, 336.

Ford, I. J. and Matthews, J. R. (1989). Proc. 19th Canadian Fracture Conf., Ottawa, and A S Kransz, Kluwer, Toronto.

Ford, I. J., (1988) Harwell research report AERE-M3650.

Frenkel, J., (1945) J. Phys. (Moscow) 9, 385.

Friedel, J., (1964) Dislocations, Pergamon Press, Oxford.

Garlick, A. and Gravenor, J. G., (1981) Proc. Topical Mtg. on Water Reactor Fuel Performance, ANS, St Charles, Illinois, p.305.

Garofalo, F., (1965) Fundamentals of Creep and Creep Rupture in Metals, MacMillan, New York.

Greenwood, G. W., Foreman, A. J. E. and Rimmer, D. E., (1959) J. Nucl. Mater. 4, 305.

Griffith, A.A., (1920) Phil. Trans. Roy. Soc. A221, 163.

Gurson, A. L., (1977) J. Eng. Mater. and Techn. 99, 2.

Hall, E. O., (1951) Proc. Phys. Soc. B64, 747.

Heald, P. T. and Speight, M. V., (1974) Phil. Mag. 29, 1075.

Hermann, L. R., (1965) Am. Inst. Av. & Aer. Jul. 3, 1896.

Herring, C. V., (1950) J. Appl. Phys. 21, 437.

Herring, C., J. Appl. Phys. 21, 437.

Hill, R., (1950) Plasticity, Oxford University Press, Oxford.

Hindle, E. D., Haste, T. J. and Harrison, W. R., (1987) Proc. Conf. on Materials for Reactor Core Applications, BNES, Bristol, vol. 1, p.79.

Hirth, J. P., (1980) Met. Trans. 11A, 861.

Hirth, J. P.and Lothe, J., (1982) Theory of Dislocations, Zud ed. Wiley, New York.

Hoff, N. J., (1953) J. Appl, Mech. 20, 105.

Hondros, E. D., and Seah, M. P., (1983) in Physical Metallurgy, eds. R. W. Cahn and P. Haasen, North Holland, Amsterdam, vol 1, p.856.

Hyam, E. D. and Sumner, G., (1962) Proc. Conf. on Radiation Damage in Solids, IAEA, Vienna, vol. 1, p.233.

Irwin, G.R., (1948) Fracturing of Metals, Amer. Soc. Metals, Cleveland, Ohio.

Johnson, D. L., (1969) J. Appl. Phys. 40, 192.

Kelly, A. and MacMillan, N. H., (1986) Strong Solids, 3rd edition, Oxford University Press, Oxford.

Kingery, W. D. and Berg, M., (1955) 26, 1205.

Kreig, R. D., (1977) Proc. 4th Int. Conf. on Structural Mechanics in Reactor Technology, San Francisco, paper M6/4*.

Kreig, R. D., (1977) Proc. 4th Int. Conf. on Structural Mechanics in Reactor Technology, San Francisco, paper M6/4*.

Kroener, E., (1958) Continuum Theory of Dislocations and Self Stresses, Ergebrisse der Angewandeten Mathematik, vol. 5, pub. Springer-Verlag, Berlin, available as a translation by I Raasch and C S Hartley, University of Florida, 1971.

Kuczyuski, G. C., (1949) Trans. AIME 185, 169.

Labusch, R., (1970) Phys. Stat. Sol. 41, 659.

Landau, L. D. and Lifschitz, E. M., (1959) Theory of Elasticity, vol. 7 Course on Theorectical Physics, in translation, Pergammon Press, London.

Lawn, B. R. and Wilshaw, T. R., (1975) Fracture of Brittle Solids, Cambridge University Press, Cambridge.

Liftshitz, I. M. and Slyozov, V. V., (1961) J. Phys. Chem. Solids 19, 35.

Manson, S. S., (1954) NACA Technical Note 2933.

Marshall, W., (1982) An Assessment of the Integrity of PWR Pressure Vessels, Issued by UKAEA.

Matthews, J. R. and Small, G. J., (1988) in Proc. IAEA Mtg. on Water Reactor Fuel Element Computer Modelling in Steady State Transient and Accident Conditions, Preston, IAEA-71-7c-657, paper 4.1.

Matthews, J. R. and Wood, M. H. (1984) Eur. Appl. Res. Rept. - Nucl. Sci. Technol. 5, 1685.

Matthews, J. R. and Wood, M. H., (1980) J. Nucl. Mater. 91, 241.

Matthews, J. R., (1970) Nucl. Eng. Des. 12, 291.

Matthews, J. R., (1979) J. Nucl. Mater. 87, 356.

Matthews, J. R., (1980) Acta Met. 22, 275.

Matthews, J. R., (1985) A simple dislocation model for high temperature deformation, Harwell Laboratory report AERE-R11564.

Matthews, J. R., (1985) Nucl. Eng. and Design, 88, 111.

McLean, M., (1985) Acta Met. 33, 545.

Mikhhin, E. Y., (1979) 87, 405.

Miller, A. G., (1987) Review of limit loads of structures containing defects, 3rd edition, CEGB report TPRD/B/0093/N/83 (rev. 2).

Milne, I. and Goodall, I. W., (1988) CEBG Research May 1988 issue, p.48. See also CEGB report R/H/R6(Rev. 3) issued May 1986.

Monkman, F. C. and Grant, N. J., (1956) Proc. ASTM 56, 593.

Morris, D. G. and Harries, D. R., (1977) Harwell Laboratory report AERE-R8811.

Mukherjee, S., (1982) Boundary Element Methods in Creep and Fracture, Applied Science Publisher, London.

Nabarro, F. R. N., (1948) Proc. Conf. on Strength of Solids, Bristol, p.75.

Nabarro, F. R. N., (1967) Theory of Crystal Dislocation, Oxford University Press, Oxford.

Nabarro, F. R. N., (1985) Dislocations and Properties of Real Materials, Proc. Conf. at Royal Society London, Metals Soc., p.152.

Nabarro, F. R. N., (1985) Dislocations and the Properties of Real Materials, Proc. Conf. at Royal Society London, Metals Soc., p.151.

Nichols, F. A. and Mullins, W. M., (1965) J. Appl. Phys. 36, 1826.

Nixon, W. and MacInnes, D. A., (1981) J. Nucl. Mater. 101, 192.

Odqvist, F. K. G., (1974) Mathematical Theory of Creep and Creep Rupture, 2nd Edition, Oxford University Press, Oxford.

Old, C. F., (1980) J. Nucl. Mater. 92, 2.

Orowan, E., (1948) Proc. Symposium on Internal Stresses in Metals, Inst. of Metals, London, p.451.

Orowan, E., (1949) Rep. Prog. Phys. 12, 185.

Owen, D. R. and Hinton, E., (1980) A Simple Guide to Finite Elements, Pineridge Press, Swansea.

Paris, P. C. and Erdogen, (1963) J. Basic Eng. Trans. ASME 85, 528.

Peach, M. O. and Koehler, J. S., (1950) Phys. Rev. 80, 436.

Pearson, S., (1972) Eng. Fracture Mechanics 2, 9.

Peierls, R., (1940) Proc. Phys. Soc. (London) 52, 23.

Perryman, L. J. and Goodhew, P. J., (1988) Acta Met. 36, 2685.

Perryman, L. J. and Goodhew, P. J.,(1988) Action.Met. 36, 2685.

Petch, N. J., (1953) J. Iron and Steel Inst., 173, 25.

Pickman, D. O., (1975) Nucl. Eng. Design 33, 141.

Rice, J. R., (1968) in Fracture, ed. H Liebowitz, Academic Press, New York, vol II, Chap. 3.

Rice, J., (1968a) J. Appl. Mech. 35, 13.

Robinson, D. N., Pugh, C. E. and Corum, J. M., (1976) 'Constitutive Equations for Describing High Temperature Inelastic Behaviour of Structural Alloys', in Proc. IAEA International Working Group on Fast Reactor Specialists Mtg. on High Temperature Structural Design Technology, IWGFR-7.

Robinson, E. L. , (1952) Trans. Amer. Soc. Mech. Engineers 74, 777.

Sadananda, K. and Shaninian, P., (1979) Int. J. Fracture, 15, R81.

Schultz, B., (1981) High Temp. - High Pres. 13, 649.

Shaarfe, B. vander and Marshall, P., (1983) Proc. Int. Conf. on Dimensional Stability of Irradiated Metals and Alloys, BNES, Brighton, vol. 1, p.143.

Speight, M. V. and Beere, W., (1975) Met. Sci. 9, 190.

Stroh, A. N., (1954) Proc. Roy. Soc. 223A, 404.

Suzuki, H., (1971) Nachr. Akad. Wis. Göttingen Math.-Phys., K1, 113.

Takeuchi, S. and Argon, (1976) J. Mat. Sci. 11, 1542.

Thompson, N., Wadsworth, N. J. and Louat, N., (1956) Phil Mag. 1, 113.

Thomson, R. M., (1978) J. Mater. Sci. 13, 128.

Thomson, R.M., (1983) Ch. 23 in Cahm and Haasen (1983).

Timoshenko, S. and Goodier, J.N., (1951) Theory of Elasticity, 2nd edition, McGraw-Hill, New York.

Timoshenko, S., (1934) Theory of Elasticity, McGraw-Hill, New York.

Treharne, G., (1971) Thesis 'Application of the Finite Element Method to the Stress Analysis of Materials Subject to Creep', Dept. of Civil Engineering, University of Wales, Swansea.

Tucker, M. O., (1981) in Cavities and Cracks in Creep and Fatigue, ed. J. H. Gittus, Applied Science Publishers, London, Chap. 3.

Tvergaard, V., (1981) Int. J. Fracture. 17, 389.

Tvergaard, V., (1982) Int. J. Fracture. 19, 163.

Valentin, R. A. and Carey, J. J., (1970) Nucl. Eng. & Des. 12, 277.

Wareing, J., Tomkins, B. and Bretherton, I., (1983) Proc. Seminar on Flow and Fracture at Elevated Temperatures, ed. R. Raj, ASME, Philadephia, Penn.

Watkins, J. S., (1984).

Willis, J., (1980).

Woo, C. H., (1984) J. Nucl. Mater. 120, 55.

Wulf, J., (1964) ed. The Structure and Properties of Materials, in 4 volumes, Wiley, New York.

Zienkiewicz, O., (1971) The Finite Element Method in Engineering Science, 2nd Edition, McGraw-Hill, London, 4th Edition now available (1989).

Glossary

Adatoms	-	A surface point defect, where an atom is detached from the surface and can migrate. Surfaces prefer to lie on high density crystal planes. Adatoms are emitted and absorbed at ledges on these planes.
Austenitic steel	-	Ferrous alloys which have predominantly the fcc structure; the γ phase in the iron phase diagrams. Ni tends to stabilise this phase and austenitic structures are seen in stainless steels and high nickel alloys.
bcc	-	body centred cubic. This is a crystal structure found in low alloy steels (ferritic steels) and refractory metal alloys (Nb, Mo, W).
Burgers vector	-	The Burgers vector is the vector that characterises the *slip* propagated by a dislocation. On making a circuit of the dislocation by moving from lattice position to lattice position, the Burgers vector is the vector that is required to complete the circuit after a series of moves that would have completed the circuit in the absence of the dislocation.
Cleavage	-	Crack propagation by the separation of the crystal lattice. In some materials cleavage is constrained to particular orientations that coincide with planes of high atomic density.
Climb	-	Motion of the edge component of a dislocation out of its slip plane. This motion is non-conservative, i.e. requires the emission or absorption of point defects, c.f. *glide*.
Cold work	-	Strain accumulated at temperatures low enough to prevent annealing. Material in a cold worked state is often used in engineering structures because of its higher strength, but this is at the expense of *ductility*.
Creep	-	The continued plastic deformation of a body on the application of a load. Creep is characteristic of the high temperature deformation of materials.
Cross slip	-	Glide of a dislocation on a new *slip* plane (i.e. other than the primary slip plane). Cross slip is only possible with the *screw* component of a dislocation, as the motion would be non-conservative (*climb*) for the *edge* component.
Dead load	-	A load that does not vary during deformation, e.g. hanging a weight on a bar or pressurising a tube with an infinite gas reservoir.
Dipole	-	A pair of dislocations lying on different glide planes that achieve an equilibrium configuration through the interaction of their elastic fields. A multipole bundle is a configuration of three or more dislocations in this way.
Dislocation	-	A line defect marking the boundary between slipped and unslipped regions of crystal. A dislocation is defined by its *Burgers vector*, see also *edge* and *screw*.
Dislocation	-	A dislocation configuration that permits the further generation of

source - dislocation line length, usually by the emission of dislocation loops. The simplest type is the Frank-Read source which simply consists of a dislocation segment between two nodes, which may be part of a dislocation network. This segment bows-out and if the applied stress is large enough it can form a complete loop and the original segment snaps back to start the process again.

Displacement damage - Radiation damage where an atom is knocked out of its lattice position by a fast neutron, a recoil ion or an incident charged particle, see *Frenkel pair*.

Ductility - The ability of a material to undergo plastic strain and is measured by the plastic or creep strain at failure. The work originally referred to the property of being able to be drawn into wire and was one of the properties that defined a metal.

Edge Dislocation - The edge component of a dislocation is that where the *Burgers vector* is normal to the dislocation line.

Epitaxy - Growth of a crystal on the surface of another crystal, not necessarily of the same phase, where the underlying crystal determines the structure and orientation of the new crystal.

Explicit calcualtions - In solving time dependent problems by taking difference approximations for time differentials, an explicit method is one where the value of a quantity at a new time is defined only in terms of values at previous times steps. The simplest example is the Enter backward method where:

$$\frac{dq}{dt} \cong \frac{q_1 - q_o}{\delta t} = f(q_o)$$

where q_1 refers to the value of q at t.

Fatigue - The property of a material to fail by the propagation of cracks on the application of a cyclic load.

fcc - faced centred cubic. This is a close packed crystal structure frequently found in stainless steels (Austenitic steels) and high nickel alloys.

Ferritic steel - Ferrous alloys which have predominantly the bcc structure; the α phase in the iron phase diagram. Cs tends to stabilise this phase and ferritic structures are seen in carbon steels.

Flow stress - The external stress required to produce dislocation glide motion.

Frenkel pair - Displacement damage produces Frenkel pairs which consist of two point defects: a *vacancy* and a self *interstitial* atom.

Glide - Motion of a dislocation within its slip plane. This motion is conservative, i.e. does not require the emission or absorption of point defects, c.f. *climb*.

Global function - A function that describes some field quantity for the whole of a body, c.f. piece-wise function.

Grain boundary - A two dimensional defect which separates two regions of differently orientated crystal.

hcp - Hexagonal close packed. This is a close packed crystal structure with hexagonal symmetry found in Mg, Ti, Zr and other non-ferrous alloys.

Hot pressing - The consolidation of a body composed of separate particles by the application of an external pressure. Hot pressing is also used to describe pressure driven reconfiguration of pores within a material, c.f. *sintering*. HIP, hot isostatic pressing, is an important new process for producing components from metal powders that would otherwise not be possible by conventional metallurgy.

Implicit calculations - Insolving time dependent problems by taking difference approximations for time differentials, an implicit method is one where the value of a quantity at a new time is defined in terms of the values at the new time step rather than previous time steps. The simplest example is the Euler forward method where:

$$\frac{dq}{dt} \cong \frac{q_1 - q_o}{\delta t} = f(q_1)$$

where q_1 refers to the value of q at $t+\delta t$ and q_o refers to the value of q at t.

Intergranular - Between grains, i.e. grain boundary processes, see *intragranular*.

Interstitial - A point defect where an atom is squeezed into a position between normal lattice positions. Self interstitial atoms are of the same type as the atoms on regular lattice positions and interstitial solutes are formed with foreign atoms.

Interstitial solute - Foreign atoms that lie between the crystal lattice positions.

Intragranular - Inside grains, i.e. processes that occur in the interior of grains as opposed to processes that occur on grain boundaries, see *intergranular*.

Jog - A jog on a dislocation is a step one atomic spacing high with a component normal to the glide plane, cf. *kink*.

Kink - A kink on a dislocation is a step one atomic spacing wide lying in the glide plane, cf. *jog*.

Lattice vector - A vector that will transpose a point from one lattice position to another.

Mixed dislocation - A dislocation with both *edge* and *screw* components.

Neutral sink - A sink for point defects; the sink strength does not distinguish between interstitials and vacancies.

Packing fraction - The volume fraction of solid matter in a conglomeration of particles.

Partial dislocation - A dislocation where the *Burgers vector* is not a lattice vector as opposed to a perfect dislocation.

Peierls stress - The local shear stress required to move a dislocation.

Piece-wise function - A function that describes some field quantity for a body in terms of a set of functions that apply over elements (or zones) that cover the whole of the body. In a piece-wise continuous function each of the functions in the set is continuous at the boundaries.

Plane strain - An assumption that permits problems where one dimension is large compared to the others to be reduced to two dimensions and axisymmetric problems to one dimension. The long dimension is assumed to be infinite and strains having components in that direction are assumed to be zero. In generalised plane strain uniform strains in the long direction are permitted if they are uniform over the cross section.

Plane stress - An assumption that permits thin plate problems to be reduced to two dimensions. Stress components which act on the plane lying parallel to the plaste are assumed to be zero.

Principal stresses - Any arbitrary stress state of a body may have finite values of all the stress components σ_{ij}. It can be shown that by choosing a suitable co-ordinate system a stress tensor with $\sigma_{ij}' = 0$ for $i = j$ can be found. The finite components of σ_{ij}' fir $i = j$ are known as the principal stresses.

PWR - Pressurised water reactor.

Recovery - The process where the internal energy of the microstructure is reduced by dislocation anihilation or by the formation of low energy configurations such as subgrain boundaries.

Recrystallisation - The lowering of the internal energy of the microstructure by the sweeping away of the old structure by the formation of a new grain structure. This occurs in two stages: primary recrystallisation where a new fine grain structure is formed from a high dislocation density; and secondary recrystallisation when this structure coarsens by grain growth further reducing the dislocation density.

Screw dislocation - The screw component of a dislocation is that where the *Burgers vector* is parallel to the dislocation line.

Segregation - Preferential concentrations of components of an alloy or impurities at an interface or a dislocation.

Sintering - The consolidation of a body composed of separate particles by the formation of continuous material at the points of contact driven by surface energy. Sintering may or may not result in densification of the resulting body depending on the mass transfer processes involved. Sintering is also used to describe surface energy driven reconfiguration of pores within a material, c.f. *hot pressing*.

Slip - Local shear of crystal when there is a relative movement of the material above and below the slip plane that is parallel to the plane. In crystals slip is confined to particular orientations usually coinciding with planes of high atomic density. There is usually a hierarchy of slip systems that are activated by increasing loads.

Stacking fault - A two dimensional defect where the normal sequence of close packed planes in a lattice is disturbed. A stacking fault is bounded by *partial dislocations* and in some cases,when stacking fault energies are low, perfect dislocations dissociate into two partials separated by a strip of stacking fault. Stacking faults are also often formed when point defects precipitate on planes.

Stiff equations - In solving time dependent problems, usually parabolic in character, the resulting systems of equations are termed stiff if the time constants governing changes in the system vary widely over the domain of the calculation, i.e. the eigen values of the equations have a large range. Such problems are frequently encountered in chemical rate theory and in creep. Implicit methods are required to provide stability to the calculations.

Stress corrosion cracking - An intergranular failure mechanism where a crack extends under a load by progressive dissolution of material at the crack tip.

Substantial solute - Foreign atoms that replace the host material on lattice positions.

Super dislocation - Dislocations with a Burgers vector that is a mulitple of a lattice vector.

Superplasticity - The property of some metals and ceramics to undergo very large plastic strains (>1000%) under tensile load. This occurs usually in the creep regime and often with two phase structures.

Texture - In a polycrystalline material if the crystals are not alligned completely randomly, the material is said to have texture.

Trial function - A function used to describe some field quantity for a body. This function has the correct symmetry and some degrees of freedom that are used to fit the function to the desired solution by a minimisation procedure.

Twin boundary - A two dimensional defect which separates two regions of crystal where there is reflection symmetry of the lattice across the boundary. By their nature twin boundaries are planar and the orientations of the crystals with respect to the boundary are fixed. Twinning occurs frequently in *hcp* and *bcc* crystals during deformation because of constraints on dislocation slip.

Vacancy - A point defect where an atom is absent from its lattice position.

Yield stress - Applied uniaxial stress required to produce significant macroscopic yield. This definition requires that some threshold plastic strain is defined for the yield stress to be determined experimentally, e.g. 0.2%.

Lecture 2 Internal Interfaces

2.1 Interfacial Energy

In this Lecture we describe processes that are largely controlled by interfacial energies. These processes are central to many engineering and metallurgical problems, but the area is generally neglected. The subject is particularly relevant to a course on thermo-mechanics, because at high temperatures diffusive processes of various types are active making possible the structural evolutions we are concerned with. A fuller description of the topic of interfacial energy and the related problem of *segregation* can be found in Hondros and Seah (1983).

There are three types of interfaces we are interested in here: surfaces that may form the boundary of a structure or the surface of a cavity; grain boundaries; and the interfaces between phases, mainly at precipitates or inclusions in an alloy. Each type of interface has an energy characterised by γ_i the interfacial energy with dimensions of energy per unit area. Alternatively γ_i is referred to as the interfacial tension and its dimension can be expressed as force per unit length. This is familiar to us in the context of soap bubbles. We will use the convention of γ_s to refer to the interfacial energy of a free surface and γ_{gb} to refer to the grain boundary interfacial energy.

At the junction of three phases the forces on the interfaces must balance and thus constrain the angles at the junction. From Fig. 2.1 for equilibrium we must have:

$$\gamma_{12}/\sin\phi_3 = \gamma_{23}/\sin\phi_1 = \gamma_{23}/\sin\phi_2 \qquad (2.1)$$

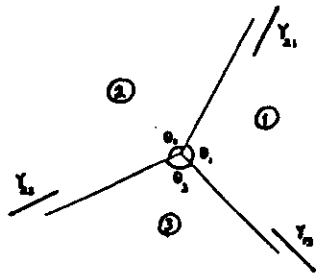

Fig.2.1

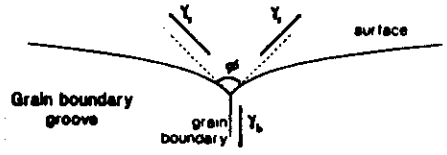

Fig.2.2

A frequently encountered case is where two of the energies are identical, e.g. where a grain boundary meets a surface making a surface groove or where a pore or precipitate sits on a grain boundary, see Fig. 2.2. In this situation equilibrium is given by

$$\gamma_{gb} = 2\gamma_s \cos(\phi/2) \tag{2.2}$$

where ϕ is referred to as the dihedral angle.

Surfaces would prefer to be flat and surface tension will pull the network of grain boundaries in a polycrystal into polyhedra. The driving force for many microstructural processes is interfacial curvature. To define the curvature of any interface in three dimensions requires two principal radii of curvature. For a sphere these radii are the same and equal to sphere radius. For a cylindrical surface one radius curvature is the cylindrical radius, the other infinite. For most surfaces the radii of curvature must be defined locally and they vary with position. Increasing the curvature of the interface increases the interfacial area and increases the interfacial energy. In terms of atomic movements the chemical potential of an atom at an interface is a function of the curvature. If we define the geometric curvature of the interface as $\kappa = 1/\rho_1 + 1/\rho_2$ where ρ_1 and ρ_2 are the principle radii of curvature the chemical potential is (Herring 1950):

$$\mu_s = \mu_o - \gamma_s \Omega \kappa . \tag{2.3}$$

This form of chemical potential will drive atoms from regions of high curvature to low curvature, leading to the equilibrium shape of inclusions, voids and bubbles as spheres, provided the interfacial energy is isotropic.

Bubbles or inclusions in equilibrium on grain boundaries are constrained by the requirement to have the correct dihedral angle and to have constant curvature. This results in a lenticular bubble made up of spherical caps, see Fig. 2.3. The radius of this bubble r_b is related to the radius of curvature and the characteristic dihedral angle by:

$$r_b = \rho_o \sin(\phi/2) . \tag{2.4}$$

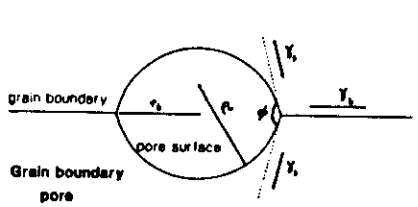

Fig.2.3

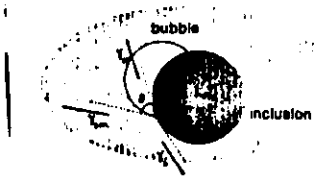

Fig.2.4

A more complex example arises when a bubble is nucleated at a precipitate, Fig. 2.4. If the precipitate is large compared with the bubble and has mass transfer rates that are slower than the matrix, then the bubble will take the form of a spherical cap at the matrix precipitate interface. The configuration is defined by the angle θ with the relationship:

$$\gamma_i = \gamma_{ip} + \gamma_{im} \cos\theta . \tag{2.5}$$

If $\gamma_{ip} + \gamma_{im} < \gamma_i$ then the bubble will enclose the precipitate as $\theta = 0°$ but if $\gamma_i + \gamma_{im} < \gamma_{ip}$ then the bubble will be distinct from the precipitate. These findings reflect the coherency of the precipitate with the matrix and could form one definition of coherency. A coherent precipitate is one where there is close atomic matching between the precipitate and the matrix, which requires near coincidence between the precipitate and matrix crystal lattices. An example of coherent precipitates are the γ' precipitates in super alloys (see section 1.3). At a coherent interface γ_i will be low. An incoherent interface has little atomic matching across the interface and hence the interfacial energy is high and may approximate $\gamma_{ip} + \gamma_{im}$. Example of incoherent precipitates are carbon (graphite) in iron, or generally oxide slag inclusions in metals.

Coherent interfaces, surface energies and grain boundaries all exhibit anisotropy to some degree. Anisotropy means that the interfacial energy will be a function of crystal orientation of the phases concerned relative to the interface. Coherency between two phases is only likely to be possible with limited ranges of orientation and this constrains coherent precipitates to parallelopipeds, sheets, needles etc characteristic of particular combinations of phases. Surfaces are mildly anisotropic in metals with high density planes having the lowest surface energy. Ionic crystals have very large

anisotropies of both grain boundary and surface energy. Small bubbles or cavities in both metals and ceramics are frequently seen to be in the form of faceted polyhedra, rather than in the form of spheres expected from curvature constraints.

An important point to note, before we move on to interfacial energy driven processes, is the importance of segregation. The driving force for segregation is frequently the change in interfacial energy on segregation. If a component segregates preferentially to an interface it will inevitably mean that the interfacial energy will be reduced. This has very large consequences on the fracture of materials where impurities or alloy components segregate to surfaces and reduce the surface energy. In other cases segregation decreases the driving force for sintering and can change the characteristic angles at interfaces.

2.2 Sintering and Hot Pressing

Sintering and *hot pressing* are the main techniques available for the fabrication of large ceramic components, a situation which is forced by the high melting points of these materials. More recently powder metallurgy has become more widely applied not only for refractory metal fabrication but also to produce alloys and composites that cannot be fabricated in other ways because of thermodynamic constraints. Sintering and hot pressing processes are also related to the behaviour of cavities that are residual to fabrication or arise from deformation. In the past the processes were treated separately but it is informative to treat them together as in most realistic situations both surface tension and external loads have an effect to some degree.

It is convenient to split sintering and hot pressing into three stages: (i) the initial stage where necks between contacting particles are formed; (ii) the intermediate stage where porosity is still interconnected but the curvature of the pores is basically concave rather than convex; and (iii) the final stage where the pores are isolated. In the consolidation of a powder aggregate all three stages must be passed through. Sintering processes may or may not result in the densification of the aggregate, depending on the controlling mechanism, but hot pressing always results in densification. The non-densifying sintering mechanisms just involve the redistribution at surfaces and comprise: surface diffusion, vapour transport and lattice diffusion with surface sources and sinks. The hot-pressing and densifying sintering mechanisms involve movement of material between the surface and the interior and comprise: grain boundary diffusion, lattice diffusion with surface sources and interior sinks, creep and plastic flow. Intermediate to these mechanisms is sintering by means of a liquid or glassy second

phase, which produces some densification but also relies on surface redistribution. This last mechanism is the one that operates in the firing of pottery, but we will restrict ourselves here to single phase processes.

Our understanding of the first stage of sintering rests on the early work of Kuczynski (1949) and Kingery and Berg (1955). Here we will use my own interpretation of the processes including macroscopic deformation (Matthews, 1979 and 1980). The first stage of sintering or hot pressing can be identified by the contact of a pair of spheres of radius and after some time a neck of radius x is established. The neck geometries for the various sintering processes are shown in Fig. 2.5. In Fig. 2.5

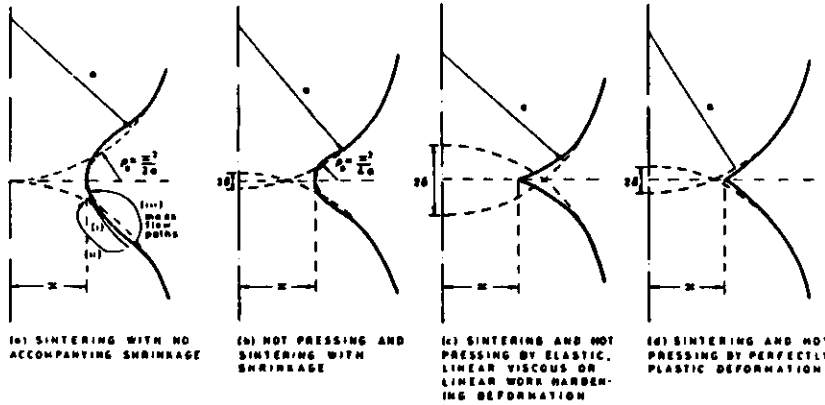

Fig.2.5

cases b, c and d involve densification and the centres of the spheres move together by a distance 2δ as the neck is formed. In cases a and b in Fig. 2.5 at the neck a radius of curvature ρ_o is established. The geometric curvature at the neck is:

$$\kappa_1 = (1/\rho_o) - (\cos\alpha)/x \quad (2.6)$$

The driving force for sintering is the difference in the curvature at the neck and away from the neck where the radii of curvature is the original sphere radius:

$$\Delta\kappa = (1/\rho_o) - (\cos\alpha)/x - 2/a \quad (2.7)$$

The angle $\alpha = (\pi - \phi)/2$ where ϕ is the dihedral angle at the interface. If the spheres were single crystal there would be a grain boundary at the interface and ϕ would be given by eq. (2.2).

For sintering with no densification the radius of curvature is given to a good approximation (Johnson 1969) by:

$$\rho = {}^1/_2 \, x^2/[a(1-\sin\alpha) - x)] \tag{2.8}$$

but for a first order approximation this may be simplified and we can replace eq. (2.7) by:

$$\Delta\kappa \equiv 2a/x^2 \, . \tag{2.9}$$

If the main process is sintering with densification, surface redistribution processes will still be important in determining the neck shape. The distance the particles move together during neck growth is given by:

$$\delta \equiv x^2/4a \tag{2.10}$$

and the next radius of curvature is $\rho_o \equiv x^2/4a$ which gives a driving force for redistribution of:

$$\Delta\kappa \equiv 4a/x^2 \, . \tag{2.11}$$

In cases where sintering is a combination of densification and no densification the driving force will lie between (2.9) and (2.11). The force normal to the interface is given by:

$$2\pi \int_o^x \sigma_n(r)\, r\,dr = 2\pi x \gamma_s \cos\alpha + F_a \equiv F_a \tag{2.12}$$

where F_a is the applied force normal to the boundary and $\sigma_n(r)$ is the local normal stress at the interface. At the neck the stress normal to the interface is:

$$\sigma_n = \gamma_s [(\cos\alpha)/x - 1/\rho_o] \equiv -\gamma_s/\rho_o \tag{2.13}$$

The distribution of stress over the interface is determined by satisfying the continuity equation for the mass flow over the boundary.

When the sintering or hot pressing is controlled purely through plastic deformation or creep the formation of a curved neck at the interface through surface diffusion may be disregarded and the geometry is that shown in Figs. 2.5 c and d. The shape of the neck is determined by the creep stress index (see section 1.3) or the work hardening index (see section 1.2). If we take n for the creep stress index or n = 1/m for work hardening the relationship between the movement of the particles towards each other and the neck size is (Matthews 1980):

$$\delta \equiv [2n/(2n+1)]^{2(n-1)} x^2/a \, . \tag{2.14}$$

For small n ($n \sim 1$) the configuration is close to Fig. 2.5c and for large n ($n \to \infty$) the configuration is close to Fig. 2.5d.

Using these relationships expressions can be developed for the growth of necks between particles for different mechanisms. These are listed in Table 2.1. Some explanation is required of how these mechanisms were derived. The surface diffusion mechanism is based on the work of Nichols and Mullins (1965) which showed that a simple circular cross section for the neck was a bad approximation. It did not predict the observation of undercutting at the neck and a continuously changing radius of curvature is required to produce surface flow. The flux of material at the surface is given by:

$$J_s(S) = -(\delta_s D_s \gamma_s/kT)\, d\kappa/ds \tag{2.15}$$

where s is the distance along the surface following the maximum gradient in curvature. The expression in Table 2.1 was derived taking this into account (Matthews 1979) and has $\dot{x} \propto a^2/x^5$ rather than $\dot{x} \propto a^3/x^6$ which was the result originally derived by Kuczynski (1949). The lattice and grain boundary diffusion expressions are those of Johnson (1969). It should be noted that if the neck radius is controlled by surface diffusion, there may still be significant densification for grain boundary diffusion. The evaporation and condensation mechanism is that of Kingery and Berg (1955) but it should be noted that if the pressure of gas in the system is high the vapour transport

Table 2.1 Mechanisms for the Initial Stage of Sintering

Surface Diffusion	$\frac{dx}{dt} = \frac{25}{6}\frac{a^2}{x^5}\frac{\delta_s D_s}{kT}\Omega\gamma_s$	$\frac{d\delta}{dt} = 0$	In most materials this is the dominant mechanism at high temperatures for small necks.
Lattice Diffusion (surface redistribution)	$\frac{dx}{dt} = \frac{25}{3}\frac{a}{x^3}\frac{D_L}{kT}\Omega\gamma_s$	$\frac{d\delta}{dt} = 0$	This mechanism is rarely seen because of the larger surface diffusion rate.
Evaporation and Condensation	$\frac{dx}{dt} = \frac{25}{12x}\left(\frac{\Omega}{kT}\right)^{3/2}\frac{P_e\gamma_s}{\sqrt{2\pi\rho_D}}$	$\frac{d\delta}{dt} = 0$	This mechanism is only seen in materials with a high vapour pressure and for larger particles.
Grain Boundary Diffusion	$\frac{dx}{dt} = \frac{32a^2}{x^5}\frac{\delta_g D_g}{kT}\Omega\left(\gamma_s + \frac{F_a}{4\pi a}\right)$	$\frac{d\delta}{dt} = \frac{x}{2a}\frac{dx}{dt}$	This is the dominant mechanism for most materials at lower temperatures with small necks.
Lattice Diffusion (internal sinks)	$\frac{dx}{dt} = \frac{8a}{x^3}\frac{D_L\Omega}{kT}\left(\gamma_s + \frac{F_a}{4\pi a}\right)$	$\frac{d\delta}{dt} = \frac{x}{2a}\frac{dx}{dt}$	This mechanism is for many materials at high temperature when the neck size is large.
Creep Deformation	$\frac{dx}{dt} = \frac{9\pi B}{8}\left[\frac{(2n+1)}{3nx}\left(\gamma_s + \frac{F_a}{2\pi x}\right)\right]^n$	$\frac{d\delta}{dt} = \varphi\frac{x}{2a}\frac{dx}{dt}$ $\varphi = \left(\frac{2n}{2n+1}\right)^{2(n-1)}$	This mechanism usually only occurs for hot pressing but can be important if diffusion and creep is significant in large particles.
Work hardening plasticity	$x = \frac{9\pi a}{8}\left[\frac{(2+m)}{3x}\left(\gamma_s + \frac{F_a}{2\pi x}\right)\right]^{1/m}$	$\delta = \left(\frac{2}{2+m}\right)^{\frac{(2-2m)}{m}}\frac{x^2}{a}$	Plasticity is the main mechanism for initial consolidation during hot pressing.
Perfect plasticity	$3\sigma_Y = \frac{\gamma_s}{x} + \frac{F_a}{\pi x^2}$	$\delta = \frac{ex^2}{a}$	
Elasticity	$\frac{8\mu x}{3\pi(1-\upsilon)a} = \frac{\gamma_s}{x} + \frac{Fa}{\pi x^2}$	$\delta = \frac{x^2}{a}$	This is the limiting case for low temperatures with no load.

rates may be controlled by gaseous diffusion rather than evaporation kinetics. The creep deformation and work hardening plasticity results are derived from my own work (Matthews 1979 and 1980). A similar expression was also proposed for linear viscous behaviour by Frenkel (1945). The neck radii have to be derived by solving the algebraic expressions provided in the plasticity and elastic cases.

The intermediate stage of sintering is reached when the necks between particles become so large that the original curvature of the particles is destroyed. Interconnected porosity surrounds the particles in a complex catenoidal configuration; an example from Tucker (1981) is shown in Fig. 2.6. This network of porosity will continue to collapse, with or without shrinkage, until tetrahedroidal pores are left at the corners. If the dihedral angle at the interface between the pores is large (i.e. $\phi \rightarrow 180°$) the network can be thought of as a series of cylindrical sections and the final residual pores as spheres. Once the porosity is no longer interconnected the final stage of sintering has been reached. At the end of the intermediate stage the concept of a neck radius becomes meaningless.

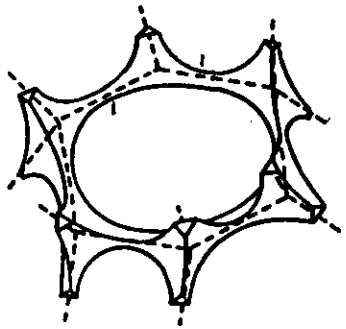

Fig. 2.6

The problem of the geometry of pores on grain boundaries during the intermediate stage of sintering is formidable. Various idealised models have been constructed based on toroidal or cylindrical tunnels and criteria have been derived for the stability of the tunnels and whether they collapse centrally or break into a series of smaller pores. The simplest way of dealing with the problem is to employ the equation for the initial stages of sintering up to a maximum value of x which is defined by the initial *packing fraction* of particles modified to take into account the shrinkage from densifying processes. It is also necessary to use a more accurate curvature of the surface of the pores. An example of the variation of curvature with densification of a close packed assembly of spheres by grain boundary diffusion is given in Fig. 2.7 (Matthews and Wood 1980). Two examples of curvature are given one for a grain boundary dihedral angle of 180^0 and one for a dihedral angle of 100^0. It is clear that the effect of the grain boundary energy on the geometry of the porosity is strong and should not be

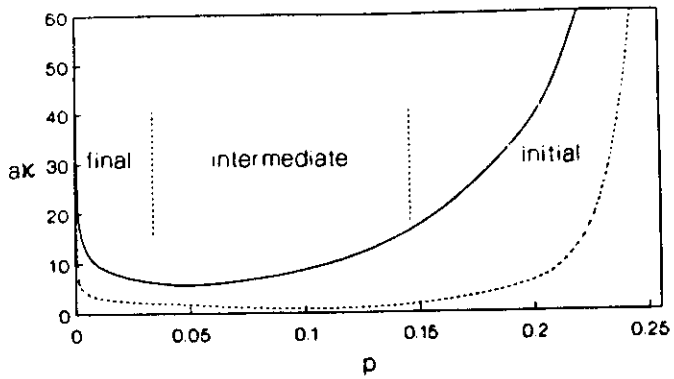

Fig.2.7

ignored. The effect is similarly important in the final stages of sintering. A tetrahedroidal cavity left at a corner where four grains meet will have a much smaller value than that of an equivalent sphere if the dihedral angle is significantly less than 180°, see Fig. 2.8. The geometry is tedious and expressions for the volume and surface areas of various grain boundary inclusion configurations can be found in Clemm and Fisher (1955) for a dihedral angle of 100° the volume of the cavity is $\sim 0.155\rho^3_o$ compared with $\sim 4.19\ \rho^3_o$ for a sphere.

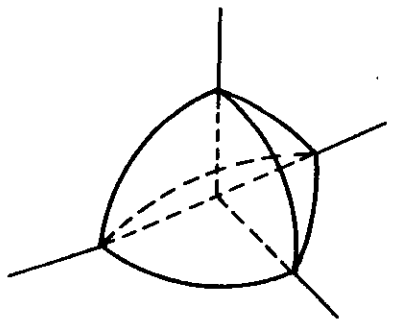

Fig. 2.8

In the final stage of sintering the surface curvature driving force, which was reduced to small values in the intermediate stage of sintering, now rises again. The main obstacle to removing all traces of porosity is the presence of gas in the pores. Gas is trapped during the transition from the intermediate to the final stage of sintering and this gas is compressed during the final stage until a balance is reached between the external load, the surface tension of the pores and the gas pressure. This effect can be removed by carrying out the sintering or hot pressing process in a vacuum, but this is expensive and for many fabrication processes the

chemistry of the material has to be controlled with either oxidising or reducing atmospheres. The residual porosity can be minimised or the levels of residual porosity controlled by influencing the operating mechanisms for sintering. A useful tool in planning sintering processes is the sintering diagram suggested by Ashby (1974), which shows the dominant sintering mechanisms at each stage of the process for various temperatures. Example diagrams are shown in Figs. 2.9 to 2.11 for UO_2 with and without an applied pressure using the data in Matthews (1979) and for iron using the data in Chuang et al (1979). High densities are achieved by avoiding sintering processes where there is no shrinkage, i.e. surface diffusion. The objective is to have as small a value of pore fraction as possible at the time of pore closure. The final porosity is given approximately by the expression:

$$p_f = (4\pi/3)(T_f\, 3\, P_c\, p_c\, a/8\pi\, T_c)^{3/2} \qquad (2.16)$$

where p_f is the final pore fraction, T_f is the final temperature, P_c, p_c and T_c are the gas pressure, pore fraction and temperature at closure. Other sintering schedules can be constructed in a similar manner

2.3 Bubbles and Cavities under Tension

In the previous section we have looked at the collapse of pores during sintering and hot pressing. No expressions were developed for the final stages of sintering because in this section we will investigate the reverse process of growth of bubbles where many of the expressions are identical. We will use the word cavity to refer generally to the range of different features that include bubbles, which generally are pressurised with gas, pores which strictly speaking are interconnected, and voids which are empty.

Cavities are in equilibrium when the forces acting on the surface are in equilibrium. This is expressed for a spherical cavity as the condition:

$$P_g - \frac{2\gamma_i}{r_c} + \sigma = 0 \qquad (2.17)$$

where P_g is the gas pressure in the bubble, r_c is the cavity radius and σ is the far field hydrostatic stress. Deviation from this condition will lead to the cavity shrinking or growing by plastic, creep or diffusional processes. In the case of faceted cavities an

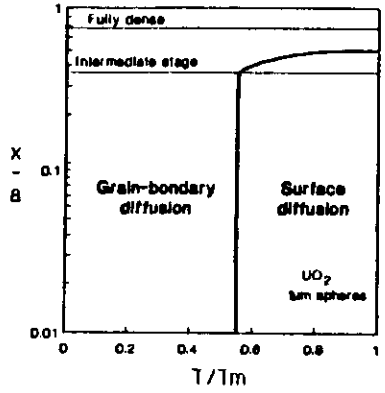

Fig. 2.9

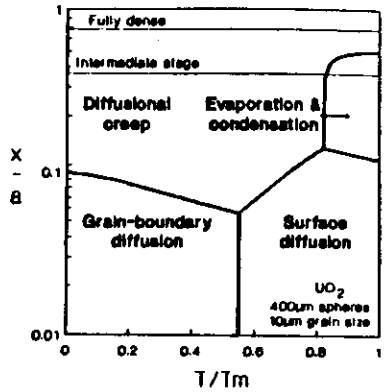

Fig.2.10

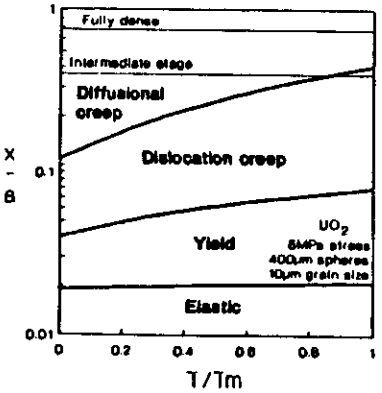

Fig.2.11

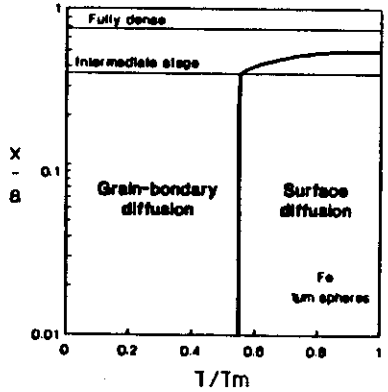

Fig.2.12

equivalent expression can be constructed in terms of a parameter related to the inverse size of the cavity.

The gas pressure P_g is related to the bubble volume and the number of gas atoms in the bubble by the equation of state of the gas. For large bubbles the gas can be described by the ideal gas law, but for small bubbles the finite size and the cohesion of the gas atoms requires a more complicated equation of state. An example of such an equation of state is the hard sphere gas law (Brearley and MacInnes 1980), but for most purposes the reduced Van der Waal's relation is adequate and it allows the behaviour of small bubbles to be simply demonstrated:

$$P_g (V_c - b_v n_c) = n_c kT \tag{2.18}$$

where V_c is the cavity volume, and b_v is the Van der Waal's constraint which is around $8 \times 10^{-29} m^3$/atom for noble gases. For equilibrium spherical bubbles the number of gas atoms in a bubble of radius r_c is:

$$n_c = \frac{(2\gamma_i / r_c - \sigma) 4\pi r_c^3}{3[kT + b_v (2\gamma_i / r_c - \sigma)]} . \tag{2.19}$$

For bubbles greater than around 50 nm this expression can be simplified to:

$$n_c = (2\gamma_i / r_c - \sigma) 4\pi r_c^3 / 3 kT . \tag{2.20}$$

Below around 2nm the justification of a continuum treatment for bubbles is difficult. The energy of the bubble will be a function of the exact configuration of lost atoms and there will be interactions between the atoms in the bubble wall and the gas atoms. There is evidence for such small bubbles in metals, below a critical temperature, for the formation of solid inclusions from inert gases (Evans and Mazey 1985). In these cases the gas atoms form a lattice that is *epitaxial* with the host lattice.

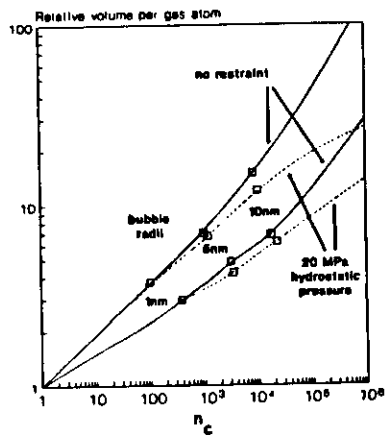

Fig.2.13

In Fig. 2.13 the effect of equilibrium bubble size on the volume occupied by each gas atom is illustrated. It is seen that the number of vacancies required to bring a bubble into equilibrium increases dramatically with bubble size. It is also seen that external loads have little effect on small bubbles but dominate the behaviour of larger bubbles.

We will now turn to the problem of the stability of cavities. Cavities without gas are inherently unstable. The equilibrium cavity size for a given bulk hydrostatic stress is simply:

$$r_c = 2\gamma_s/\sigma . \tag{2.21}$$

An increase in load will cause the cavity to grow indefinitely and a decrease in load will cause the cavity to shrink to nothing. The addition of gas stabilises the bubble size to that defined by eq. (2.19) or (2.20) and changes in load merely result in a new equilibrium being attained. However, this stability only holds for a range of loads. If the load is too large the stability is lost. We can see this for the ideal gas law by examining the differential of σ with respect to r_c for given n_c and T. There is a maximum in the stress that defines a critical bubble radius and applied stress above which the bubble will grow unstably (Hyam and Sumner, 1962). These critical values are:

$$r_{crit} = (9n_c kT/8\pi\gamma_s)^{1/2} \tag{2.22}$$

and

$$\sigma_{crit} = (8/9)(2\pi\gamma_s^3/9n_c kT)^{1/2} . \tag{2.23}$$

So far we have looked at bubbles in terms of a fixed number of gas atoms that are insoluble in the host material and have large vapour pressures, i.e. noble gases.

Bubbles are often formed from gases that have some solubility in the material, e.g. H_2 or N_2. An increase in compressive load increases the solubility of the gas but a tensile load results in further precipitation of gas into the bubble. In such cases the effect of a tensile load is magnified and the cavity growth rate increased. A related problem is where there are inclusions which generate gas in order to maintain an equilibrium pressure. Examples of this are hydride or nitride inclusions in metals which produce H_2 or N_2, carbon or carbide inclusions in oxide ceramics which produce CO and CO_2, or volatile materials which try to establish an equilibrium vapour pressure, e.g. Cs Te as fission products in nuclear fuels. Provided there are no other gases present bubbles generated by such inclusions are always unstable. There will be an equilibrium pressure P_e, which is usually a strong function of temperature. The bubble will grow indefinitely or until the inclusion is destroyed if $[P_e(T) + \sigma] > 2\gamma_s/r_i$, where r_i is the radius of the inclusion. If $[P_e(T) + \sigma] < 2\gamma_s/r_i$ the bubble will shrink down onto the inclusion.

Cavities can only change their size by movement of the host material. This can either by deformation of the material around the cavity or by the absorption or emission of point defects at the cavity surface. If the cavity is small compared to the scale of the microstructure in the material it may grow by punching out dislocation loops provided the excess pressure in the cavity is high enough (Greenwood, Foreman and Rimmer 1959)

$$P_{ex} = (P_g - 2\gamma_s/r_c + \sigma) \geq \mu b/r_c . \tag{2.24}$$

For larger bubbles the macroscopic constitutive relations can be used. Plastic flow can occur at a bubble when $P_{ex} > \sigma_Y/2$. The deformation around cavities is discussed in more detail in Lectures 4 and 5, but an important point to note is that when macroscopic deformation laws are used the cavity size only appears in the excess pressure terms and the resulting macroscopic deformations are dependent only on the shape of the cavities and their volume fraction.

The diffusive growth of cavities in most materials is controlled by the absorption and emission of vacancies at the cavity. For intragranular spherical cavities the flow of vacancies to and from the cavities is dependent on the relative chemical potentials of the vacancies at the cavities and at other sources or sinks of vacancies. Without other sources and sinks the cavities cannot grow or shrink. Other sinks may be dislocation or grain boundaries. In Lecture 1 we introduced the concept of rate equations and sink strengths. In the absence of radiation damage, we have a very

simple rate equation for vacancies (assuming we are always close to dynamic equilibrium):

$$K_c - c_v k_c^2 = 0 . \tag{2.25}$$

When cavities, dislocations and grain boundaries are all present we have (Bullough 1985):

$$k_c^2 = k_d^2 + k_c^2 + k_b^2 \tag{2.26}$$

where $k_d^2 = \rho_d$, $k_c^2 = 4\pi r_c C_c$ and $k_b^2 = (\sigma/d_b)(k_c^2 + k_d^2)^{1/2}$; the last term is a reasonable approximation if $(k_c^2 + k_d^2)^{1/2} >> d_b/6$. If the equilibrium vacancy concentration is c_v^e and a hydrostatic stress is applied the thermal vacancy concentration at the dislocation and grain boundaries is $c_v^e \exp(\sigma\Omega/kT)$. Near the cavities the equilibrium thermal vacancy concentration is $c_v^e \exp[-(P_g - 2\gamma_s/r_c)\Omega/kT$.

The rate equation for vacancies (2.25) becomes:

$$c_v^e \left\{\exp(\sigma\Omega/kT)(k_s^2 + k_b^2) + \exp[-(P_g - 2\gamma_s/r_c)\Omega/kT]k_c^2\right\} - c_v (k_d^2 + k_b^2 + k_c^2) = 0 \tag{2.27}$$

The net flow of vacancies to cavities is:

$$j_v^c = 4\pi D_v r_c C_c \{c_v - c_v^e \exp[-(P_g - 2\gamma_s/r_c)\Omega/kT]\} .$$

Substituting the value for c_v from eq. (2.27) we get

$$j_v^c = 4\pi r_c D_v c_v^e \left\{\frac{(k_d^2 + k_b^2)}{(k_d^2 + k_c^2 + k_b^2)}\left(\exp\left(\frac{\sigma\Omega}{kT}\right) - \exp\left[-\frac{(P_g - 2\gamma_s/r_c)}{kT}\Omega\right]\right)\right\}$$
$$= 4\pi \frac{r_c D_L}{kT} \beta (P_g + \sigma - 2\gamma_s/r_c)\Omega \tag{2.28}$$

which holds if $P_{ex}\,\Omega << kT$ which is true for most materials. This gives a cavity growth rate of:

$$\frac{dr_c}{dt} = \frac{j_v^c \Omega}{4\pi r_c^2} = \frac{\beta D_L P_{ex}}{r_c kT}\Omega \tag{2.29}$$

The above equation with β=1 is often quoted for the shrinkage rate in the final stages of sintering or hot pressing. It is only reasonable if the strength of other sinks is high enough and the cavities are not on the grain boundaries.

We have already seen in section 2.2 that cavities on grain boundaries have awkward geometries. This complicates the calculation of their growth on boundaries considerably. The simplest example is for an isolated cavity lying on a grain face, Fig. 2.3. The radius of the cavity on the grain boundary is related to the radius of curvature by:

$$r_c = \rho_c \sin(\phi/2) \tag{2.30}$$

and the volume of the cavity is:

$$V_c = 4\pi \alpha r_c^3/3 \tag{2.31}$$

where

$$\alpha = [1 - \cos^3(\phi/2)]/[\sin(\phi/2)(1+\cos(\phi/2)].$$

Calculating the growth rate of the cavity on the grain boundary requires a calculation of the rate of production of vacancies over the boundary in equilibrium with a redistribution of normal forces on the boundary. This was first rigorously done by Speight and Beere (1975). The distribution of vacancies on the boundary is given by:

$$\frac{D_v}{r}\frac{d}{dr}r\frac{d}{dr}c_v = \beta \tag{2.32}$$

where β is the vacancy production rate. When the process is in dynamic equilibrium β must be constant over the boundary otherwise the stress distribution on the boundary would change. Eq. (2.32) is solved a cavity radius r_c sitting in a circular region radius C representing the area of the boundary available to the cavity and 2C is approximately the cavity spacing. For r=c the dc_v/dr=0 at r=r_c the vacancy concentration is that at the cavity surface:

$$c_v(r_c) = c_v^e \exp[(\gamma_s \sin(\phi/2)/r_c - P_g)\Omega/kT]$$
$$\approx c_v^e \{1 + [\gamma_s \sin(\phi/2)r_c - P_g]\Omega/kT\} \quad (2.33)$$

On the boundary the vacancy concentration is determined by the local stress which governs the chemical potential for vacancy formation:

$$c_v(r) = c_v^e \exp[\sigma_n(r)\Omega/kT]$$
$$= c_v^e [1 + \sigma_n(r)\Omega/kT] \quad (2.34)$$

We find β by integrating $\sigma_n(r)$ over the boundary not occupied by the cavity to match with an applied tensile stress σ_a. The volume change in the cavity comes from two sources, (i) the direct increase from the absorption of vacancies into the cavity and (ii) an equal increase produced by the jacking apart of the boundary when the vacancies are formed. The final rate of cavity growth is given by:

$$\frac{dr_c}{dt} = \frac{2}{\alpha r_c^2} \frac{\delta_b D_b \Omega}{kT} \frac{[P_g - 2\gamma_s \sin(\phi/2)/r_c + \sigma_a]}{q} \quad (2.35)$$

where σ_a is the applied stress normal to the grain boundary and for the Speight and Beere model:

$$q = 4 \ln(c/r_c) - (1 - r_c^2/c^2)(3 - r_c^2/c^2)$$

where 2c is the spacing of the cavities. This model assumes no associated plastic flow around the cavity, the free production of vacancies on the boundary and rapid surface diffusion to maintain constant curvature over the cavity surface.

2.4 Swelling Under Irradiation

There are two sources of swelling during irradiation: swelling from the generation of gases from fission or from (n,α) reactions; and swelling due to supersaturations of vacancies that cause cavities to grow larger than their thermal equilibrium sizes.

Calculation of swelling from gas generation is simple provided we know the amount of gas in cavities and the density of cavities. From Fig. 2.12 we can deduce

that a large number of small cavities will have a smaller amount of swelling compared with a smaller number of large cavities with the same amount of gas. The nucleation of cavities is thus the critical factor in determining the final swelling. The cavities may be nucleated on pre-existing features such as inclusions, residual fabrication pores, the dislocation network or the grain boundaries or fission spikes or displacement cascades. Alternatively they can nucleate homogeneously by random walk encounters. This last process requires some knowledge of the stability of small gas atom clusters and simple expressions for the final concentration of cavities are not easily derived. In general it can be stated that the nucleation density is inversely related to the gas diffusion coefficient, giving higher cavity concentrations for lower temperatures.

The subject of fission gas swelling is in nuclear fuels is complex, involving fission fragment effects. There is no space to give adequate attention to the subject here. Matthews and Wood (1984) and Matthews and Small (1988) deal with the subject for oxide fuels, including current issues that are yet to be adequately resolved.

Nucleation of cavities is also central to the problem of swelling in materials subjected to fast neutron irradiation damage. We have already seen in section 1.6 that dislocations have a preference for the interstitial produced by atomic displacements. The sink strengths of cavities are relatively insensitive to the type of point defect they absorb and are thus often classed as neutral sinks. Taking the simple model for radiation damage with just cavities and dislocations we find the cavity growth rate is:

$$\frac{dr_c}{dt} \cong \frac{C_c}{r_c}\left[\frac{\Delta F(\eta) K \rho d}{(4\pi r_c C_c + \rho_d)^2} + \frac{K_s}{(4\pi r_c C_c + \rho_d)} - D_L \exp\left[-\frac{(P_s - 2\gamma_s/r_c)}{kT}\right]\right]. \quad (2.36)$$

The first part of the expression gives the rate of growth of the cavities from the Frenkel pair production rate K and the dislocation bias Δ. The second and third terms describe the thermal emission terms which will shrink the cavity in the absence of the displacement damage. When the sink strength of the dislocations is large compared to that of the cavities we see that the swelling rate is proportional to the cavity concentration. For low dislocation densities, which is the case at high temperature, the selling rate is larger with small cavity densities. Homogeneous nucleation is inhibited at higher temperatures and the nucleation of cavities on precipitates with a relatively low density can lead to a second peak in swelling in some stainless steels.

We have seen that the density of cavities affects the swelling rate during radiation damage but there is also an important incubation effect on the nucleation of cavities. Before a cavity can grow by absorbing vacancies from the supersaturation it has to reach a critical size, which is sensitive to temperature, the dislocation bias and the recombination rate. Below this size thermal emission of vacancies will remove any fluctuations. If the critical size is small enough cavities may be nucleated on vacancy clusters in cascades. The presence of gas will stabilise the cavity nucleus and also reduce the critical size. If the critical size is large, which is the case at high temperature and for materials with strong impurity trapping of point defects, then cavity nucleation is only possible on coarse precipitates, particularly if they are incoherent and have gas associated with them.

2.5 Microstructural Evolution

Holding a material at high temperature for long periods inevitably will result in microstructural changes. We have already met recovery and recrystallisation in Lecture 1, but cavities, precipitates and grain boundaries also undergo many changes, controlled by diffusive processes.

One of the most important processes driven by interfacial energy is Ostwald ripening, i.e. the coarsening of precipitate structures by thermal ageing. The smaller precipitates shrink and the larger precipitates grow. This is because the interfacial energy per unit area of interface is higher for the smaller precipitates and this increases locally the solubility of the components. Simple expressions for this process can be constructed using a single mean size parameter (Lifshitz and Slyozov 1961). For spherical precipitates where r_p represents the mean precipitate radius the coarsening rate is given by:

$$\frac{dr_p}{dt} = \frac{\alpha}{r_p^2} D_a c_a C_p \frac{\gamma_p \Omega}{kT} \qquad (2.37)$$

where α is a constant generally found to be around $1/3$, D_a is the diffusivity of the limiting component a of the precipitate, c_a is the thermal equilibrium concentration of a, C_p is the volume fraction of precipitates and γ_p is the interfacial energy at the precipitate. Ostwald ripening may also take place for cavities, in which case:

$$\frac{dr_c}{dt} = \frac{4\pi r_c}{3} C_c D_L \frac{\gamma_c \Omega}{kT} . \qquad (2.38)$$

Coarsening of this type can take place even during sintering if the strength of sinks for vacancies is small compared with that of the cavities. Such effects are seen during the annealing of fast neutron induced swelling of steels (Watkins, 1984).

Similar expressions can be derived for the coarsening of precipitates of other shapes and for those laying on grain boundaries. Such coarsening is important in determining thresholds for recrystallisation and in the nucleation of cavities during creep.

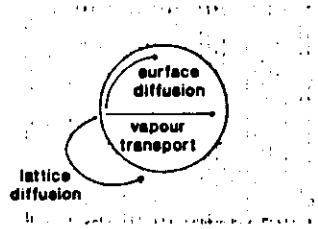

Fig.2.14

Cavities and precipitates are also mobile to some extent, by lattice diffusion, interfacial diffusion and in the case of cavities vapour transport. (See Fig. 2.14). The topic of cavity migration has been reviewed recently by Perryman and Goodhew (1988). The basic bubble diffusivity from each of the basic mechanisms is:

Lattice Diffusion

$$D_C = 3D_L\Omega/4\pi r_c^3 \qquad (2.39)$$

Vapour Transport

$$D_C = 3\Omega_\beta^3 P_{vap} D_g /4\pi kT r_c^3 \qquad (2.40)$$

where β is a measure of the departure from ideality of the gas in the cavity, D_g is the diffusivity of the vapour in the gas and P_{vap} is the vapour pressure of the host material.

Surface Diffusion

$$D_c = 3\delta_s D_s \Omega W(n_c)/2\pi r_c^4 \qquad (2.41)$$

and where $W(n_c)$ is a factor giving the effect of gas in the cavity. These basic mechanisms show that small cavities are more mobile than large ones, but there are other factors which diminish the mobility of very small cavities. Firstly small cavities tend to be faceted and this can inhibit all three mechanisms for bubble mobility, as the *adatoms* responsible for surface diffusion, the vacancies for lattice diffusion and the vapour are most easily produced at defects in the perfection of the surface. In this case the diffusion rate is limited by the nucleation rate of ledges on the facets giving a bubble diffusion rate of:

$$D_b' = (D_b/a)\, L \exp(-\pi E_L L/2kT) \tag{2.42}$$

where L is the length of the facet ($\sim r_c$) and E_L is the energy to form the ledge. This term reduces the mobility of very small bubbles by surface diffusion. Larger cavities are not generally affected, as they are not faceted and have more disorder surfaces. The effect also disappears at high temperatures when the anisotropy of surface energy is reduced. Lattice diffusion can also be reduced in very small faceted cavities. This is because certain configurations of small bubbles have lower energies and this raises the energy to emit or absorb vacancies at the cavity.

The pressure of gas in a cavity will inhibit both surface diffusion and vapour transport, because of direct interaction between gas atoms adatoms or vapour. The term $W(n_c)$ in eq. (2.41) comes from a model by Mikhlin (1979) which was improved by Nixon and MacInnes (1981):

$$W(n_c) = \exp\left[-\frac{3n_c q}{4\pi r_c^3}\left(\frac{1+2y}{(1-y^2)}\,\frac{2y^2}{(1-y)^3}\right)\right] \tag{2.43}$$

where q is the volume when the adatoms are excluded by the gas and y is the reduced density, i.e. n_c times the molecular volume of the gas divided by the cavity volume. This gives a strong inhibition to surface diffusion in bubbles less than 20 nm in radius. The gas diffusivity in eq. (2.40) is inversely proportional to the gas pressure and dependent on the relative molecular weights of the vapour and gas species..

The cavity mobility allows small cavities to migrate by Brownian motion but larger cavities may move under the influence of an applied force. The cavity velocity in these cases is given by the Einstein equation:

$$V_c = D_b F_c/kT \tag{2.44}$$

where V_c is the velocity of the cavity and F_c is the force. The force may be directly from a grain boundary or it could be generated by a gradient in stress or temperature. Precipitate can migrate in a similar manner to cavities, either by lattice diffusion if the components are to some extent soluble in the host lattice or by interfacial diffusion. Eqs. (2.39) and (2.41) apply replacing D_L by $D_a c_a$ (analogous to eq. (1.37) and $\delta_s D_s$ by $\delta_i D_i$.

The final topic on microstructural evolution to be dealt with is grain growth. By this I mean *normal* grain growth rather than the development of new grain structures that occur *during* recrystallisation. Normal grain growth is a continual process of the elimination of the smaller grains in a distribution and the growth of larger ones. The process is driven by the grain boundary energy. The driving force is proportional to γ_b/r_b. If the mobility of the boundary is independent of the grain size then the grain growth rate is given by (Burke and Turnbull 1952)

$$\dot{r}_b = K_b/r_c \tag{2.45}$$

and

$$r_b^2 - r_{b0}^2 = 2K_b t \tag{2.46}$$

where K_b is a temperature dependent coefficient and r_b is the initial grain size. In pure materials K_b is controlled by the rate of diffusion of material across the grain boundary (e.g. see Atkinson 1988) but for real materials containing cavities and precipitate the boundary mobility will be controlled by these obstacles. In many cases the grain growth rate will be controlled by the mobility of the cavities or precipitates. This can lead to other types of dependency of the grain growth rate on the grain size, as particles accumulate on the boundaries. As the driving force for grain growth diminishes with increasing grain size the particles may eventually stop grain growth if the mobility is low. For small grains with low particle fraction it may be possible for the boundaries to by-pass precipitates by bowing round them in a manner analogous to dislocation interactions with precipitates.

2.6 Pores and Properties

The presence of cavities and precipitates have strong effects on properties which cannot be ignored, particularly when the microstructure is changing during deformation, irradiation or even during ageing at high temperature. The effect on thermal conductivity is an important example. A general approach to this problem has been developed by Shultz (1981) and others. This enables the thermal conductivity of composites of any shape and property to be estimated, including anisotropic effects. The basic relation is:

$$(1 - f_b) = \left(\frac{k_a}{k_{ab}}\right)^m \frac{(k_b + k_{ab})}{(k_b - k_a)} \left(\frac{k_{ab} - n\,k_b}{k_a - n\,k_b}\right)^q \qquad (2.47)$$

where k_a is the host material conductivity, k_b is the conductivity of the inclusion, k_{ab} is the composite conductivity, f_b is the volume fraction of inclusions and

$$m = \frac{F(1-2F)}{1-(1-F)\cos^2\alpha - 2F(1-\cos^2\alpha)}$$

$$n = \frac{1-(1-f)\cos^2\alpha - 2F(1-\cos^2\alpha)}{2F(1-\cos^2\alpha) + (1-F)\cos^2\alpha}$$

$$q = m + \frac{(1-F)2F}{2F(1-\cos^2\alpha) + (1-F)\cos^2\alpha} - 1 .$$

The parameter F gives the effect of the shape of the inclusions, see Fig. 2.15. The

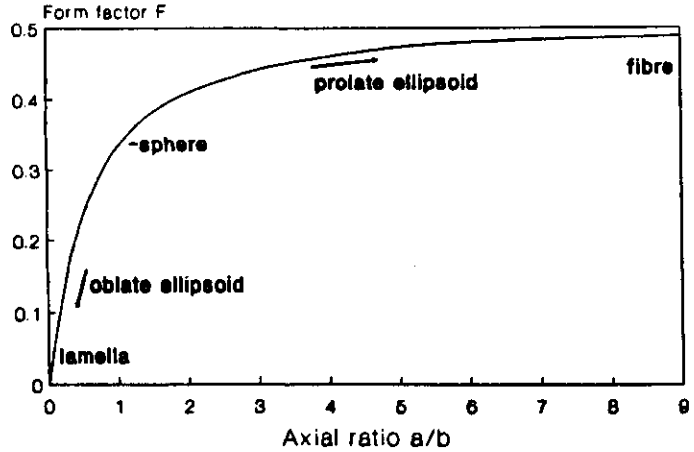

Fig.2.15

inclusions are modelled as ellipsoids with axial ration of a/b. For long fibres F tends to 0.5, for flat sheets F tends to zero and for spheres F tends to 1/3. The angle α gives a measure of the anisotropy induced by preferred orientation of the inclusions. For random orientation a value of $\cos^2\alpha = 1/3$ is used.

An important example of the use of eq. (2.47) is the effect of cavities on thermal conductivity. For small cavity fractions the cavity conductivity can be taken as zero. This gives the conductivity of the porous material as:

$$k_{ca} = k_a (1 - p_c)^X \qquad (2.48)$$

$$\text{where } X = \frac{1-\cos^2\alpha}{1-F} + \frac{\cos^2\alpha}{2F} .$$

For spherical pores this reduces to

$$k_{ca} = k_a (1 - p_c)^{1.5}. \qquad (2.49)$$

During sintering the porosity undergoes a wide range of shape changes and during the initial stages X will have a larger value. In such cases it is necessary to take into account the conductivity of the gas in the pores and at high temperatures the effect of thermal radiative heat transfer.

The effect of inclusions and cavities on other linear properties can be derived in a similar way. Thermal expansion is relatively unaffected by cavities unless there is a strong texture in non-spherical porosity. Elastic modulii are reduced by the presence of cavities and often the measured effect is stronger than expected by a $(1-p_c)^{1.5}$ type of correction term. Generally the bulk modulus is affected more strongly than the shear modulus which gives a Poisson's ratio that reduces as the cavity concentration increases (Christensen 1979).

Other mechanical properties are affected but the treatment of second phases on the plastic behaviour is both important and difficult. Gurson (1977) has provided a framework for calculating the effect of inclusions and pores or the yield stress and this can be generalised to work hardening and viscous behaviour e.g. for cavities see Tvergaard (1981 and 1982). The yield condition for single phase material, that the yield stress σ_y equals the Von Mises stress σ_e, is replaced in a material with cavities by:

$$\frac{\sigma_e^2}{\sigma_y^2} + 3p_c \cosh\left(\frac{3\sigma}{2\sigma_y}\right) - 1 - \frac{4}{9}p_c^2 = 0 \quad . \tag{2.50}$$

The effect of the cavity fraction on yield condition is shown in Fig. 2.16. For finite values of cavity fraction yield can occur in purely hydrostatic stress conditions. This yield criterion can be used to generate creep and work hardening plastic flow rules.

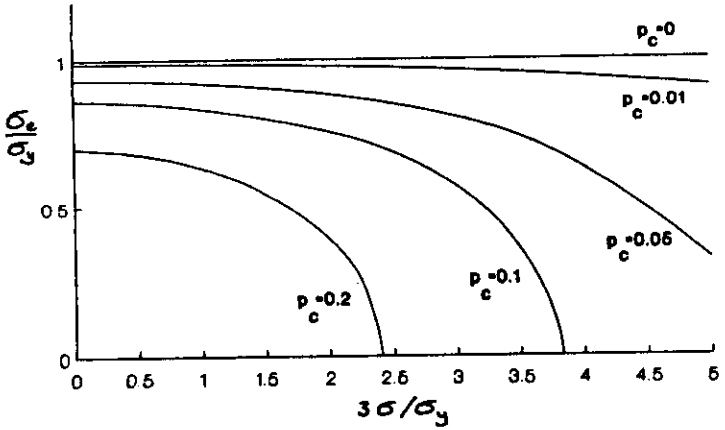

Fig.2.16

2.7 Cracks

We will be discussing the growth of cracks in section 5.2 as part of the Lecture on Failure of Structures. This section is included for those who have not encountered LEFM (Linear Elastic Fracture Mechanics) previously.

Our understanding of cracking as an interfacial process was stated clearly by Griffith (1920) in an attempt to understand the brittleness of glass. In this section we will follow Griffith and disregard the possibility of local plastic deformation.

Consider an elliptical hole passing though a plate, which is thin enough to allow us to assume *plane stress*. The dimensions of the hole are assumed to be small

compared to the width of the plate; the configuration is shown schematically in Fig 2.17.

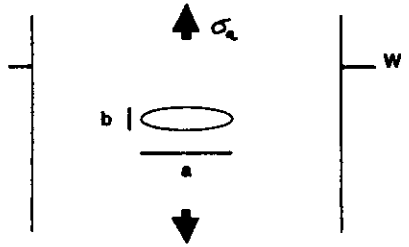

Fig.2.17

If a uniaxial stress σ_a is applied to the plate normal to the long axis of the hole, the reduction elastic strain energy per unit thickness of the plate from the presence of the hole is (Timoshenko and Goodier 1951):

$$V_e = \pi a^2 \sigma_a^2 / E \quad . \tag{2.51}$$

If we increase the length of the crack infinitesimally by δa the elastic energy changes by:

$$\delta V_e = 2\pi a \sigma_a^2 \, \delta a / E \quad . \tag{2.52}$$

Now when the crack increases in size its surface area increases and hence the surface energy. For a thin crack this increase is given by:

$$\delta V_s = 2 \gamma_s \, \delta a \quad . \tag{2.53}$$

Griffith established his crack growth criterion by proposing that if the elastic strain energy released by the extension of the crack is greater than the increase in surface energy then the crack will grow spontaneously i.e. when $\delta V_e > \delta V_s$. The critical stress for crack growth σ_f is given from (2.52) and (2.53) as:

$$\sigma_f = (2E\gamma_s / \pi a)^{1/2} \quad . \tag{2.54}$$

Similar expressions can be obtained for other configurations:

plane strain (thick Plate)	$\sigma_f = [2E\gamma_s / \pi a(1-\nu^2)]^{1/2}$
circular crack in an infinite body	$\sigma_f = [\pi E\gamma_s / 2a(1-\nu^2)]^{1/2}$.

The Griffith criterion is found to apply to very brittle materials and can be used directly to calculate the strength of defected structures built from glass or ionic crystals at reasonably low temperatures. At higher temperatures and for most other materials even if their failure is brittle in nature the failure stress under tension is higher than that given by the Griffith criterion. Despite this the failure stress is commonly found to be proportional to $1/a^{1/2}$. This led Irwin (1948) to propose an effective surface energy γ_f to replace γ_s in the fracture criterion. This effective energy was to account for other processes that increased the work of fracture such as plasticity, but we will return to this in section 5.2.

So far the shape of the crack has not explicity entered into the discussion. As we have seen, the introduction of any cavity into a stressed body will locally raise the stress near the cavity. If we return to our problem of an elliptical hole in a plate subjected to a uniaxial load as the aspect ratio of the ellipse increases the local stress as the hole increases.

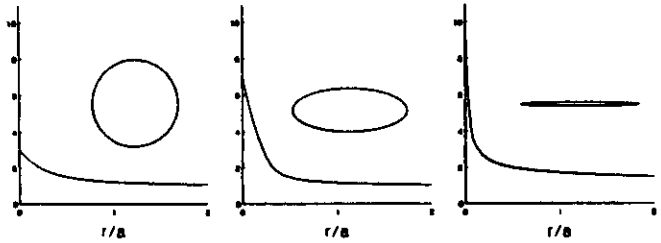

Fig.2.18

Fig 2.18 shows plots of the stress component in the direction of the load as a function of distance from the hole for three aspect ratios: (a) 1:1 a circular hole; (b) 3:1 an elliptical hole; and (c) ∞ :1 a flat crack. The tensile stress at the hole may be expressed as (Kelly and MacMillan 1986):

$$\sigma_{max} = \sigma_a (1 + 2a/b) = \sigma_a[1 + 2(a/\rho_c)^{1/2}]. \qquad (2.55)$$

where b is the thickness of the hole and ρ_c is the local radius of curvature at the crack top. It is clear from (2.55) that the stress concentration becomes singular for the flat crack. This result was used by Orowan (1949) to provide an ingenious second derivation of the Griffith criterion. For very sharp cracks there is a limit to the radius of

curvature at the crack tip which cannot become much smaller than the atomic spacing. Hence,

$$\sigma_{max} \cong 2\sigma_a (a/a_o)^{1/2} . \qquad (2.56)$$

At the crack tip failure will occur when the material reaches its theoretical strength of the material. Orowan used an atomic cohesion argument to estimate the magnitude of theoretical strength:

$$\sigma_{th} \cong (E\gamma_s/a_o)^{1/2} . \qquad (2.57)$$

Equating σ_{max} and σ_{th} we may obtain an expression for the size of the applied stress to produce failure:

$$\sigma_{fA} \cong (E\gamma_s/4a)^{1/2} \qquad (2.58)$$

which is very close to the Griffith expression.

In practical terms the processes at the crack tip are not very important. Most fracture mechanics calculations are made using the stress intensity factor K. Close to the crack tip the stress field in the surrounding material is defined as:

$$\sigma_{ij} = \frac{K}{(2\pi r)^{1/2}} f_{ij}(\theta) \qquad (2.59)$$

Fig.2.19

where r and θ are the polar co-ordinates relative to the crack tip (see Fig 2.19). The singularity at the crack tip is of type $r^{-1/2}$ and K determines its magnitude. The type of loading we have been discussing so far is classed as type I and with the stress intensity factor K_I.

Cracks may also propagate with shear loading; K_{II} is for shear loads normal to the crack and K_{III} for shear loads parallel to the crack. The normal stress component in the direction of the load for mode I is:

$$\sigma_{yy} = \frac{K_I}{(2\pi r)^{1/2}} \cos(\theta/2)\,[1 - \sin(\theta/2)\sin(3\theta/2)] \quad (2.60)$$

The other stress components for mode I and the other two modes are given by Thomson (1983). The value of K is to some extent a function of the configuration of the structure but in the limit of a small crack $K = \sigma_\infty(\pi a)^{1/2}$ where σ_∞ is the stress far away from the crack and is the appropriate one for the crack loading modes, i.e. $\sigma_\infty = (\sigma_{yy})_\infty$ for mode I, $(\sigma_{yz})_\infty$ for mode II and $(\sigma_{yz})_\infty$ for mode III. For other configurations K is multiplied by a factor m (Lawn and Wilshaw 1975, Rice 1968). For an edge crack of depth a in a semi-infinite body m=1.12 and for penny shaped crack radius a in an infinite body $m = 2/\pi$. For a cracks in a plate of finite width W, m is a function of the ratio of the crack size to the specimen size:

$$m = [(W/\pi a)\tan(\pi a/W)]^{1/2} . \quad (2.61)$$

The Griffith criterion can be re-expressed in terms of the stress intensity factor, which is convenient for application in elastic structural analysis. The crack propagation criterion is given by the critical values of the stress intensity factors. For the three loading modes they are for isolated cracks in an infinite body:

$$K_{Ic}^2 = K_{IIc}^2 = 2\gamma_f E/(1-\nu^2);\ K_{IIIc}^2 = 2\gamma_f E/(1+\nu) . \quad (2.62)$$

Lecture 3 Thermo-elasticity

3.1 Stresses and Strains

To prepare for our discussion of thermo-elastic and inelastic problem solving we w riefly review the main features of stresses and strains. We will use the simplified tensor notation throughout (covariant and contravariant tensors will not be distinguished). The usual conventions will be used of repeated indices implying summation, i.e. $\sigma_{ii} = \sigma_{11} + \sigma_{22} + \sigma_{33}$, and differentiation with respect to spatial dimensions by a comma, i.e. $\sigma_{ij,k} = \partial\sigma_{ij}/\partial x_k$. A fuller discussion of background of stress and strain can be found in Landau and Lifschitz (1959).

Stress is an intensive quantity that describes how forces are propagated through a body. The most important property in formulating our problem is equilibrium. In rectangular co-ordinates this is expressed as:

$$\text{div}\,\sigma = \sigma_{ij,j} = F_i$$

and

$$\sigma_{ij} = \sigma_{ji} \tag{3.1}$$

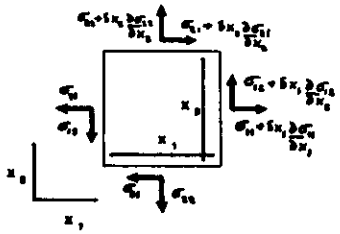

Fig. 3.1

where F_i represents body forces, gravitation being the most usually encountered one. The equilibrium relations can be simply derived by balancing the forces on a body element and taking the infinitesimal limit. As an example in two dimensions we have from Fig. 3.1 the first order terms:

in the x_1 direction

$$\left[\sigma_{11} + \frac{\partial\sigma_{11}}{\partial x_1}\delta x_1\right]\delta x_2 + \left[\sigma_{12} + \frac{\partial\sigma_{12}}{\partial x_2}\delta x_2\right]\delta x_1 = \sigma_{11}\delta x_2 + \sigma_{12}\delta x_1 + F_1\,\delta x_1\,\delta x_2$$

in the x_2 direction

$$\left[\sigma_{22} + \frac{\partial \sigma_{22}}{\partial x_2}\,\delta x_2\right]\delta x_1 + \left[\sigma_{21} + \frac{\partial \sigma_{21}}{\partial x_1}\,\delta x_1\right]\delta x_2 = \sigma_{22}\,\delta x_1 + \sigma_{21}\,\delta x_2 + F_2\,\delta x_1\,\delta x_2$$

and the rotational couple

$$1/2\,\sigma_{12}\,\delta x_1\,\delta x_2 = 1/2\,\sigma_{21}\,\delta x_2\,\delta x_1 \,. \tag{3.2}$$

This gives the equilibrium equations on taking δx_1, and $\delta x_2 \to 0$.

$$\frac{\partial \sigma_{11}}{\partial x_1} + \frac{\partial \sigma_{12}}{\partial x_2} = F_1$$
$$\frac{\partial \sigma_{22}}{\partial x_2} + \frac{\partial \sigma_{12}}{\partial x_2} = F_2$$

and

$$\sigma_{12} = \sigma_{21}. \tag{3.3}$$

Strain is an extensive quantity that measures the deformation of the body. It is related to the displacement of points within the body, in rectangular co-ordinates, by the compatibility relation:

$$\varepsilon_{ij} = 1/2\,(u_{i,j} + u_{j,i} + u_{k,i}\,u_{k,j})\,. \tag{3.4}$$

For elastic calculations the gradients of displacement and hence the strains are small so the first order approximation of (3.4) is used:

$$\varepsilon_{ij} = 1/2\,(u_{i,j} + u_{j,i})\,. \tag{3.5}$$

Beware of the engineering convention of missing out the 1/2 in the definition of shear strains $i \neq j$, e.g. in Timoshenko (1934). In all our applications eq. (3.5) will be used and any large deformations will be handled by changing the co-ordinate system as it deforms. The continuity relation (volume conservation) is expressed by the volume strain ε:

$$\varepsilon = \varepsilon_{ii}. \tag{3.6}$$

The definition of strain also implies:

$$\varepsilon_{ij} = \varepsilon_{ji}. \tag{3.7}$$

The most common types of problem we encounter are problems which are best described in cylindrical co-ordinates and spherically symmetric problems. The equilibrium equation for the cylindrical co-ordinates r, θ and z are:

$$\begin{aligned}
&\frac{\partial \sigma_{rr}}{\partial r} + \frac{1}{r}\frac{\partial \sigma_{r\theta}}{\partial \theta} + \frac{\partial \sigma_{rz}}{\partial z} + \frac{\sigma_{rr} - \sigma_{\theta\theta}}{r} = -F_r \\
&\frac{\partial \sigma_{rz}}{\partial r} + \frac{1}{r}\frac{\partial \sigma_{\theta z}}{\partial \theta} + \frac{\partial \sigma_{zz}}{\partial z} + \frac{\sigma_{rz}}{r} = -F_z \\
&\frac{\partial \sigma_{r\theta}}{\partial r} + \frac{1}{r}\frac{\partial \sigma_{\theta\theta}}{\partial \theta} + \frac{\partial \sigma_{\theta z}}{\partial z} + \frac{2\sigma_{r\theta}}{r} = -F_\theta
\end{aligned} \tag{3.8}$$

The corresponding strain-displacement relationships are:

$$\begin{aligned}
&\varepsilon_{rr} = \frac{\partial u_r}{\partial r},\ \varepsilon_{\theta\theta} = \frac{1}{r}\frac{\partial u_\theta}{\partial \theta} + \frac{u_r}{r},\ \varepsilon_{zz} = \frac{\partial u_z}{\partial z} \\
&\varepsilon_{\theta z} = \frac{1}{2}\left(\frac{1}{r}\frac{\partial u_z}{\partial \theta} + \frac{\partial u_\theta}{\partial z}\right),\ \varepsilon_{rz} = \frac{1}{2}\left(\frac{\partial u_r}{\partial z} + \frac{\partial u_z}{\partial r}\right) \\
&\text{and } \varepsilon_{r\theta} = \frac{1}{2}\left(\frac{\partial u_\theta}{\partial r} - \frac{u_\theta}{r} + \frac{1}{r}\frac{\partial u_r}{\partial \theta}\right).
\end{aligned} \tag{3.9}$$

The expressions for spherically symmetric problems in spherical co-ordinates are much simpler. The equilibrium equation is:

$$\frac{d\sigma_{rr}}{dr} + \frac{2(\sigma_{rr} - \sigma_{\theta\theta})}{r} = F_r \tag{3.10}$$

and the strain-displacement relations are

$$\varepsilon_{rr} = \frac{\partial u_r}{\partial r}\,;\ \varepsilon_{\theta\theta} = \frac{u_\theta}{r}\,. \tag{3.11}$$

3.2 Solving Elastic Problems

There is only space in this course to consider isotropic elasticity, which is a good approximation for most polycrystalline materials. The elastic behaviour of isotropic materials is described in terms of two elastic constants out of a set of four that are commonly used.

For uniaxial loading of an applied stress $\sigma_a = \sigma_{11}$:

$$\sigma_{11} = Ee_{11} = -Ee_{22}/\nu = -\nu Ee_{33}/\nu \tag{3.12}$$

where E is the Young's modulus and ν is Poisson's ratio. We will use e_{ij} to define thermo-elastic strains and from now on reserve ε_{ij} for total strains including inelastic effects. For a hydrostatic loading where $\sigma_{11} = \sigma_{22} = \sigma_{33} = \sigma$:

$$\sigma = Ke = Ke_{ii}\ , \tag{3.13}$$

where K is the bulk modulus. Finally if a simple shear stress is applied $\tau_a = \sigma_{12}$:

$$\sigma_{12} = 2\mu e_{12}\ , \tag{3.14}$$

where μ is the shear modulus.

The four elastic moduli are related by:

$$\mu = \frac{E}{2(1+\nu)}\ ,\ K = \frac{E}{3(1-2\nu)}$$
$$\text{and } \nu = \frac{(3K-2\mu)}{2(3K+\mu)}. \tag{3.15}$$

Many of the problems we will deal with include the effects of isotropic thermal expansion. The thermal strain for each strain component is given by:

$$e_{11}^{th} = e_{22}^{th} = e_{22}^{th} = \alpha(T-T_o) \tag{3.16}$$

where α is the thermal expansion coefficient and T_o is some reference temperature. The volume conservation condition is given by:

$$e = \sigma/K + 3\alpha(T-T_o)\ . \tag{3.17}$$

The isotropic thermo-elastic constitutive relations can be concisely expressed as:

$$\sigma_{ij}/2\mu = e_{ij} + \delta_{ij}[\nu e_{kk} - \alpha(1+\nu)(T-T_o)]/(1-2\nu) \tag{3.18}$$

or

$$e_{ij} = \sigma_{ij}/2\mu - \delta_{ij}[\nu\sigma_{kk}/2(1+\nu)\mu - \alpha(T-T_o)]\ . \tag{3.19}$$

The elastic field may be described entirely in terms of the displacements by combining the constitutive relation (3.18) with the equilibrium and compatibility equations (3.1) and (3.5) to get for rectangular coordinates:

$$u_{i,kk} + \frac{1}{(1-\nu)}u_{i,ij} = \frac{Fi}{\mu} + 2\alpha\frac{(1+\nu)}{(1-2\nu)}T_{,i} \tag{3.20}$$

or more generally:

$$\nabla^2\mathbf{u} + \frac{1}{(1+2\nu)}\,\mathbf{grad}\ \mathrm{div}\ \mathbf{u} = \frac{\mathbf{F}}{\mu} + \frac{2\alpha(1+\upsilon)}{(1-2\nu)}\,\mathbf{grad}\ T \tag{3.21}$$

where $\nabla^2$is the appropriate Laplacian operator for the co-ordinate system. These expressions assume that the elastic properties are constant over the body to which they are applied. The field equations for material with properties that vary over the body can be easily derived but are significantly more complicated to implement.

The system of equations are elliptic in form and require the boundary conditions to be defined for each displacement component (Dirichlet conditions); alternatively stresses or some linear combination of the gradients of the displacements may be defined. Another way of describing the elastic field is to define a scalar potential or stress function, χ that uniquely defines the fields. This may be found for each co-ordinate system to give a biharmonic equation (Landau and Lifschitz 1959):

$$\nabla^2\nabla^2\chi = 0\ . \tag{3.22}$$

For rectangular co-ordinates we have:

$$\sigma_{ij} = \chi_{,ij} \ , \ i = j$$
$$\sigma_{ij} = -\chi_{,ij} \ , \ i \neq j \qquad (3.23)$$

The stress function was one of the main vehicles for solving elastic problems before the development of computers and the economic application of numerical methods.

Problems can frequently be approximated by two dimensional treatments. These are of two classes: plain strain approximation for long structures where end effects are not important; and plain approximations for thin plates where deformation out of the plane of the plate is important. In plain strain the strain components in the direction normal to the section of the body are made zero. This approximation is appropriate for an infinitely long structure but a better approximation is generalised plane strain where finite deformations in that direction are allowed but they are made constant over the section, i.e. $e_{33} = w$. The thermo-elastic constitutive relation is given by:

$$\sigma_{ij}/2\mu = e_{ij} + \delta_{ij}\,[\nu(e_{kk} + w) - \alpha(1+\nu)(T - T_0)]/(1-2\nu), \qquad (3.24)$$

but i and j can be 1 to 2, rather than 1, 2 and 3. The displacement field equation (3.20) applies, but just for some components. The stress components normal to the section are given by:

$$\sigma_{33} = \nu(\sigma_{11} + \sigma_{22}) - 2\mu(1+\nu)[\alpha(T - T_0) - w]$$

and

$$\sigma_{23} = \sigma_{13} = 0. \qquad (3.25)$$

The normal strain is found by imposing:

$$\int_s \sigma_{33}\, dS = F_{ax}, \qquad (3.26)$$

where F_{ax} is the total force applied to the section.

In the plane stress approximation the section is assumed to be thin enough for the stress components normal to the section to be ignored, $\sigma_{33} = \sigma_{31} = \sigma_{32} = 0$. The strain normal to the section is given by:

$$e_{33} = [\alpha(1+\nu)(T - T_0) - \nu(e_{11} + e_{22})]/(1-\nu). \qquad (3.2$$

This makes the constitutive relation:

$$u_{ij}/2\mu = e_{ij} + \delta_{ij}\,[\nu e_{kk} - \alpha(1+\nu)(T - T_0)]/(1-\nu), \qquad (3.28)$$

and the displacement field equation is:

$$u_{i,kk} + \frac{(1+\nu)}{(1-\nu)} u_{i,ij} = \frac{Fi}{\mu} + 2\alpha\frac{(1+\nu)}{(1-\nu)}\alpha T, \qquad (3.29)$$

where i and j can be 1 or 2.

Similar approximations can be made for problems in cylindrical co-ordinates corresponding to long rods and tubes or thin discs. We will look at the axisymmetric plane strain formulation as an example. The displacement equation is:

$$\frac{d}{dr}\frac{1}{r}\frac{d}{dr} r u_r = \frac{(1-2\nu)}{(1-\nu)}\frac{F_r}{2\mu} + \alpha\frac{(1+\nu)}{(1-\nu)}\frac{dT}{dr}. \qquad (3.30)$$

This can be directly integrated if F_r and T are explicit functions of r to give:

$$u_r = \frac{C_1}{r} + C_2 r + \frac{(1-2\nu)}{(1-\nu)}\frac{1}{2\mu r}\int r\int F_r\, dr'\, dr + \frac{\alpha}{r}\frac{(1+\nu)}{(1-\nu)}\int (T - T_0)\, r dr. \qquad (3.31)$$

The component of stress from eq. (3.24) is:

$$\sigma_{rr} = \frac{2\mu}{(1-2\nu)}\left[(1-\nu)\frac{du_r}{dr} + \nu\frac{u_r}{r} + \nu w - \alpha(1+\nu)(T - T_0)\right]$$

$$\sigma_{\theta\theta} = \frac{2\mu}{(1-2\nu)}\left[(1-\nu)\frac{u_r}{r} + \nu\frac{du_r}{dr} + \nu w - \alpha(1+\nu)(T - T_0)\right]$$

$$\sigma_{22} = \nu(\sigma_{rr} + \sigma_{\theta\theta}) - 2\mu(1+\nu)[\alpha(T - T_0) - w]. \qquad (3.32)$$

Either displacement or stress boundary conditions can be applied and for solid rod problem $C_1 = 0$. The normal strain component w is found by the condition:

$$2\pi \int \sigma_{zz}\, r\, dr = F_{ax}. \tag{3.33}$$

Two examples we will use later are for a pressurised closed tube and for tubes with a radial temperature variation. For the tube inner radius a and outer radius b with an internal pressure p_i but no external pressure we have $\sigma_{rr} = p_i$ at a and p_i $\sigma_{rr} = 0$ at b. The axial force acting on the section is $F_{ax} = \pi a^2$. The stress components are found to be:

$$\sigma_{rr} = \frac{p_i b^2 a^2}{(b^2 - a^2)}\left[\frac{1}{b^2} - \frac{1}{r^2}\right],\ \sigma_{\theta\theta} = \frac{p_i b^2 a^2}{(b^2 - a^2)}\left[\frac{1}{b^2} + \frac{1}{r^2}\right]$$
$$\sigma_{zz} = \frac{p_i\, a^2}{(b^2 - a^2)}. \tag{3.34}$$

The radial displacement is:

$$u_r = \frac{p_i\, a^2}{2\mu\,(b^2 - a^2)}\left[\frac{b^2}{r} + \frac{(1+2\nu)r}{(1+\nu)}\right] \tag{3.35}$$

and the axial strain is:

$$w = \frac{(1-2\nu)\, a^2\, p_i}{2\mu\,(1+\nu)(b^2 - a^2)}. \tag{3.36}$$

For the tube with a radial temperature variation but no external load we have the stress components:

$$\sigma_{rr} = 2\mu\alpha\frac{(1+\nu)}{(1-\nu)}\left[\frac{a^2}{(b^2-a^2)}\left(\frac{1}{a^2} - \frac{1}{r^2}\right)\int_a^b (T - T_o)\, r\, dr\right]$$
$$\sigma_{\theta\theta} = 2\mu\alpha\frac{(1+\nu)}{(1-\nu)}\left[\frac{a^2}{(b^2-a^2)}\left(\frac{1}{a^2} + \frac{1}{r^2}\right)\int_a^b (T - T_o)\, r\, dr + \frac{1}{r^2}\int_a^r (T - T_o)\, r\, dr - (T - T_o)\right]$$
$$\sigma_{zz} = 2\mu\alpha\frac{(1+\nu)}{(1-\nu)}\left[\frac{1}{(b^2-a^2)}\int_a^b (T - T_o)\, r\, dr - (1-2\nu)(T - T_o)\right]. \tag{3.37}$$

The radial displacement is:

$$u_r = \alpha\frac{(1+\nu)}{(1-\nu)}\left[\frac{1}{(b^2-a^2)}\left(\frac{a^2}{r} + \frac{(1-2\nu)r}{(1+\nu)}\right)\int_a^b (T - T_o)\, r\, dr + \frac{1}{r}\int_a^r (T - T_o)\, r\, dr\right] \tag{3.38}$$

and the axial strain is:

$$w = \frac{\alpha}{(b^2-a^2)}\frac{(1-2\nu)}{(1-\nu)}\int_a^b (T - T_o)\, r\, dr. \tag{3.39}$$

Another approximation of interest is for thin shells or membranes, where pressure differentials across the shell are balanced by forces in the plane of the shell, permitted by the membrane curvature. The simplest case is that of a cylindrical shell or thin tube where:

$$\sigma_{\theta\theta} = R\,(P_i - P_o)/h \tag{3.40}$$

where R is the shell radius, h is the tube thickness, P_i is the inner pressure and P_o is the outer pressure, or more accurately:

$$\sigma_{\theta\theta} = (aP_i - bP_o)/(b - a). \tag{3.41}$$

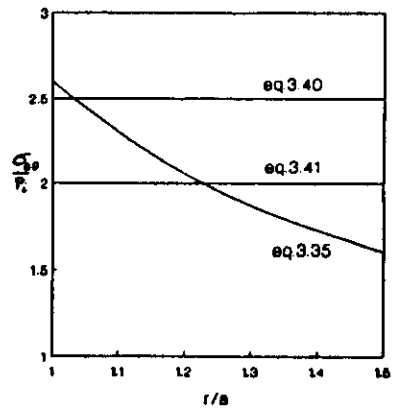

Fig.3.2

These approximations can be used to produce reference stresses for quite thick shells, with reasonable accuracy. This can be seen in Fig. 3.2 where the thin shell approximations are compared with the value of $\sigma_{\theta\theta}$ from eq. (3.35) for the case where b/a = 1.5.

The bending of elongated and plate-like structures are also of frequent interest in structural calculations. Let us consider a prismatic beam

of arbitrary cross section, but long compared with its thickness. We will only consider deflections of the beam that are small enough for the planes in the section to remain plane and that bending only takes place in a single plane. If the beam is aligned along the x_2 axis and bent in the x_2, x_3 plane at a point the originally straight beam is bent to a radius of curvatureon the neutral surface that passes through the centroid of the beam section. On this neutral surface the material experiences no deformation in the x_2 direction. If we measure z as the distance through the section in the x_3 from the centroid we find

$$e_{22}(z) = z\frac{\partial^2 u_{22}}{\partial x_2^2} = z/\rho_c \tag{3.42}$$

and the stress in the section is simply

$$\sigma_{22} = zE\frac{\partial^2 u_{22}}{\partial x_2^2} = zE/\rho_c. \tag{3.43}$$

This stress when averaged over the section of the beam is zero. We can now define the bending moment M as:

$$M = \int_{-z_1}^{z_2} \sigma_{22}\, z\, w(z)\, dz = \frac{E}{\rho_c}\int z^2 w(z) dz = \frac{EI}{\rho_c}$$

where I the moment of inertia of the section and w(z) is the width of the section, see

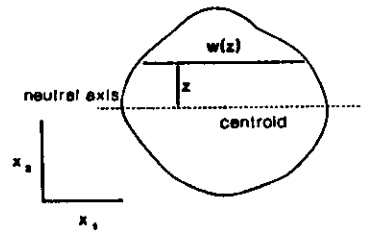

Fig. 3.3

Fig. 3.3. This simple relation can be used to analyse the bending of arbitrarily shaped beams. The magnitude of the bending moment can be found for point forces by calculating the couples or moments with respect to support points. The problems are frequently complicated by the direction of the applied force changing as the beam deforms.

The linear nature of elastic fields means that both stress and displacements resulting from different types of loading can be super-imposed. This is useful for

thermo-elastic problems which can be solved separately from the deformations produced by external loading as from body forces. This property also permits another approach to solving elastic problems. Applied stresses at surfaces or body forces can be described by a distribution of point forces using Green's functions. This is particularly useful for problems with local stress concentrations which can be treated as semi-infinite bodies. Often only the surface displacements are required or alternatively the surface stresses resulting from applied displacements. As an example we will look at the classic problem of the elastic indentation of a surface by a rigid sphere.

The displacement at x produced by a point force at x' in an infinite body is given by:

$$u_i(x) = G_{ij}(x-x')\, P_j(x') \tag{3.45}$$

where G_{ij} is the Green's tensor. The displacements on a surface given by a distribution of point forces on the surface are agiven by:

$$u_i(x) = \int_s G_{ij}(x-x')\, P_j(x')\, ds. \tag{3.46}$$

For the spherical indentor problem we are only interested in displacements and forces normal to the surface and in this case the Green's function is (Landau and Lifshitz 1959):

$$G_{33} = \frac{(1-\nu)}{2\pi\mu}\frac{1}{[(x_1-x_1')^2 + (x_2-x_2')^2]^{1/2}}. \tag{3.47}$$

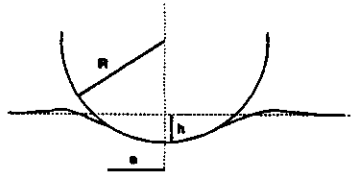

Fig. 3.4

The displacements are fixed for the problem by the sphere radius R and the depth of the indentation h, see Fig. 3.4. We get the integral equation:

$$h - \frac{(x_1^2 + x_2^2)}{2R} = \frac{(1-\nu)}{2\pi\mu}\iint \frac{P_3(x_1', x_2')\, dx_1'\, dx_2'}{[(x_1-x_1')^2 + (x_2-x_2')^2]^{1/2}}. \tag{3.48}$$

This has the solution

$$P_3(r) = 3F_a\,(1 - r^2/a^2)/2\pi a^2 , \tag{3.49}$$

where a is the radius of the indentation:

$$a = (3F_a\,(1 - \nu)/8)^{1/3} , \tag{3.50}$$

F_a being the applied force and $r = (x_1^2 + x_2^2)^{1/2}$.

3.3 Numerical Approximations

Many elastic problems may be solved in terms of series solutions of harmonic functions or in terms of Bessel's functions or other special functions for other co-ordinate systems, but even for simple problems the solutions are complicated and slow to evaluate numerically. There are advantages in closed form solutions in enabling important features of the elastic field to be identified, but this may nearly always be done by simplifying the problems and directing the solution at the key issues. Examples of this are the characteristics of stress concentrations and the definition of reference stresses for structures. The nature of the boundary conditions, the coupling to other interacting systems (e.g. thermal or fluid dynamic), the complexity of shape of the structure, composite structures and heterogeneity of properties are factors that lead inevitably to the choice of numerical approximate solution to problems. The drive is even stronger when inelasticity also has to be coped with.

An example of how complex the analytical solution can be for a relatively straightforward thermo-elastic problem can be found for the distortions of a free heat generating finite cylinder. The analytical solution in terms of ordinary and modified Bessel functions is fiercely complicated and expensive to evaluate (Valentin and Carey 1970). This can be compared with the simplicity of a finite-difference approach to the problem (Matthews 1970).

The finite-difference method was the first numerical approximation applied to elastic and thermo-elastic problems. The usual way it is applied is to make the approximation on the second order equations for the displacement field. For problems in rectangular co-ordinates the structure to be analysed has a rectangular grid of points super-imposed on it; less regular grids produce difference approximations of

undesirable complexity. Some degree of refinement is possible by varying the spacing of the grid. The differential equations are then approximated by differences taken at each point on the grid. Most rigorously central differences should be used and a regularly spaced grid is required for confidence in the approximation. Only the lowest order difference approximations are generally u: As an example we may take differences for eq. (3.30). The grid spacing is δr anc grid radii are labelled r (I) and the displacements u_r (I):

$$\frac{u_r(I+1) - 2u_r(I) + u_r(I-1)}{\delta r^2} + \frac{u_r(I+1) - u_r(I-1)}{2\delta r\, r(I)} - \frac{u_r(I)}{r(I)^2}$$

$$= \frac{(1+2\nu)}{(1-\nu)}\frac{F_r(I)}{\mu} + \frac{\alpha(1+\nu)}{(1-\nu)}\frac{[T(I+1) - T(I-1)]}{2\delta r}. \tag{3.51}$$

The boundary conditions are applied directly at boundary grid points; forward or backward differences are applied as appropriate. The outer boundary condition of $\sigma_{rr} = P_o$ would be given by:

$$(1-\nu)\frac{[u_r(N) - u_r(N-1)]}{\delta r} + \nu\frac{u_r(N)}{r(I)} + \nu w - \alpha(1-\nu)(T(N) - T_o) = P_o\frac{(1-2\nu)}{2\mu} \tag{3.52}$$

where r(N) = b. In this case the coefficients of the linear equations for u(I) form a tri-diagonal matrix that can be solved very quickly for Gaussian elimination. The unknown axial strain w has to be simultaneously calculated from numerical integration of eq. (3.33) which provide an additional linear equation that can be incorporated into the Gaussian elimination without destroying the overall sparsity of the problem.

The above finite difference formulation does not permit the elastic moduli to vary with position. This can limit the usefulness of the method for problems with large temperature variations or when the characteristics of the material change within position from variations in porosity etc. This handicap may be removed by taking differences only on first order differential equations, but at the expense of larger number of variables. The differences are taken on the stress equilibrium equations and the compatibility relations. An alternative is to derive a second order equation taking differentials on all of the elastic moduli, which leads to very complicated coefficients.

The other main advantage of the low order method is that it provides values of stresses as well as displacements at the grid points without need of further calculation.

The other main group of methods of tackling elastic problems is the use of trial functions to describe the elastic field. One way of approaching this is to use a variational method (Rayleigh - Ritz method). For elastic problems this corresponds to minimising the strain energy of the system. This can be shown simply using Euler's theorum. If we take a function:

$$\chi = \int_v f(x_i, u_i, u_{ij})\, dv + \int_s (a_1 u_i + a_2 u_i^2/2) ds \tag{3.53}$$

which is to be minimised and vary the displacements, the variational principle can be expressed as:

$$\delta\chi = \int_v \delta u_i \left[\frac{\partial f}{\partial u_i} - \frac{\partial}{\partial x_j}\left(\frac{\partial f}{\partial u_{i,j}}\right)\right] dv + \int_s \delta u_i \left[a_1 + a_2 u_i + n_j \frac{\partial f}{\partial u_{i,j}}\right] ds \tag{3.54}$$

where n_j are the direction cosines of the co-ordinate system with the normal vector to the surface. For a minimum to be achieved for an arbitrary variation of δu_i we have in the interior of the structure:

$$\frac{\partial f}{\partial u_i} - \frac{\partial}{\partial x_j}\left(\frac{\partial f}{\partial u_{i,j}}\right) = 0 \tag{3.55}$$

and on the boundary:

$$a_1 + a_2 u_i + n_j \frac{\partial f}{\partial u_{i,j}} = 0 \tag{3.56}$$

If we use the stress equilibrium, the compatability and constitutive equations to define the field, permitting the elastic moduli thermal expansion coefficient to be a function of position we find:

$$f = u_i F_i - 1/2\, e_{ij}\, \sigma_{ij} \tag{3.57}$$

The variational principle can now be expressed as:

$$\delta\chi = \delta \int_v (1/2\, e_{ij} - u_i F_i)\, dv + \int_{s'} \sigma^*_{ij}\, n_j\, u_i\, ds \tag{3.59}$$

where σ^*_{ij} indicates that the stress is an imposed boundary stress and s' indicates that portion of the boundary where the stress boundary condition applies. Displacement boundary conditions are normal directly imposed on the trial function.

To show how the variational approach works in practice we will use our axisymmetric plain strain example. The variational principle is given by:

$$\delta\chi = \delta \int_a^b \left\{\mu\left[\left(\frac{du_r}{dr}\right)^2 + \left(\frac{u_r}{r}\right)^2 + w^2 + \frac{\nu}{(1-\nu)}\left(\frac{du_r}{dr} + \frac{u_r}{r} + w\right)^2\right]\right\}$$

$$\left\{\left[+\frac{\alpha(1+\nu)}{(1-2\nu)}\alpha(T-T_0)\left(\frac{du_r}{dr} + \frac{u_r}{r} + w\right)\right] - u_r F_r\right\} 2\pi r\, dr$$

$$+ \delta 2\pi \left[a\, u_r(a) P_i + b u_r(b) P_o\right] = 0. \tag{3.60}$$

Some function with unknown coefficients is used to describe the displacement field. The trial function should reflect the symmetry of the problem and normally consists of a set of independent functions such as a harmonic or polynomial series. The more degrees of freedom the function has the better the anticipated result. For our example we will use a polynomial for u_r up to order 3:

$$u_r = b_0 + b_1 r + b_2 r^2 + b_3 r^3. \tag{3.61}$$

Substituting (3.62) into (3.60) and integrating explicitly we obtain an equation which is quadratic in the coefficients b_i. This is differentiated with respect to each coefficient in turn and a set of linear equations is found which may be easily evaluated. Additionally an equation giving the axial force (3.3) must be included so that w may be determined.

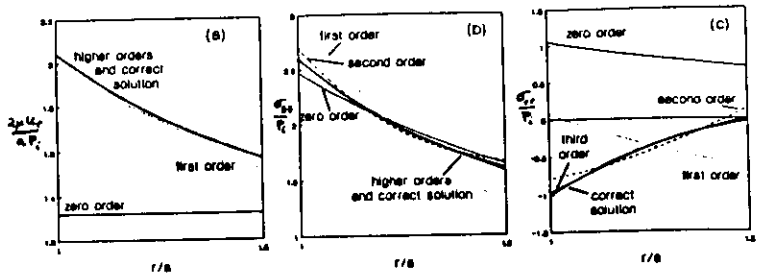

Fig.3.5

We have done this for $P_o = 0$ and with no temperature field and compare the resulting displacements and stresses in Fig. 3.5 with those obtained directly from eqs. (3.34) and (3.35). In these plots resuls are shown for various orders of polynomial in (3.61). The displacements are reasonably estimated even for a first order trial function. The stresses are more difficult. A second order trial function is required to a reasonable representation for the hoop stress,but the radial stress is poorly represented even by the 3rd order function.

There are many disadvantages with this method of solving problems for all except the simplest configurations. The method requires large numbers of terms which are slow to evaluate directly and difficult to write as algorithms. It is almost impossible to cope with structures with low symmetry and indented boundaries. Such trail functions which extend over the whole structure are termed global functions. A solution to the problems of the variational method is the use of *piece-wise* trial functions and finite elements. A brief introduction to the background to finite elements may be found in Owen and Hinton (1980) and the best comprehensive treatise is by Zienkiewicz (1971 and 1989).

The structure is divided into an assembly of conveniently shaped regions, termed elements and the trial function is defined by some simple function in each region. The functions in each element are constrained to be continuous to some extent with its neighbours. Various degrees of continuity have been experimented with, e.g. the use of cubic splines which are continuous to the second order have been tried. The finite element method has developed by using low order polynomial functions that are defined by the displacements at nodes. Where these nodes lie on the boundaries between elements continuity is ensured. The simplest functions are linear with the nodes defined only at the boundaries between the elements for one dimensional calculations, with nodes at the corners of triangular elements in two dimensional

calculations and at the corners of tetrahedral elements in three dimensional calculations. Higher order trial functions require additional nodes. For a second order trial function in one dimensional problems an additional node is added in the interior or the element. For two and three dimensional calculations the nodes may be added at the interior of the element or on the boundaries. Frequently the elements used in t· · and three dimensional calculations are simple straight sided blocks, tetrahedr iangul · prisms, but curved elements may also be used at the expense of a signific.. increase ... complexity. The use of straight sided elements means that curved structures have to be approximated by polyhedra and a large number of elements used make the representation adequate.

The displacements at the nodes become the unknowns in the problem. The simplest example is the one dimensional case where within an element defined by the radii r_i and r_{i+1} the displacement is given by:

$$u_r(r) = \frac{\left[u_r(r_{i+1})(r_{i+1} - r) + u_r(r_i)(r - r_i)\right]}{(r_{i+1} - r_i)} \qquad (3.62)$$

More generally the displacements can be represented in terms of the nodal displacements by:

$$\mathbf{u} = [N]\{u\}^e \qquad (3.63)$$

where $\{u\}^e$ signifies the set of nodal displacements defining that element and [N] is the corresponding matrix of functions of position called the shape function. Equation (3.63) can be extended to represent the whole structure rather than just one element by defining the values of the components of [N] to be zero outside their relevant node. We can now use {u} to represent the whole ensemble of nodal displacements in the structure. We can generate a matrix of functions [B] which relate the strains at any point with the nodal displacements:

$$\mathbf{e} = [B]\{u\}. \qquad (3.64)$$

For our one dimensional example for the element lying between r_i and r_{i+1} [B] is given by:

$$(e_{rr},\ e_{\theta\theta}) = \begin{bmatrix} -1/\delta r_i\ ,\ 1/\delta r_i \\ -(1 - r_{i+1}/r)/\delta r_i\ ,\ (1 - r_i/r)/\delta r_i \end{bmatrix} \begin{pmatrix} u_r(r_{i+1}) \\ u_r(r_i) \end{pmatrix}. \tag{3.65}$$

The stresses in the structure are related to the strain by a matrix of elastic moduli [D]:

$$\sigma = [D]\,(e - e_o), \tag{3.66}$$

where e_o are termed prior strains and correspond here to the thermal strains. Equation (3.66) is simply an alternative way of writing the constitutive relation eq. (3.28) but is more general as [D] can be formulated for materials with anisotropic elastic and thermal expansion behaviour. We now substitute (3.63), (3.64) and (3.66) into the variational principle (3.59) and after differentiating with respect to the unknown nodal displacements we obtain a set of linear equations:

$$[K]\{u\} + \{F\}_i + \{F\}_o + \{F\}_b = 0 \tag{3.67}$$

where the stiffness matrix is:

$$[K] = \sum_e \int_e [B]^T [D][B]\, dv \tag{3.68}$$

the nodal forces from body forces are:

$$\{F\}_i = \sum_e \int_e [N]^T F\, dv \tag{3.69}$$

the forces from prior strain are:

$$\{F\}_o = \sum_e \int_e [B]^T [D]\, e_o\, dv \tag{3.70}$$

and the nodal forces from imposed boundary stresses are:

$$\{F_o\} = \sum_e \int_b [N]^T \sigma n\, ds \cdot \tag{3.71}$$

For structures described by many elements the stiffness matrix is sparse and symmetric and generally quick to solve, but care has to be taken to ensure that the solution method takes advantage of these characteristics.

The finite element method can be derived by several other means besides the use of a variational principle. The most usual method is that of weighted residuals using the trial functions themselves as the weights; the Galerkin method. This is somewhat more general and can be applied to problems where a variational principle cannot be derived.

Finite element techniques are simple to write as computer algorithms and provide rapid methods of coping with the deformation of complex structures. It is relatively straightforward to treat stress concentrations by having a local fine array of elements. Finite element calculations can be made easier to implement and quicker to evaluate by making approximations to the integrals in eqs. (3.26) to (3.71). If an order of integration is taken one lower than the order of the trial function there is little loss of accuracy and in some cases the quality of the result is improved provided sufficient refinement of the elements has been taken in the first place. So for a linear trial function a single point integration is adequate, i.e. the values of the quantities to be integrated are taken at the centroid of the element and multiplied by the volume, area or length of the element as appropriate. There are drawbacks, however. The gradients in displacements are discontinuous at the boundaries between elements so the stresses are only well defined at the integration points. It is thus necessary during calculations to out-put stresses from these positions and then interpolate if values are required elsewhere.

Before moving on to examples and the implementation of finite differences and finite elements to thermo-elastic problems we will briefly mention the boundary element method. This method has proved particularly successful where the main interest is the displacements at the surface or where the distribution of loads on the surface is complex. A description of the basis of the method and how it is used for a wide range of problems can be found in Banerjee and Butterfield (1981). The basic relationship that underpins the method is that:

$$u_j(x) = \int_s \{u_{ij}(x, x')\,\sigma_{ik}(x')\,n_k - T_{ij}(x, x')\}\,u_i(x')\,ds$$

$$+ \int u_{ij}(, x')\,F_i(x')\,dv + \int 2\mu\, u_{ij,k}(x, x')\,e^o_{ik}(x')\,dv \tag{3.72}$$

where u_{ij} is the function that gives the displacements in the i direction from a unit point force in the j direction, similarly T_{ij} is the function that gives a traction in the i direction from a unit displacement in the j direction. The forms of these functions for two and three dimensional problems can be found in Banerjee and Butterfield (1981). The displacements and tractions on the surface are represented by nodal values for an array of elements covering the surface. Eq. (3.72) then gives on integration a series of linear equations in terms of these nodal values. The prior strains, including thermal expansions, and body forces have to be integrated on a mesh over the interior of the structure, but where these are absent the integrals are confined to the surfaces. The resulting set of equations is generally lower order than that for the finite element method for the same accuracy, but the matrix of coefficients is not sparse. The boundary element method is more complex to implement than finite elements for most problems, but is superior in performance in many cases. Axisymmetric problems are more difficult than most other configurations to model using boundary elements. This is because the stress distribution functions contain elliptic integrals which are slow to evaluate and difficult to manipulate.

Lecture 4 Plasticity and Creep

4.1 Deformation under Multiaxial Stress

In the first three sections of this lecture we will use some very simplified models of plastic and creep deformation and in the fourth section we will briefly look at more complex and hence realistic models. In some cases we will look at concurrent inelastic and elastic deformations but in many cases we may ignore elastic effects and simply look at inelastic consitutive relations.

The simplest model of plasticity is the perfectly plastic material, where for uniaxial loading the material yields when $\sigma_a = \sigma_y$. Most materials exhibit some degree of work hardening so we will express this generally by:

$$\sigma_y = \sigma_0 + H(\varepsilon_p). \tag{4.1}$$

For creep deformation we will make the strain rate a simple function of the applied stress:

$$\dot{\varepsilon} = f(\sigma_a). \tag{4.2}$$

We will assume that the sign of the stress is not significant, with complete reversability and that the plastic strain ε_p in (4.1) is obtained by integrating the modulus of the strains.

Most real problems require the treatment of multiaxial stress states and changing stress states. Some method of coping with this problem is needed. A discussion of the formulation of plastic problems can be found in Hill (1950) and a very accessable treatise on creep problems is provided by Odqvist (1974). Further assumptions are required to provide a sufficiently simple framework for problem solving. The first is that the material is completely isotropic, which is initially a good assumption for many polycrystalline engineering alloys, but as we shall see not so good after large deformations. The second is that plastic and creep deformations are volume conserving and are insensitive to the hydrostatic components of stress. This again is a good assumption for materials that do not contain significant volume fractions of cavities. For very porous materials a new form of flow rule is required, as has already been discussed in section 2.6.

The rate of work done during plastic deformation is:

$$\dot{W} = \sigma_{ij} \dot{\varepsilon}_{ij} . \tag{4.3}$$

We define the stress deviation tensor or deviatoric stress as:

$$s_{ij} = \sigma_{ij} - \delta_{ij} \sigma_{kk}/3 = \sigma_{ij} - \sigma . \tag{4.4}$$

Volume conservation requires $\dot{\varepsilon}_{kk} = 0$ so we may rewrite eq. (4.3) as:

$$\dot{W} = s_{ij} \dot{\varepsilon}_{ij} . \tag{4.5}$$

It would be desirable to describe the plastic state of the body in terms of some scaler quantity and this might be found in the invariants of the stress tensor. Any second order tensor has three independent invariants these are:

$$J_1 = \sigma_{kk} = 3\sigma \; ; \; J_2 = 1/2 \; s_{ij} \, s_{ij} \text{ and}$$
$$J_3 = 1/3 \; s_{ij} \, s_{jk} \, s_{ki}. \tag{4.6}$$

We have already excluded the possibility of J_1 controlling plastic strain so we are left with J_2 and J_3. The next simplest possibility is that J_2 provides the criterion. This corresponds to the von Mises stress σ_e where:

$$\sigma^2_e = 3 \; s_{ij} \, s_{ij}/2. \tag{4.7}$$

This has some justification as σ_e is a measure of the state of shear in the body as it corresponds to the shear stress acting on the octahedral planes (the octahedron referred to is that superimposed on the axes of the principal stress system). Yield results when σ_e reaches σ_y. We would therefore expect $\dot{W}$ to be a function of σ_e, hence:

$$\dot{\varepsilon}_{ij} = \frac{d\dot{W}}{d\sigma_e} \frac{d\sigma_e}{ds_{ij}} = \frac{3}{2} \frac{d\dot{W}}{d\sigma_e} \frac{s_{ij}}{\sigma_e} . \tag{4.8}$$

All we need do now is constrain $\dot{W}$ to make eq. (4.8) give the appropriate value for uniaxial deformation, when $\sigma_e = \sigma_{11} = \sigma_a$, $s_{11} = 2\sigma_{11}/3$ and $s_{22} = s_{33} = -\sigma_{11}/3$. For creep we have:

$$\dot{\varepsilon}_{11} = \frac{3}{2} \frac{d\dot{W}}{d\sigma_e} \frac{2}{3} \frac{\sigma_{11}}{\sigma_{11}} = f(\sigma_{11}) \tag{4.9}$$

so that

$$\frac{d\dot{W}}{d\sigma_e} = f(\sigma_e) \tag{4.10}$$

and

$$\dot{\varepsilon}_{ij} = \frac{3}{2} f \frac{(\sigma_e)}{\sigma_e} s_{ij} . \tag{4.11}$$

For plastic deformation when $\sigma_e = \sigma_y$:

$$\dot{\varepsilon}_{11} = \frac{d\dot{W}}{d\sigma_e} = g'(\sigma_{11}) \dot{\sigma}_{11} \tag{4.12}$$

where $g(\sigma_e)$ is obtained by replacing σ_y by σ_a in eq. (4.1) and inverting to give the accumulated plastic strain as a function of applied stress. The final expression often referred to as the Reuss equation is:

$$\dot{\varepsilon}_{ij} = \frac{3}{2} g'(\sigma_e) \frac{s_{ij}}{\sigma_e} \dot{\sigma}_e . \tag{4.13}$$

Equations (4.11) and (4.13) will form the basis of our problem solving in the next two sections.

Before moving it is worth defining a von Mises equivalent strain ε_e as:

$$\varepsilon^2_e = \frac{2}{3} \varepsilon_{ij} \, \varepsilon_{ij} , \tag{4.14}$$

with the additional requirement that there is no volume strain arising from ε_{ij}. The yield condition is redefined for multiaxial stress states as:

$$\sigma_e = \sigma_y = \sigma_o + H(\varepsilon_{e\text{-plastic}}) . \tag{4.15}$$

4.2 Solving Creep and Plastic Flow Problems

Before going on to describe the numerical implementation of inelastic deformations in structural analysis it is worth looking at the direct solution of some example simple problems. The range of problems that can be tackled in this way is small because of the intrinsic non-linearity of plasticity. There is, however, the advantage that the condition of incompressibility gives on constraining the form of the strains and displacements.

Let us first of all look at the deformation of a pressurised thick cylinder. If plastic flow has propagated through the section of the tube and if elastic strains can be ignored the form of the radial displacement is fixed by the volume conservation condition:

$$\varepsilon_{kk} = \frac{du_r}{dr} + \frac{u_r}{r} = 0, \tag{4.16}$$

which may be integrated to give:

$$u_r = \frac{c_1}{r}. \tag{4.17}$$

It should be noted that the axial strain is zero for an internally pressurised tube during incompressible plastic or creep deformation and that this arises automatically from axial force balance considerations. The stresses of interest in the problem are:

$$\sigma_{zz} = \frac{1}{2}(\sigma_{rr} + \sigma_{\theta\theta}) \quad , \quad s_{rr} = -\frac{1}{2}(\sigma_{\theta\theta} - \sigma_{rr})$$
$$s_{zz} = 0,\ s_{\theta\theta} = \frac{1}{2}(\sigma_{\theta\theta} - \sigma_{rr}) \text{ and } \sigma_e = \left(\sqrt{3/2}\right)(\sigma_{\theta\theta} - \sigma_{rr}). \tag{4.18}$$

The stress equilibrium condition is given by:

$$\frac{d\sigma_{rr}}{dr} + \frac{(\sigma_{rr} - \sigma_{\theta\theta})}{r} = 0. \tag{4.19}$$

From eq. (4.17) the plastic strain components are:

$$\varepsilon_{rr} = -c_1/r^2,\ \varepsilon_{\theta\theta} = c_1/r^2$$
$$\text{and } \varepsilon_e = 2c_1/\sqrt{3}\,r^2. \tag{4.20}$$

If we take a particular form of the flow rule (4.15):

$$\sigma_e = \sigma_y = (\sigma_o + \sigma_p \varepsilon_e^m), \tag{4.21}$$

where σ_o, σ_p and m are materials constants. From eqs. (4.18) and (4.20) we have

$$\sigma_{\theta\theta} - \sigma_{rr} = \left(2/\sqrt{3}\right)\left[\sigma_o - \sigma_p \left(2c_1/\sqrt{3}\right)^m / r^{2m}\right] \tag{4.22}$$

and hence from (4.19):

$$\frac{d\sigma_{rr}}{dr} = \frac{2}{\sqrt{3}r}\left[\sigma_o + \sigma_p \frac{\left(2c_1/\sqrt{3}\right)^m}{r^{2m}}\right]. \tag{4.23}$$

Integrating and setting $\sigma_{rr} = 0$ at $r = b$ and $\sigma_{rr} = -P_1$ at $r = a$ we find:

$$\sigma_{rr} = \frac{2}{\sqrt{3}}\left\{-\sigma_o \ln(b/r) - \frac{\left[\left(\sqrt{3/2}\right)P_1 - \sigma_o \ln(b/a)\right]}{(a^{-2m} - b^{-2m})}\left(\frac{1}{r^{2m}} - \frac{1}{b^{2m}}\right)\right\}$$
$$\sigma_{\theta\theta} = \frac{2}{\sqrt{3}}\left\{\sigma_o [1 - \ln(b/r)] + \frac{\left[\left(\sqrt{3/2}\right)P_1 - \sigma_o \ln(b/a)\right]}{(a^{-2m} - b^{-2m})}\left(\frac{(2m-1)}{r^{2m}} + \frac{1}{b^{2m}}\right)\right\}$$
$$u_r = \frac{\sqrt{3}}{2r}\left[\frac{2m\left[\left(\sqrt{3/2}\right)P_1 - \sigma_o \ln(b/a)\right]}{\sigma_e (a^{-2m} - b^{-2m})}\right]. \tag{4.24}$$

This expression is only valid for reasonably small strains (<10%), but shows how the character of the stress distribution changes when work hardening becomes important.

A similar distribution is found for creep deformation and for a creep law of the type $\dot{\varepsilon} = B\sigma_e^n$ the distribution is identical for work hardening with m = 1/n and the initial yield stress zero:

$$\sigma_{rr} = -P_i\left(r^{-2/n} - b^{-2/n}\right)/\left(a^{-2/n} - b^{-2/n}\right)$$
$$\sigma_{\theta\theta} = P_i\left[\left((2m-1)\,r^{-2/n} + b^{-2/n}\right]/\left(a^{-2/n} - b^{-2/n}\right)\right.$$

(4.25)

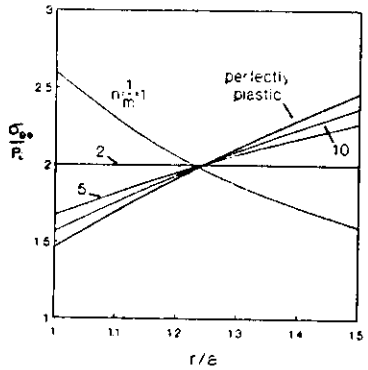

Fig.4.1

The effect of the creep or the work hardening inex on the hoop is shown in Fig. 4.1 for the example previously used where b/a = 1.5. The effect of increasingly non-linear deformation is to shift the maximum normal stress from the inside wall of the tube to the outside.

To evaluate partial yielding it is necessary to include the effect of elasticity. The initial elastic state of the tube is given by eqs. (3.34). The von Mises stress distribution through the wall is given by:

$$\sigma_e = \frac{\sqrt{3}\,P_i\,a^2b^2}{(b^2 - a^2)r^2},$$

(4.26)

so the yielding will start at the clad inside surface when the internal pressure reaches the threshold value of:

$$P_i = (b^2 - a^2)\sigma_y/\sqrt{3}b^2.$$

(4.27)

Calculating the progression of yielding through the tube wall is more difficult because of the complications arising from the axial loading conditions (Hill 1950). The problem can be solved easily if the axial component of axial strain remains zero throughout the propagation. This is not a bad approximation and is correct at the start of yielding, as eqs. (3.34) give $s_{zz} = 0$, and this is also true once the whole of the tube is undergoing plastic strain. The approximation also coincides with the Tresca yield criterion. We will therfore assume that eqs. (4.18) hold in the plastic region throughout the process we will start with the internal pressure at the threshold value given by eq. (4.26) and then increase it. The plastic region is bounded by the radius c which starts at the inner radius a and reaches b when yield across the section is complete. In the plastic region r≤c eq. (4.19) together with (4.18) and the yield condition gives:

$$\frac{d\sigma_{rr}}{dr} = \frac{(\sigma_{\theta\theta} - \sigma_{rr})}{r} = \frac{2}{\sqrt{3}}\frac{\sigma_e}{r} = \frac{2}{\sqrt{3}}\frac{\sigma_y}{r}.$$

(4.28)

On integration and matching with the elastic solution at r = c the stress distributions in the elastic and plastic regions can be found.

Elastic region $c \le r \le b$

$$\sigma_{rr} = \frac{\sigma_y}{\sqrt{3}}\frac{c^2}{b^2}\left(\frac{b^2}{r^2} - 1\right)$$
$$\sigma_{\theta\theta} = \frac{\sigma_y}{\sqrt{3}}\frac{c^2}{b^2}\left(\frac{b^2}{r^2} + 1\right)$$
$$\sigma_{zz} = \frac{\sigma_y}{\sqrt{3}}\frac{c^2}{b^2}.$$

(4.29)

Plastic region $a \le r \le c$

$$\sigma_{rr} = \frac{2}{\sqrt{3}}\sigma_y\left[\frac{c^2}{2b^2} - \frac{1}{2} - \ln(c/r)\right]$$
$$\sigma_{\theta\theta} = \frac{2}{\sqrt{3}}\sigma_y\left[\frac{c^2}{2b^2} + \frac{1}{2} - \ln(c/r)\right]$$
$$\sigma_{zz} = \frac{2}{\sqrt{3}}\sigma_y\left[\frac{c^2}{2b^2} - \ln(c/r)\right].$$

(4.30)

The relationship between P_i and c is found by taking the values of σ_{rr} from (4.30) for r = a:

$$P_i = \frac{2\sigma_y}{\sqrt{3}}\left[\frac{1}{2} - \frac{c^2}{b^2} + \ln(c/a)\right]$$

(4.31)

and propagation of yielding through the section is complete when

$$P_i = \frac{2\sigma_y}{3}\left[\ln (c/a) - \frac{1}{2}\right].$$

(4.32)

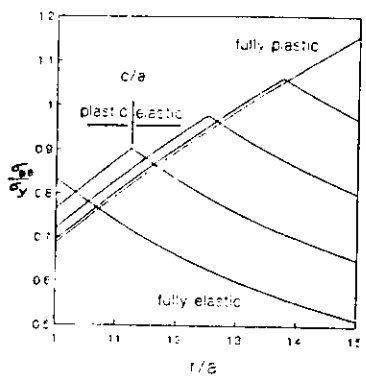

Fig.4.2

Comparison of σ_{zz} calculated from eqs. (4.29 and (4.30) reveals a discrepancy at r = c which arises from our assumption of no axial deformation. The redistribution of hoop stress across the tube wall during propagation of yield is shown in Fig. 4.2.

This example of yield propagation in a structure is one of the simplest cases that we encountered. More typically yield propagation has to be modelled in terms of incremental elasto-plastic constitutive relations. These are rarely soluble analytically. The resulting equations are hyperbolic in character and the solution method has to reflect this aspect.

Before turning to other structures, it is convenient to use the pressurised tube example to illustrate another aspect of creep deformation. This is that creep is very sensitive to temperature and structures undergoing creep may have large variations in creep strength if there are temperature gradients. As a thermally activated process creep may often be described by an equation of the type:

$$\dot{\varepsilon} = B_o \exp(-Q/T)\sigma_e^n .$$

(4.33)

If the temperature varies through the thickness of the tube wall, the hoop stress given in eq. (4.24) would change to:

$$\frac{\sigma_{\theta\theta}(r)}{P_i} = \frac{r^{-2/n}\exp[Q/nT(r)] \cdot \int_r^b r^{-2/n}\exp[Q/nT(r)]dr}{\int_a^b r^{-2/n}\exp[Q/nT(r)]dr}$$

(4.34)

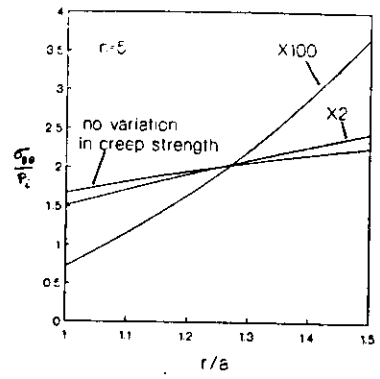

Fig.4.3

In Fig. 4.3 we show the examples of the variation in hoop stress for a tube with a linear variation of temperature resulting in a factor 2 and 100 increase in crep rate for a given stress. The main effect is to increase the stress in the outer regions of the tube where the material is stronger. A reference stress and temperature can still be used to characterise the rate of diameter increase of the tube, but these will not be a good guide to the local stresses which could determine failure.

The growth or collapse of spherical cavities by plastic deformation is of great interest for the theory of both hot pressing and failure processes. The treatment of creep deformation is simplest as we can assume that the whole of the material is undergoing creep. We have a cavity of radius a and an internal pressure P_i in a medium with a uniform hydrostatic pressure σ. The radial displacements centred on the cavity are determined by the volume conservation condition.

$$\dot{\varepsilon}_{rr} + 2\dot{\varepsilon}_{\theta\theta} = \frac{d\dot{u}_r}{dr} + \frac{2\dot{u}_r}{r} = 0 ,$$

(4.35)

which on integration give displacements of the form:

$$\dot{u}_r = c_1 / r^2 .$$

(4.36)

The stress components gives of interest are:

$$s_{rr} = -(2/3)(\sigma_{\theta\theta} - \sigma_{rr}),\ s_{\theta\theta} = (1/3)(\sigma_{\theta\theta} - \sigma_{rr})$$
$$\text{and } \sigma_e = |\sigma_{\theta\theta} - \sigma_{rr}|$$

For power law creep and using the spherically symmetric stress equilibrium equation (3.10) we find:

$$\frac{d\sigma_{rr}}{dr} = 2\frac{(\sigma_{\theta\theta} - \sigma_{rr})}{r} = \left(\frac{2c_1}{B}\right)^{1/n} \frac{1}{r^{3/n+1}}. \tag{4.37}$$

On integrating and using the boundary condition of $\sigma_{rr} = -P_1$ at $r = a$ we get:

$$\sigma_{rr} = P_1 + \frac{2n}{3}\left(\frac{2c_1}{B}\right)^{1/n}\left(\frac{1}{a^{3/n}} - \frac{1}{r^{3/n}}\right). \tag{4.38}$$

Examination of the solution reveals that the hydrostatic stress is constant and undetermined by this procedure. Another condition is required to fix the solution. If we consider that the cavity is part of a volume concentration of cavities C_c then one model of the system is to surround our cavity by a sphere of radius $R = (3/4\pi C_c)^{1/3}$ and make $\sigma_{rr} = \sigma$ at the surface of the sphere. This fixes the value of C_1:

$$C_1 = \frac{B}{2}\left[\frac{2n(\sigma - P_1)}{3(a^{-3/n} - R^{3/n})}\right]^n. \tag{4.39}$$

Defining the volume fraction of cavities as:

$$p_c = \frac{4\pi}{3} a^3 C_c = \frac{a^3}{R^3}, \tag{4.40}$$

the rate of change of porosity is given by:

$$\frac{dp_c}{dt} = -\frac{B}{2}\left[\frac{2n(\sigma - P_1)}{3(p_c^{1/n} - 1)}\right]^n. \tag{4.41}$$

Equation (4.41) is a useful expression to put alongside the others in section 2.3.

Plastic yielding around cavities is a much more difficult topic and discussions may be found in Hill (1950) and Gurson (1977). Amongst the results one that is useful is that the internal pressure required to expand a cavity in a thick shell is approximately:

$$P_i = \frac{2}{3}\sigma_y\left[1 + \ln\left(\frac{E}{3(1-\nu)\sigma_y}\right)\right], \tag{4.42}$$

and the ratio of plastic radius to cavity radius is approximately:

$$\frac{c}{a} = \left[\frac{E}{3(1-\nu)\sigma_y}\right]^{1/3}. \tag{4.43}$$

When work hardening is present eq. (4.42) still holds, but with an additional hardening term.

Despite the complexity of non-linear creep and plastic stress distributions, simple expressions can be obtained for the bending of sections. Following the same notation as section 3.2 the rate of change of strain in the x_2 direction is related to the deflections in the x_3 direction by:

$$\dot{\varepsilon}_{22} = z\frac{\partial^3 \dot{u}_{22}}{\partial x_2^2} = B\sigma_{22}^n. \tag{4.44}$$

The equivalent to eq. (3.44) is:

$$M = \int_{-z_1}^{z_2} \sigma_{22}\, z\, w(z)\, dz = \frac{I_n}{B}\frac{\partial^3 \dot{u}_{22}}{\partial x_2^2} \tag{4.45}$$

where I_n replaces the moment of inertia of the section and is defined by:

$$I_n = \int_{-z_1}^{z_2} z^{1+1/n}\, w(z)\, dz. \tag{4.46}$$

The rate of bending of the section is given by:

$$\frac{\partial^3 \dot{u}_{22}}{\partial x_2^2} = \frac{BM}{I_n}. \tag{4.47}$$

This simple expression is integrated over the length of the section according to the loading conditions in the same way as for elastic structures. Similar expressions may be derived for work hardening deformation.

4.3 Incorporating Creep in Structural Mechanics Calculations

The most frequent and direct approach to incorporating inelastic deformation into structural mechanics calculations is to simply add the strain from this source as prior strains and for this reason is referred to as the initial strain method. To do this we split the strain into elastic and inelastic parts:

$$\varepsilon_{ij} = e_{ij} + \gamma_{ij} = \frac{1}{2}(u_{i,j} + u_{j,i}). \tag{4.48}$$

Wherever elastic strains are encountered in the formulation of the structural analysis they are replaced by $\varepsilon_{ij} - \gamma_{ij}$, hence the constitutive relation (3.18) becomes:

$$\sigma_{ij} = \varepsilon_{ij} - \gamma_{ij} + \delta_{ij}[\nu\varepsilon_{kk} - \alpha(1+\nu)(T-T_0)]/(1-2\nu) \tag{4.49}$$

remembering that $\gamma_{kk} = 0$. By doing this inelastic strains can be incorporated into an existing method of solving elastic problems - direct, finite difference, finite element or boundary element.

As an example we can take the case of the axisymmetric plane strain case and replace eq. (3.30) by:

$$\frac{d}{da}\frac{1}{r}\frac{d}{dr}ru_r = \frac{(1-2\nu)}{(1-\nu)}\frac{F_r}{2\mu} + \alpha\frac{(1+\nu)}{(1-\nu)}\frac{dT}{dr} + \frac{(1-2\nu)}{(1-\nu)}\left[\frac{d\gamma_{rr}}{dr} + \frac{(\gamma_{rr}-\gamma_{\theta\theta})}{r}\right] \tag{4.50}$$

which is integrated to give (neglecting body forces):

$$u_r = \frac{c_1}{r} + c_2 r + \frac{\alpha}{r}\frac{(1+\nu)}{(1-\nu)}\int (T-T_0)\,r\,dr + \frac{(1-2\nu)}{2(1-\nu)}\left[\frac{1}{r}\int(\gamma_{rr}+\gamma_{\theta\theta})\,r\,dr + r\int\frac{(\gamma_{rr}+\gamma_{\theta\theta})}{r}dr\right]. \tag{4.51}$$

Alternatively the finite difference formulation replaces the difference equation (3.51) with:

$$\frac{u_r(I+1)-2u_r(I)+u_r(I-1)}{\delta r^2} + \frac{u_r(I+1)-u_r(I-1)}{2\delta r\, r(I)} - \frac{u_r(I)}{r(I)^2}$$

$$= \frac{(1-2\nu)}{(1-\nu)}\frac{F_r(I)}{\mu} + \frac{\alpha(1+\nu)}{(1-\nu)}\frac{[T(I+1)-T(I-1)]}{2\delta r}$$

$$+ \frac{(1-2\nu)}{(1-\nu)}\frac{[\gamma_{rr}(I+1)-\gamma_{rr}(I-1)]}{2\delta r} + \frac{(1-2\nu)}{(1-\nu)}\frac{[\gamma_{rr}(I)-\gamma_{\theta\theta}(I)]}{r(I)}. \tag{4.42}$$

Similarly and more generally for finite elements we extend the definition of e_0 in eq. (3.70) to include the inelastic strains. The same is done for boundary elements in eq. (3.72) and the inelastic strains have to be integrated over the volume of the structure (Mukherjee, 1982).

Once the elastic-inelastic problem is formulated in one of the above ways the inelastic strains are determined incrementally. For an elasto-plastic problem the stress distribution is first calculated from a purely elastic constitutive relation. These stresses are then used to estimate the plastic strains, γ_{ij}, which are then used to re-estimate the stresses. The procedure is iterated until hopefully a converged set of stresses and plastic strains is obtained. The method is reasonably reliable for materials showing significant work hardening and where the plastic strains are small. It is often necessry to carefully increment the load and to iterate on each increment. For creep, the creep strains are incremented over a time step using the stresses obtained from the previous step. This can be done *explicitly* by just retaining the strains from the stresses from the previous step or the result can be iterated to obtain an *implicit* or semi-implicit value for the strains. Where creep strains are small this method is both reliable and efficient, as the numerical solutions to the stiffness matrix or its equivalent (usually in triagnularised form) can be re-used on each time step. The method, however, is limited in the amount of creep strain that can be accumulated and in some cases it is difficult to obtain a stable solution.

The most important limitation to the use of the above method of implementing creep deformation in structural calculations is where the creep strength is low and particularly where there is a wide range of creep strength across the structure giving a *stiff* problem. If we have a structure with a part which is relatively strong and a part which creeps rapidly, on loading the stresses redistribute rapidly in the weaker part, but over a longer time the overall deformation will be determined by the stronger part. One could imagine taking small timesteps to cope with the initial transient and then increase

the timesteps once the system had settled. However, when an explicit scheme is used any stress errors generated in the weaker section result in large errors in creep strain and the timesteps have to be kept small. The use of iteration to provide an implicit scheme is only partially successful as some form of explicit estimate is required to start the iteration and frequently a stable procedure cannot be found. One useful technique is not extrapolate stress but rather the total strain. This is then used with the constitutive relation to generate a stress estimate for the new timestep and from that the next inelastic strain increment. The stress estimate can be used to provide a prior stress value to make up the difference between the stresses from a purely elastic calculation and the new estimate, for this reason the method is sometimes called the initial stress method. This scheme works adequately for problems where the loading is internal (e.g. from thermal expansions) or is controlled by imposed strains, but is of limited success with gas pressure or deadloading. There is also a penalty in materials with complicated constitutive relations as a relatively slow numerical procedure is required to relate the new stress estimates to the total strains.

The most satisfactory way of dealing with creep problems is sometimes called the softened or variable stiffness method. If we confine ourselves to volume conserving creep deformation we might describe an increment in the shear strains in the material by:

$$\delta\left(\varepsilon_{ij} - \delta_{ij}\frac{\varepsilon_{kk}}{3}\right) = \frac{\delta s_{ij}}{2\mu} + \delta t H s_{ij} \tag{4.53}$$

where H is a measure of the creep strength of the material. The shear modulus could then in the elastic calculation be replaced by a reduced value G where:

$$G = (2\,\delta t H + \mu)^{-1} . \tag{4.54}$$

This formulation is straightforward if we are dealing with a linear viscous material but generally creep is non-linear. If creep is described by equation (4.11) then some means of linearising the problem must be found. For some cases all that is necessary is to use estimated values for the von Mises stress i.e.

$$\dot{\gamma}_{ij} = \frac{3}{2}\frac{f(\dot{\sigma_e})}{\dot{\sigma_e}} s_{ij} \tag{4.55}$$

where $\dot{\sigma}'_e$ is an estimated value of $\dot{\sigma}_e$ from a previous calculation. Once implemented the calculation can be iterated to convergence. This procedure does not work well if creep is very non-linear in character. It is more satisfactory to make a first order Taylor expansion (Matthews 1985)

$$\dot{\gamma}_{ij} = \frac{3}{2}\left[f(\dot{\sigma_e})\, s_{ij} - \frac{df(\dot{\sigma_e})}{d\dot{\sigma_e}}\,\dot{\sigma_e}\, s'_{ij} + \frac{3}{2}\frac{df(\dot{\sigma_e})}{d\dot{\sigma_e}}\frac{s'_{ij}}{\dot{\sigma_e}}\,(s'_{kl}\, s_{kl})\right]. \tag{4.56}$$

This looks complex but it is straightforward to introduce into finite difference or finite element procedures. In some cases the initial stresses at the start of the step can be used for $\dot{\sigma}_e$' but for most non linear creep problems a predictor corrector method is necessary with iteration to convergence. The use of the softened stiffness method enables long time steps to be taken for the most extreme cases once the initial transients have settled. Work hardening plasticity using the Reuss equations can be implemented in a similar manner (Ford 1988).

When plastic and creep strains become very large the usual elastic methods become less adequate. The infinitesimal strain approximation becomes invalid and also the stiffness matrix, or the equivalent matrix of coefficients in the finite difference approximation, becomes increasingly ill-conditioned. This arises because as volume conserving inelastic deformation becomes dominanat the effective Poisson's ratio tends to 0.5 and the (1-2v) term in the constitutive relations make the stiffness matrix go singular. In order to overcome this problem Herrmann (1965) proposed that the continuity equation is added explicitly to the set of equations and a new variable, σ, is added to the displacements for solution. Firstly we modify the stress equilibrium equation (3.1) to separate the hydrostatic stress component:

$$\sigma_{,i} + s_{ij,j} = F_i . \tag{4.57}$$

The continuity or volume conservation condition is given by:

$$\varepsilon_{kk} - \varepsilon^{\circ}_{kk} - \frac{\sigma}{K} = 0 \tag{4.58}$$

where ε°_{kk} are prior volume strains such as those arising from thermal expansion. The constitutive relation is given by:

$$s_{ij}/2G = \varepsilon_{ij} - \varepsilon_{ij}^{o} - \delta_{ij}\,\sigma/3K, \tag{4.59}$$

where G includes the effect of inelasticity and the prior strains $\varepsilon_{ij}^{o} - \varepsilon_{kk}^{o}/3$ include any strain components arising from the linearisation of the inelastic constitutive relation. Substituting eq. (4.59) into (4.57) gives:

$$(1 - 2G/K)\,\sigma_{,i} + 2G(u_{i,kk} + u_{j,ij}) = F_i + 2G\varepsilon_{ij,j}^{o}. \tag{4.60}$$

A variational principle can now be generated from eqs. (4.57) and (4.60) using Eulers theorum:

$$\delta\chi = \delta\int_v \left[G\,\varepsilon_{ij}(\varepsilon_{ij} - \varepsilon_{ij}^{o}) + (1 - 2G/3K)\,\sigma(\varepsilon_{kk} - \varepsilon_{kk}^{o}) - (\sigma^2/2K) - u_i F_i\right] dv + \int_{s'} \sigma_{ij}^{*}\, n_j\, u_i\, ds. \tag{4.61}$$

Herrmann's method is implemented by provided a trial function for σ as well as **u**. For one dimensional problems this is straightforward and has formed the basis of the TRAFIC fuel performance code (Matthews 1984). A linear piece-wise trial function for displacements is usually paired with a point discontinuous function for σ. Higher order displacement functions would be matched by a function for σ one order lower. The problem is not so simple for two and three dimensional problems. Adding the constraint of the continuity equation reduces the number of degrees of freedom of the system. In practice using point values of σ with linear triangular elements over constrains the problem. This has been analysed by Treharne (1971) in terms of Lagrange multipliers. The solution is to provide more degrees of freedom. This can be done by either using higher order trial functions for **u** or by grouping elements and then fixing σ as a point value.

For comparison with eq. (3.60) the variational principle for the axisymmetric plane strain example is given by:

$$\delta\chi = \delta\int_a^b \left\{G\left[\left(\frac{du_r}{dr}\right)^2 + \left(\frac{u_r}{r}\right)^2 - 2\,\frac{du_r}{dr}\,\varepsilon_{rr}^{o} - \frac{2u_r}{r}\,\varepsilon_{\theta\theta}^{o}\right] + \left(\frac{1 - 2G}{3k}\right)\left[\sigma\left(\frac{du_r}{dr} + \frac{u_r}{r} + W - \varepsilon_{kk}^{o}\right) - \frac{\sigma^2}{2k}\right] - u_r F_r\right\} 2\pi r\,dr + \delta\,2\pi\left[-a u_r(a)\,P_i + b u_r(b)\,P_o\right] = 0. \tag{4.62}$$

Another consideration is the effect of large strains on the analysis. Imposing the full compatibility relation (3.4) is not practical. The most effective solution is to reformulate the analysis in terms of displacement increments instead of displacements and to then adjust the positions of nodes during deformation. This technique is also more satisfactory, from the point of view of accounting for the change in boundary conditions from large strains, than iterative technqiues.

4.4 More Complex Deformation Models

The inelastic behaviour of real materials is unfortunately rather more complex than the simple forms we have used to illustrate the analysis of the deformation of structures. The complexities are of two sorts: the way the material deforms evolves during deformation due to changes in the material microstructure; and the model of isotropic response to multiaxial and changing stress is at best an approximation but for many materials misses important aspects of their behaviour.

One problem that must be faced is the limitations imposed by available measurements of deformation on the material of interest. Measurements tend to be of two kinds: (i) tensile tests at fixed strain or displacement rates; and (ii) creep tests under constant load, often done coincidentally as part of creep rupture time determination. The results are usually forced to fit well established relationships that reflect the nature of the testing more than the applications to which the results are applied. Sometimes the results are expressed in ways that prevent consistant application. Creep effects are often confused with tensile tests particularly if the testing is done for slow strain rates at high temperature.

An important example of the difficulty in implementing experiment deformation expressions is primary creep. Creep expressions are often fitted (see section 1.3) to expressions of the type

$$\varepsilon_{creep} = a_p t^{1/3} + \dot{\varepsilon}_{ss} t \tag{4.63}$$

where a_p is experimentally determined primary creep coefficient and $\dot{\varepsilon}_{ss}$ is the secondary or steady state creep rate, both are functions of stress and temperature. For a constant load and temperature there is no problem and (4.63) can be used to calculate the creep strain in structures. Most problems have loads that vary, often in complex ways, and temperature changes also have to be accommodated. To overcome this we would use a strain rate applicable to conditions for a particular time. Unfortunately there is no unique way of doing this. We could directly differentiate (4.63) to get a creep rate:

$$\dot{\varepsilon}_{creep} = a_p/(3t^{2/3}) + \dot{\varepsilon}_{ss}. \tag{4.64}$$

This gives a 'time hardening' law. Alternatively we could imagine that the accumulated strain was a better guide to determining the creep rate, as time is more usually associated with softening or recovery processes. Substituting eq. (4.63) in (4.64) we get a 'strain hardening' law:

$$\dot{\varepsilon}_{creep} = a_p^3/\varepsilon^2 + \dot{\varepsilon}_{ss}. \tag{4.65}$$

Which strain is used is not clear, but the accumulated primary creep rate is the usual measure. To show that the difference between time hardening and strain hardening matters, we demonstrate the effect of incrementing the applied stress after a period of deformation at constant load in Fig. 4.4. A creep law where a_p and $\dot{\varepsilon}_{ss}$ are proportional

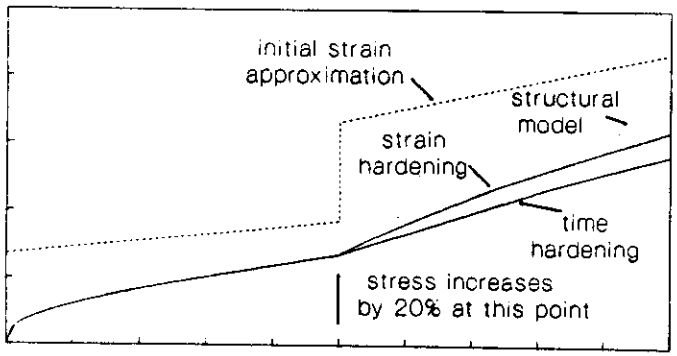

Fig. 4.4

to σ_a^4 was used and it was assumed that there was no significant time independent plastic strain. The time hardening law predicts significantly lower strains than the strain hardening law. For calculations where an upper limit to the creep strain is required for design purposes, the maximum value of the primary creep strain can be estimated for a particularly stress and temperature and this value is applied as an instantaneous initial strain every time the conditions change. This is also shown in Fig. 4.4 and unless times are long this substantially overestimates the creep strain.

The only real solution to the problem is to formulate a reliable model incorporating additional structural variables, as was discussed in section 4.1. The simplest isotropic model with a single structural varaible would be of the form:

$$\dot{\varepsilon}_{creep} = f(\sigma_a, T, \alpha), \tag{4.66}$$

and

$$\dot{\alpha} = \dot{\varepsilon}\, h(T, \alpha) - r(T, \alpha) = \psi(\sigma_a, T, \alpha) \tag{4.67}$$

where α is the structural variable, h is the hardening rate and r is the recovery rate. Such a model which gives $\dot{\varepsilon} \propto \sigma_a^4$ was chosen to reproduce the primary creep behaviour under steady load of the other example. The response of this structural model is to the load increment is also shown in Fig. 4.4. The response of the structural variable to the change in load produces a significantly larger initial strain rate and total strain than the time and strain hardening assumptions. This is in general in agreement with experiment. The main disadvantage with this approach is that much more experimental information is required to characterise a structural model and previously gathered information is usually inadequate.

Simple structural models have a disadvantage in that they cannot describe a variety of effects, where the strain rate is not co-axial with the load. These effects include reverse deformation on removing the load (anelasticity), the Bauschinger effect where the material has a lower yield stress on reversing the load and other changes in the yield surface when the stress axes are rotated. One type of model that accounts for such, describes a kinematic hardening, where the yield surface is displaced relative to stress system, in addition to changes in the yield surface normally associated with isotropic hardening (Robinson, Pugh and Corum 1976). In this model the von Mises stress and the stress deviants are replaced by new quanties:

$$s^{*}_{ij} = s_{ij} - s^{o}_{ij}$$

and

$$\sigma^{*2}_{e} = \frac{3}{2} s^{*}_{ij} s_{ij} - \alpha^{2}$$

(4.68)

where s^{o}_{ij} is a tensor internal stress deviant and α is an isotropic salar structural parameter with dimensions of stress. The multiaxial creep rates are now given by:

$$\begin{aligned}
\dot{\varepsilon}_{ij} &= f(\sigma^{*}_{e}, T)\, s^{*}_{ij}/\sigma^{*}_{e}, \\
\dot{s}_{ij} &= \dot{\varepsilon}_{ij}\, h_{o}(s^{o}_{ij}\, s^{o}_{ij}) - s^{o}_{ij}\, r_{o}\,(s^{o}_{ij}\, s^{o}_{ij}, T), \\
\dot{\alpha} &= f(\sigma^{*}_{e}, T)\, h_{\alpha}\,(\alpha) - r_{\alpha}\,(\alpha, T).
\end{aligned}$$

(4.69)

There are many variations on this type of model, but as yet none of the available models have been put on a sound physical basis.

Krieg (1977) describes how these types of models may be used in structural mechanics calculations. The large number of variables involved make this a far from simple taks. It is frequently necessary to use a fully implicit calculation, in which case the various rate equations describing the evolution of the various structural parameters are partly solved using the Newton-Raphson approximation and the solution completed after the structural calculation is done and the stresses are known. To see how this is done we will look at the simpler model given by eqs. (4.66) and (4.67) (Matthews 1983) for multiaxial stresses eq. (4.66) becomes:

$$\dot{\varepsilon}_{ij} = f(\sigma_{e})\, s_{ij}/\sigma_{e} \text{ and } \dot{\varepsilon}_{e} = f(\sigma_{e}).$$

(4.70)

During the calculation we have to solve for both the stresses and α. First of all we define Ψ from eq. (4.66):

$$\Psi = \alpha' - \alpha^{\circ} - \delta t\, \Psi(\sigma'_{e}, \alpha')$$

(4.71)

which is the residual from the forward difference approximation from the estimates of α and σ_{e} indicated by the primes. A new estimate α is found from the Newton-Ralphson approximation:

$$\alpha = \alpha' - \left[\Psi - \frac{1}{\sigma'_{e}} \frac{\partial \Psi}{\partial \sigma'_{e}} \left(\frac{3}{2} s_{kl}\, s_{kl} - \sigma''^{2}_{e}\right) \Big/ \frac{\partial \Psi}{\partial \alpha}\right].$$

(4.72)

A Taylor expansion to first order in α and s_{ij} is made for the strain rate (4.70) and (4.72) is then used to eliminate α:

$$\begin{aligned}
\dot{\varepsilon}_{ij} &= f(\sigma'_{e}, \alpha')\, s_{ij} - s'_{ij} \frac{\partial f}{\partial \alpha'} \Psi \Big/ \frac{\partial \Psi}{\partial \alpha'} \\
&\quad + \left(\frac{\partial f}{\partial \sigma'_{e}} - \frac{\partial f}{\partial \alpha'} \frac{\partial \Psi}{\partial \alpha'}\right)\left(s'_{ij}\, \sigma'_{e} - \frac{3}{2} \frac{s'_{ij}}{\sigma'_{e}} s_{kl}\, s_{kl}\right).
\end{aligned}$$

(4.73)

Eq. (4.73) can be used in the same way as eq. (4.56) to construct the stiffness matrix of a finite element calculation. The value is then determined from eq. (4.72) once the stresses have been calculated. When more than one structural variable is used or when the structural variables are tensors a set of equations like (4.72) as used to form a Jacobian matrix. This can be very large and some simplification is possible by finding scalar quantities to apply the Newton-Raphson approximation to (Kreig 1977).

One aspect not yet discussed is anisotropy of properties. This is usually related to intrinsinc anisotropy in the crystal structure of the material, although anisotropic microstructures may develop in cubic materials with high isotropy and these may result in anisotropic properties. The von Mises stress for an anisotropic material is given generally by (Hill 1950):

$$\begin{aligned}
\sigma^{2}_{e_a} &= F(\sigma_{11} - \sigma_{22})^{2} + G(\sigma_{22} - \sigma_{33})^{2} + H(\sigma_{33} - \sigma_{11})^{2} \\
&\quad + 2L\sigma^{2}_{12} + 2M\sigma^{2}_{23} + 2N\sigma^{2}_{31}
\end{aligned}$$

(4.74)

where F, G, H, L, M and N are anisotropic coefficients that have to be determined experimentally. In polycrystalline anisotropic materials the macroscopic anistropy results from *texture* of the crystal structure that results from the fabrication of the component. During deformation the texture will change as individual crystals rotate as they shear. The description of this complicated topic is outside the scope of these lectures. In applying eq. (4.74) it is found that not only are the strain rates different in different directions, but the strain rates are not co-axial with the load. From (4.8) we can find the components of strain for creep in an anisotropic material:

$$\dot{\varepsilon}_{11} = (3/2)f(\sigma_{ea})[(F+H)S_{11} - FS_{22} - HS_{33}]/\sigma_{ea}$$
$$\dot{\varepsilon}_{22} = (3/2)f(\sigma_{ea})[(F+G)S_{22} - FS_{11} - GS_{33}]/\sigma_{ea}$$
$$\dot{\varepsilon}_{33} = (3/2)f(\sigma_{ea})[(G+H)S_{33} - HS_{11} - GS_{22}]/\sigma_{ea}$$
$$\dot{\varepsilon}_{12} = (3/2)f(\sigma_{ea})L\,S_{12}/\sigma_{ea}$$
$$\dot{\varepsilon}_{23} = (3/2)f(\sigma_{ea})M\,S_{33}/\sigma_{ea}$$

and

$$\dot{S}_{31} = (3/2)f(\sigma_{ea})N\,S_{31}/\sigma_{ea}.$$

(4.75)

Reuss equations for plastic flow of anisotropic materials can be formulated in a similar manner.

Another complication that arises is the inter-dependence of the shear deformation and volume changes in materials that contain cavities. We have already seen the form of the flow rule for such cases given by eq. (2.50). This type of flow rule can be used to produce creep and plastic flow expressions that are dependent on both the von Mises and hydrostatic stresses.

Finally we should mention the effect of cracking on structural mechanics calculations, although not a plastic phenomenon it does lead to inelastic deformations. The propagation of individual cracks needs the use of a crack tip element, in finite element calculations, that can cope with the stress singularity at the crack tip. Whether the crack propagates or not depends on whether the stress intensity factor reaches a critical value, see section 5.2. Of more interest here are structures containing materials that cannot support large tensile loads, such as ceramics, concrete or rock. To model these types of material in a finite element scheme it is necessary to modify the stiffness matrix in some way. Methods that use initial stresses or strains are never really satisfactory. There are two main ways of introducing cracked regions in a continuum manner. The first is to simply make the elastic moduli depend on the sign of the stress. A scheme must be devised to change the [D] matrix (3.66) whenever a normal stress component changes sign, the Young's modulus is set to a very small value for elements of the [D] matrix which are positive. This method is very simple to implement and causes the least disturbance to the rest of the finite element algorithm, but it has the disadvantage of not giving directly a value for the internal voidage generated by the cracking. A more satisfactory method is to set up special elements for the cracked material, which set the appropriate normal stress to zero or some reference value when a cracking criterion is transgressed. This provides additional degrees of

freedom to the element which are eliminating by calculating the volume occupied by the cracks when open. Both methods are stable when used with a reliable system for setting the state of each element and convergence is guaranteed for linear elastic problems. Coping with simultaneous cracking and yield is something of a nightmare even for one dimensional calculations.

Lecture 5 Failure of Structures

5.1 Ductile Failure

Materials that deform easily by plastic or creep deformation fail at high strain. The *ductility* may be high over the whole specimen, the extreme case is *superplasticity*, or may be localised by extreme necking of the structure for tensile loads, by shearing off along a slip band or by ductile tearing. When voids or precipitates are present the ducility may be even more local with small scale necking, tearing and slipping between the heterogeneities.

Let us look at failure during time independent plasticity first. It is simple to establish the failure conditions for a perfectly plastic or an elasto-plastic material. As soon as plastic flow propagates through the cross-section of the structure failure follows. The flow is very unstable and any minor fluctuation in the load bearing area or the material properties will result in local failure. The local ductility may be infinite but the averaged strain to failure is small. Fortunately real materials display some degree of work hardening which stabilises the deformation. To illustrate this let us look at the deformation of an idealised work hardening material with a stress strain relation:

$$\varepsilon_a = (\sigma_a/\sigma_p)^{1/m} \tag{5.1}$$

where ε_a is the plastic strain in the direction of the load, σ_p is a materials constant and m is the work hardening coefficient. These properties are measured using true stress and strain values. Let us now take a bar of the material with a uniform cross sectional area A and apply a dead load which provides a force F. If the original length of the specimen is L_O and after loading L, the true strain is given by $\ln(L/L_O)$ and the true stress is given by FL/A_OL_O where A_O is the original specimen cross sectional area. Substituting into eq. (5.1) we get the force displacement relationship

$$F = (\sigma_p A_o L_o/L)[\ln(L/L_o)]^m . \tag{5.2}$$

If we differentiate F with respect to L we find that the rate of change of displacement with force is infinite when the true strain is equal to m or the engineering strain is equal to exp(m)-1. At this point the deformation becomes unstable (see Fig. 5.1 which illustrates this for parabolic hardening i.e. m=0.5).

It is clear how this instability arises for dead loading, but the criterion is similar for a strain controlled load. Let us assume that our bar is long compared to its width and that at some point there is a small defect that reduces the load bearing area by $(1 - \delta)$. If this defect is short enough to not too greatly affect the overall extension of the bar the force on the defected region is controlled by the average strain ot the bar. We thus have a fixed loading condition at the defect and the instability condition will apply when the strain reaches a value of m. We can now determine the strain in the undefected part of the bar as the load is the same in the defected and undefected regions:

$$\frac{F}{\sigma_p A_o} = m^m \exp(-m)(1-\delta) - \varepsilon_f^m \exp(-\varepsilon_f) \tag{5.3}$$

We may solve eq. (5.3) to find the uniform strain to failure ε_f by using a simple Newton-Raphson procedure (see Fig. 5.2 for an example where m=0.5). The uniform failure strain is relatively insensitive to the size of the original defect and in the limit of $\delta \rightarrow o$, ε_f becomes m. Thus any minor defect in the cross sectional area will lead to necking and local failure.

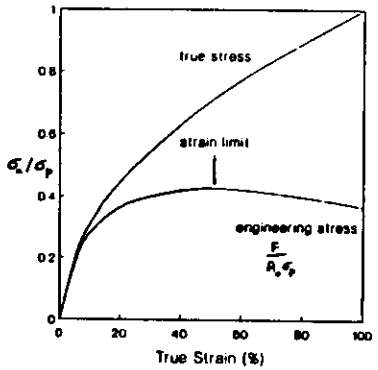

Fig.5.1

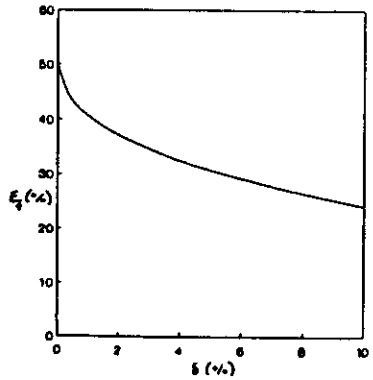

Fig.5.2

The degree of sensitivity to defects is strongly dependent on the work hardening coefficient. Fig. 5.3 shows the effect of m on the uniform strain of a rod with a defect of just 1% of the area ($\delta = 0.01$). The uniform strain to failure decreases faster than

the strain to initial the instability (m) as m is decreased. Notch sensitivity is not just a problem for brittle materials, but also for materials with minimal work hardening. It should be noted here that the strain required to induce plastic instability is not the local strain at the failure site. This could be very high and some materials can exhibit necking down to essentially a point.

Cold working is well known for decreasing the ductility of a metal and the reasons for this can be easily shown repeating the stability calculation using the following stress-strain relation instead of eq. (5.1):

$$\varepsilon_a = (\sigma_a/\sigma_p)^{1/m} - \varepsilon_{cw} \tag{5.4}$$

where ε_{cw} is the cold work strain. The plastic instability is found to start at $m - \varepsilon_{cw}$ rather than m. Similarly other forms of hardening, such as solute hardening also decrease ducility, e.g. for a stress-strain relation of the type:

$$\varepsilon_a = [(\sigma_a - \sigma_1)/\sigma_p]^{1/m} \tag{5.5}$$

where σ_1 is the new flow stress arising from the hardening. The two types of hardening from eq. (5.4) and (5.5) are compared in Fig. 5.4, where the value of the cold work was taken to be 20%, σ_1 was chosen to give the same yield stress as the cold worked case and m = 0.5. The ductility of the material obeying eq. (5.5) is smaller than the cold worked case, but the cold worked material is more sensitive to the size of the defect.

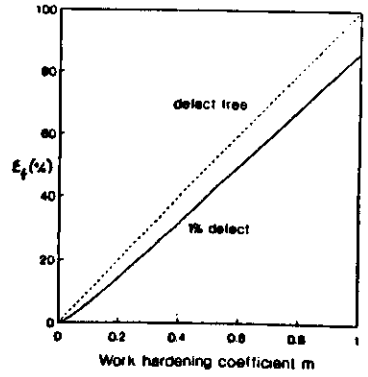

Fig.5.3

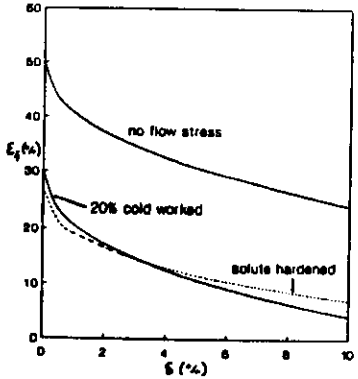

Fig.5.4

Ductile failure under creep deformation is defined by the time a structure takes to fail. For a perfectly ductile material even though the strain to failure is infinite the time to failure is finite. This can be expressed in closed form for simple power law creep of the type:

$$\dot{\varepsilon}_s = B\sigma_s^n \tag{5.6}$$

Returning to our bar of uniform cross section and applying a dead load F the deformation rate is:

$$\dot{L}/L = B(FL/A_oL_o)^n \tag{5.7}$$

The time to failure can be found by integrating eq. (5.7) for L between L_o and ∞ :

$$t_f = \frac{1}{B}\left(\frac{A_oL_o}{F}\right)^n \int_{L_o}^{\infty} \frac{dL}{L^{(n+1)}} = \frac{1}{nB(F/A_o)^n} = \frac{1}{n\dot{\varepsilon}_{so}} \tag{5.8}$$

where $\dot{\varepsilon}_{so}$ is the creep rate in the original configuration. This relationship was first pointed out by Hoff (1953).

The Hoff time to failure is very similar to the empirical observation by Monkman and Grant (1956) that the product of the steady state creep rate and time to failure is approximately a constant for a particular material, i.e.

$$\dot{\varepsilon}_s t_f = C \tag{5.9}$$

where C is in the range 0.1 to 0.3. As the creep index of most metals and alloys (see section 1.3) is between 3 and 7, eq. (5.8) and (5.9) are essentially identical. For any material with significant ductility in creep, the time to failure is determined by the plastic instability. This can be seen by integrating eq. (5.7) to a finite L:

$$t_f = [1-\exp(-n\varepsilon_s)]/n\dot{\varepsilon}_{so} \tag{5.10}$$

In Fig. 5.5 we plot $t_f\dot{\varepsilon}_{so}$ against failure strain for different values of n.

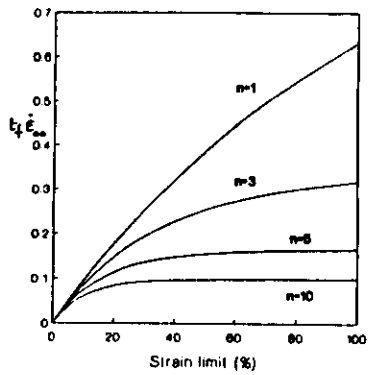

Fig.5.5

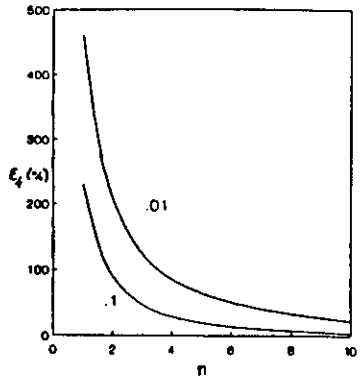

Fig.5.6

The sensitivity of ductile creep failure depends on the stress sensitivity of the creep. Taking our example of a long bar with a defect reducing the cross sectional area by $(1-\delta)$ we find a new Hoff failure time of

$$t_f = (1-\delta)^n/n\dot{\varepsilon}_{so} \tag{5.11}$$

If eq. (5.10) is equated to eq. (5.9) an estimate can be made of the uniform failure strain away from the defect at the time of failure:

$$\varepsilon_f = (1/n)\ln[1/[1-(1-\delta)^n]] \tag{5.12}$$

The uniform failure strain is plotted as a function of m for a 1% and a 10% defect in Fig. 5.6). It is clearly seen that ε_f is highest for low n and that for n=1 the failure strains are extremely large. This is the basis of superplastic deformation. However, other conditions have to be fulfilled and in particular the formation of cavities on grain boundaries has to be inhibited. Superplasticity is frequently found in materials where there is a second phase that prevents grain growth, thus enabling diffusive creep mechanisms to operate, and also lubricates the grain boundaries to permit grain boundary sliding.

The criteria for instability during work hardening and creep deformation can also be derived for thin cylindrical and spherical shells. These only differ from the

results for our bar example by a geometric factor. For example the Hoff time to failure for a pressurised tube is $t_f = 1/2n\dot{\varepsilon}_{so}$ where $\dot{\varepsilon}_{so}$ is the initial circumferencial strain rate from the pressure. The analysis of thick shells and other more complex configurations such as the bending of prismatic beams is more difficult. Odqvist (1974) gives some examples for the simple power law creep expression and also accounting for primary creep approximated by work hardening deformation. Fortunately elasticity can be neglected in these problems as the strains are high.

Let us briefly look at the effect of adding work hardening deformation to the creep of a bar under dead loading. Combining the eqs. (5.1) and (5.6) we get the constitutive relation:

$$\dot{\varepsilon}_s = \frac{d}{dt}\left(\frac{\sigma_s}{\sigma_p}\right)^{1/m} + B\sigma_s^n \quad . \tag{5.13}$$

For a fixed load F at any time during the deformation

$$\frac{1}{L}\frac{dL}{dt} = \frac{d}{dt}\left(\frac{FL}{A_o L_o \sigma_p}\right)^{1/m} + B\left(\frac{FL}{A_o L_o}\right)^n \tag{5.14}$$

which, as only L is varying during deformation, may be re-written as:

$$\frac{1}{L}\frac{dL}{dt} = \frac{B(FL/A_o L_o)^n}{[1-(1/m)(FL/A_o L_o \sigma_p)^{1/m}]} \quad . \tag{5.15}$$

Failure will thus occur when

$$\left(\frac{FL}{A_o L_o \sigma_p}\right)^{1/m} = m \tag{5.16}$$

i.e. when the previously established plastic instability criterion is reached. Integrating (5.14) to obtain the time to infinite extension we find:

$$t_f = \frac{1}{nB\sigma_{so}^n}\left\{1 - \frac{n}{(nm-1)}\left(\frac{\sigma_{so}}{\sigma_p}\right)^{1/m}\right\} + \frac{1}{n(nm-1)m^{nm}B\sigma_p^n} \tag{5.17}$$

where σ_{so} is the load in the initial configuration and which holds provided n>1/m. An example of the failure time appropriate for annealed 316 stainless steel at 700°C is given in Fig. 5.7 where m=0.5, $\sigma_p = 10^3$ MPa , n=6 and $B=10^{-16}$ MPa^{-1}hr^{-1}. This simple model reproduces many of the observations in creep rupture tests, but tends to over-estimate the failure time at low stress as it neglects other failure processes, see section 5.4.

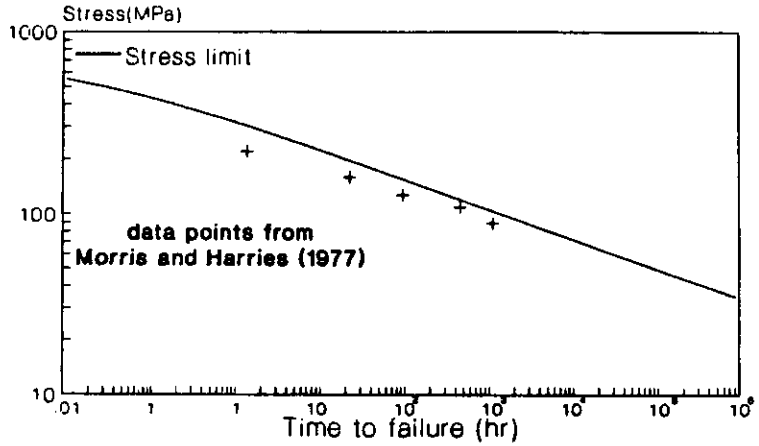

Fig.5.7

Calculation of failure time during creep deformation in real situations often means that the applied load and the temperature change. To cope with this Robinson (1952) proposed a cumulative damage law. The failure time is calculated for the current conditions and this is used in the integral:

$$D_f = \int_0^t \frac{dt}{t_f} \quad . \tag{5.18}$$

When D_f reaches 1 the failure time for the varying conditions is found. This procedure is valid for simple ductile creep problems and is widely used for both empirically and phenomenologically based rupture expressions. Approximations are frequently used in terms of reference stresses (see section 4.2) to assess creep ductile failure, as finite element calculations are very expensive with the large strains required to reach stability limits. Fortunately internal stresses, from thermal gradients etc, have little effect on failures of these types.

So far we have only discussed stability under tensile loads. The most frequent problem encountered is the buckling of beams and shells in structures under compressive loads. The main difference from the tensile load problems is that elastic deflections may be large; in fact for most structures the elastic buckling limit provides the main design constraint even though plastic deformation occurs during the collapse. A simple description of elastic buckling may be found in Crandall, Dahl and Lardner (1978). Any elastic structure, with an aspect ratio greater than 1, has a critical load for which it will buckle, due to growth of small disturbances in its configuration. The size of the critical load depends on the way the structure is constrained, but the values all have the form:

$$F_{crit} = \alpha\pi^2 EI/4L^2 \qquad (5.19)$$

where I is moment of inertia of the structure section and α is constant. Typically α=1/4 for a beam free at one end and rigidly supported at the other, α=1 for a beam hinged at both ends and α=4 for a doubly supported beam.

Plastic deformation and creep tend to concentrate the deformation at particular points in the structure forming plastic hinges. This type of behaviour becomes more acute in materials with low work hardening coefficients or large creep stress indexes. The main role of creep in buckling problems is to enhance any pre-existing defects until the elastic or plastic buckling limit is reached. The time to failure in these cases is controlled by an expression similar in form to the creep tensile failure i.e.

$$t_f \alpha\ 1/(n-1)F^n \qquad (5.20).$$

The derivation of limits in these cases is not simple and depends strongly on the shape of the structure cross-section and the nature of the initial defect.

5.2 Fracture

In section 2.7 we have described how crack propagation criteria can be constructed for truly brittle materials. Real materials, however can fail by crack propagation when they exhibit significant plasticity. We have already mentioned Irwin's (1948) proposal that an effective surface energy can be used to account for the extra energy dissipated in moving a crack in plastic material, but such an approach is not completely satisfactory. There are three main problems that have to be addressed:

(i) plastic constitutive relations invalidate the linear elastic analyses that are the basis of conventional fracture mechanics; (ii) the processes that control crack advances are on a small scale at the crack tip where macroscopic plastic relations do not hold; and (iii) in many engineering structures the region affected by plastic deformation extends across the whole section of the structure, i.e. is not confined to the crack tip, so some way of reconciling plastic collapse criteria with fracture criteria is needed. In recent years there has been a lot of progress in resolving these three problems. We will address them in order in this section.

To illustrate the effect of plasticity on cracks two types of continuum models are often used to represent deformation near the crack tip. A fuller discussion of this subject can be found in Rice (1968). The first is to assume that the material is perfectly plastic with a yield stress σ_Y. For small scale yielding this produces a plastic zone ahead of the crack tip with a diameter D_0 (Rice 1968):

$$D_o \cong K^2/\alpha\pi\sigma_Y^2 \qquad (5.21)$$

where α is 1 for a shear crack and α=4 for a tensile crack. Inside the plastic zone the stress is uniform and outside the plastic zone the elastic stress field is shifted as if the crack were extended by half the plastic zone diameter and lies at the centre of the plastic zone. A crack opening displacement may also be estimated from the plastic strain at the tip of the crack, see Fig. 5.8:

$$\delta_{COD} \cong K^2/\pi E\sigma_Y . \qquad (5.22)$$

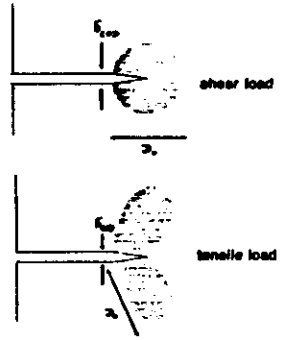

Fig.5.8

This quantity, as will be seen, is of some importance in the application of fracture mechanics with plasticity. The shape of the plastic zone will be dependent on the type of loading for shear loading mode III the plastic zone is approximately spherical but for tensile loading mode I the plastic zone is lobed as the maximum shear stresses are at 45° to the crack tip.

The second is to assume that the material work hardens, characterised by a work hardening index m (as in eq. 5.1). Solutions to this problem have not been found, but Rice (1968) has investigated a related problem of non-linear elasticity. In linear elasticity both the stress and strain fields vary as $r^{-1/2}$ from the crack tip. For the non linear problem the stress field varies as $r^{-[m/(1+m)]}$ and the strain field as $r^{-[1/(1+m)]}$ where m usually lies betwen 0 and 1. In an elasto-plastic analysis the size of the zone affected by plasticity is very sensitive to the magnitude of the external loading. In tensile loading the magnitude of the tensile stress ahead of the crack is very sensitive to the work hardening index. For lightly work hardened material the tensile stress is greatly reduced.

When the plastic region around the crack tip is small compared to both the crack and structural section sizes, it has in the past been assumed that LEFM can still be applied and that values of the fracture toughness K can be determined by elastic calculations. In many cases, however, yielding is on a large scale and the use of K in this way is not easily justified. In order to over come this Rice (1968a) suggested the use of a path integral J, first defined by Eshalby (1956), as a quantity that can be reliably measured experimentally and can be used to define a crack propagation criterion with plasticity. J can be described as the crack extension force or the crack energy release rate and has dimensions of energy per unit area. The path integral defining J is:

$$J = \int_{\Gamma} (1/2\, \sigma_{ij}\, \varepsilon_{ij}\, dx_2 - T_i \delta x_1\, ds) \qquad (5.23)$$

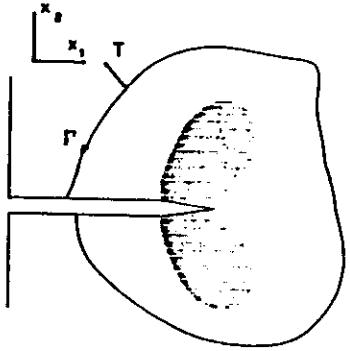

Fig.5.9

where Γ represents some arbitrary path outside the plastic region, (see Fig. 5.9), T_i are the components of the force normal to the path from the applied stress and U_i are the resulting displacements. For purely elastic materials J and the fracture toughness can be directly related:

$$J = \frac{(1-\nu^2)}{E}(K_I^2 + K_{II}^2) + \frac{K_{III}^2}{2\mu} . \qquad (5.24)$$

The path integral definition of J is not directly useful, but it can easily be shown (Rice 1968) that:

$$J = dU/da \qquad (5.25)$$

where U is the potential energy per unit length of crack, i.e. J is the energy release rate as the crack ends. Eq. (5.24) assumes that the applied force does no work, which means that any displacements are restrained during crack extension. In practice this energy release rate can be determined experimentally from the load-displacement curve of a tensile test in a deeply cracked specimen:

$$J = \alpha \int F dL/[(W-a)b] \qquad (5.26)$$

where α is a function of the specimen geometry, e.g. α=2.56 for a compact tensile test specimen, and b is the specimen thickness (Willis, 1980). The compact test specimen has a notch and a crack is introduced by fatigue. The same test can also provide a value of the critical value of J for crack growth, J_{IC} for mode I loading.

Another approach to establishing an experimental measure of fracture toughness is by the measurement of crack opening displacements. This has the advantage, in a well constructed test, of not requiring the separate monitoring of the crack extension. For small scale yielding J and the δ_{COD} are related by (Rice 1968):

$$\delta_{COD} = J/\sigma_Y . \qquad (5.27)$$

So far we have only discussed how a crack propagation criterion may be established for a material that deforms plastically. The continuum models have not provided us with a method of determining when a material will be ductile or when it will be brittle or how J_{IC} or K_{IC} are related to intrinsic properties of the material. The reason for this is that the underlying processes that control crack propagation take place at the crack tip on an atomic scale

$$\delta_{COD} = Nb_c \qquad (5.28)$$

where N is the number of dislocation and b_c is the component Burgers vector normal to the crack plane. The long range stress fields of the dislocations shield the crack tip

from the external stress. The problem is a difficult one, as the size of the dislocation interaction has to be solved self consistenly, as the dislocation redistributes in the stress field the crack. The local force balance that determines whether the crack propagates or not is still the Griffith value, i.e. $(2\mu\gamma_i)^{1/2}$, see section 2.7. Thomson (1978) finds an estimate for the fracture toughness of:

$$K_c^2 = 2\pi (2\gamma_i \mu/\pi)^{(1+m)/2m}/(c\sigma_Y^2)^{(1-m)/2m} \qquad (5.29)$$

where c is the cut of distance for the closest dislocation to the crack. The important point to note is that even for a material with substantial plasticity the fracture toughness is still proportional to a power of the surface energy or some other parameter controlling atomic cohesion. This has important consequences in the impact of environmental or local chemical changes on fracture.

Our experience of real materials is that some exhibit ductile behaviour with significant global plastic deformation and some are brittle with no significant plastic strain. In deciding whether a material is ductile or brittle there are two classes of behaviour: (i) the material may be able to fracture by crack propagation but there are no defects of sufficient size to allow crack before bulk yield; or (ii) the material may not be able to sustain crack propagation, rather the material tears plastically at defects with large energy dissipation. The first category covers bcc metals including structural materials such as low alloy steels. Whether such materials are brittle or ductile in normal operation depends on both temperature and microstructure. A lower limit to the defect size can be made with the material grain size. Local deformation in individual grains can occur before yield propagates over the material (see section 1.2). Pile-ups of dislocation at grain boundaries can generate wedge cracks that form crack nuclei (Stroh 1954) or intersecting slip bands can also nucleate cracks at the grain size (Cottrell 1958). The yield stress is weakly dependent on the grain size so we may find a criterion for brittle-ductile transition by simply equating the yield stress with the crack propagation stress and the grain size with the crack size, hence for crack propagation:

$$K_{Ic} < \sigma_Y (\pi d)^{1/2} \qquad (5.30)$$

Small grain size material is thus expected to be ductile unless larger defects are present.

A similar effect is seen with temperature in bcc metals. This is largely because the yield stress and, indirectly, the fracture toughness are sensitive to temperature. The

brittleness of materials is often evaluated using the Charpy v-notch impact test, where the energy dissipated in fracturing a small specimen is measured. Such tests on ferritic steels and other bcc alloys reveal a transition impact energy at a particular temperature, see Fig. 5.10 for the typical behaviour of a 17% Cr ferritic steel (Bagley et al 1987).

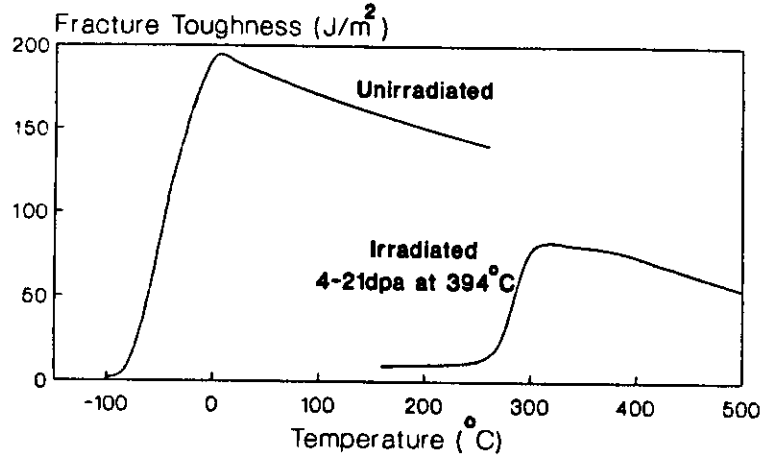

Fig.5.10

The transition temperature is sensitive to a wide range of metallurgical parameters but for nuclear reactor applications it is important as radiation hardening of the material increases the transition temperature, see Fig. 5.10. Such irradiation induced changes are themselves sensitive to the alloy composition and metallurgical state. This is important in the design of PWR pressure vessels, where problems were found in early reactors becuase of the presence of Cu as an impurity in the steels (Marshall 1982). In modern PWR pressure vessel forgings the transition temperature can increase by 30°C over the reactor life, which causes no problems during operations but care has to be taken to avoid quenching the vessel under pressure.

The second case, where under certain conditions crack propagation is extremely difficult, is relevant to many materials that are basically ductile but are strengthened by coherent precipitates etc. To identify the conditions for this type of behaviour Chan (1989) has proposed the use of the tearing modulus T_R:

$$T_R = \frac{E}{\sigma_Y^2}\frac{dJ}{da} \qquad (5.31)$$

When T_R is zero cracks can propagate freely if the fracture conditions are met. When T_R is greater than zero the crack propagates stably; the load has to be increased to continue crack growth. The crack is moved through the material by ductile tearing rather than cleavage or void coalescence ahead of the crack tip (see section 5.3), and the failure plane is not normal to the loading (for mode I) but follows the main slip direction. The conditions where this may occur are related to the local strain at the crack tip required to produce failure and is related to the critical crack opening displacement.

We now have criteria for crack propagation and for ductile failure, but often in engineering problems failure of a structure is determined by both these processes. If the defects in a structure are small the load necessary to initiate crack growth may result in the plastic deformation of the whole section. No completely rigorous approach has yet been found to the problem, but a practical solution is offered by the R6 design code developed by the CEGB (Milne and Goodall 1988). Two parameters are used to characterise the failure of a structure: (i) K_r is the crack propagation parameter which may be defined in terms of the fracture toughness

$$K_r = K_I/K_{IC} \tag{5.32}$$

or in terms of some other criterion such as J or δ_{COD} ; (ii) L_r is the plastic collapse parameter defined as

$$L_r = \sigma_{ref}/\sigma_Y \, . \tag{5.33}$$

The two parameters could be applied separately with failure occurring if $K_r < 1$ or $L_r < L_r^{max}$, with K_I and being determined by some structural mechanics calculation and L_r^{max} from investigating the plastic stability of the structure. This may not, however, be sufficiently pessimistic because of interaction between the two processes. To overcome this the failure assessment diagram (FAD) was developed. This plots K_r against L_r and a function relating the two variables defines the regions on the diagram where failure is and is not expected. Failure is determined by the relation:

$$K_r \geq f(L_r) \tag{5.34}$$

where for Option 1 of revision 3 of R6

$$f(L_r) = (1 - 0.14\,L_r^2)\,[0.3 + 0.7\exp(-0.65\,L_r^6)] \, .$$

This failure criterion, shown in Fig. 5.11, is an empirical fit for assessments of failure in structures of various configurations and is valid for a limited range of materials. The extension of the limit value along the L_r axis is due to the work hardening nature of the

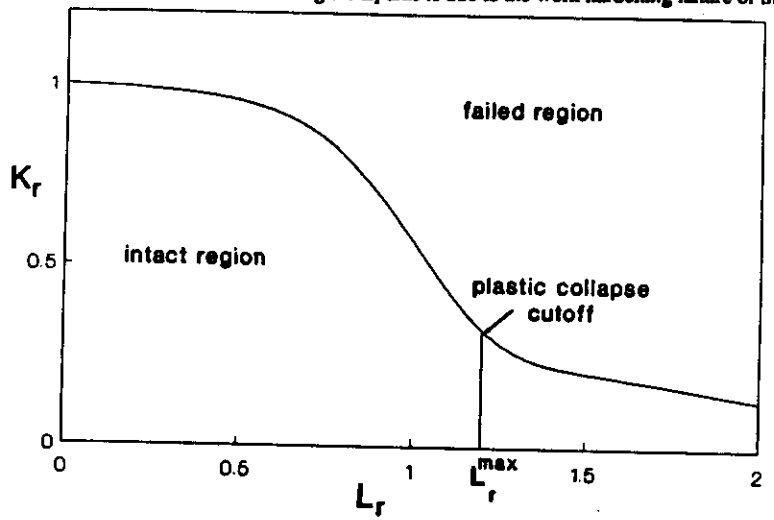

Fig.5.11

alloys and a separate L_r^{max} cut off has to be applied. Fig. 5.11 should be taken as an example, other forms of FAD are used for particular applications.

Values of K_I and σ_{ref} for use in R6 have been collected for many of the configurations found in engineering applictions (Miller 1987). Internal stresses, e.g. from thermal stress or from fabrication, create a problem as they can cause a crack to extend locally but are dissipated by the crack extension. The R6 design code sums stress intensity factors from primary loading sources and from internal stresses, but internal stresses are omitted from the determination of plastic collapse.

In assessing the failure of structures using R6 or other methods the size of defects likely to be present must be known. One way is to assume that defects are present with a size at the limit of the resolution of the non destructive testing techniques applied to the structure. This may not be sufficiently pessimistic as larger defects may be missed. To cope with this probabilistic fracture mechanics has been developed

which relates the probable distribution of defect size to the realities of testing techniques and gives the likelihood of failure for a particular load (Cameron and Temple 1988). Growth of defects, below critical size, during operation has to be anticipated; we will look at some of these mechanisms in the last three sections of this lecture.

An important concept in the area of fracture analysis is 'leak before break'. If the critical crack size, on the basis of fracture mechanics assessment for the largest load likely to be encountered, is smaller than the thickness of the wall of a pressure vessel then the vessel could fail without warning. However if the crack size is much larger than the wall thickness then the vessel will leak before it fails. Provided the growth rate of the crack during operation is slow enough for the leak to be detected then a leak before break argument can be established (Milne and Goodall 1988).

5.3 Cavities and Inclusions

In this section we will look mainly at intragranular failure processes other than cleavage. Such processes are plastic in nature, but the microstructure of strengthened material leads to the concentration of the strain locally, with the result that the uniform strain of the material is greatly reduced. There are two main types of failure: (i) the growth of cavities or voids that then coalesce leaving a dimpled failure surface: and (ii) channel fracture where strain is confined to narrow slip bands resulting in local shearing-off and failure surface that is sometimes confused with cleavage. Typical examples of the three types of structure are shown in Fig. 5.12. Let us look at cavity growth first.

Cavities may already exist, e.g. from radiation damage or residual porosity from fabrication processes, or may be nucleated at inclusions or from dislocation interactions. Failure is characterised by two local strain stages: the nucleation strain and the cavity coalescence strain. A rigid inclusion will produce a mild elastic stress concentration; an applied tensile stress will generate a tensile stress at the inclusion interface of the order of 2(1-ν) the applied stress. For an incoherent precipitate this will be enough to separate the matrix from the precipitate, but for most materials plastic deformation is required to concentrate the stress further. An essentially rigid inclusion acts as an obstacle to plastic deformation and the stress at the inclusion will be proportional to volume fraction of inclusions and the plastic strain. A cavity may also be nucleated at an inclusion by the pile-up of dislocations at the interface in a similar manner to the grain boundary crack nucleation mechanisms. Cavities are also nucleated in very pure materials with no second phases at very high strains. This is because the

work hardened dislocation structure can generate cavities or small cracks by combinations of dislocations forming locked segments in the network (Cottrell, 1958).

Once nucleated the cavity will grow by elongating in the direction of the applied shear or tensile stress. Brown and Emburg (1973) have proposed that the ligaments between cavities become unstable when the elongation of the cavities reaches a critical value of $h = (L-2r_c)$ where L is the cavity separation. Without work hardening this gives the simple criterion for strain to coalescence:

$$\varepsilon_c = \ln [(L/2r_c) - 1] \cong \ln (p_c^{-1/2} - 1) \tag{5.35}$$

where r_c is the cavity radius at nucleation and p_c is the volume fraction of cavities.

Alternatively the growth of cavities to plastic instability can be accounted for in more detail by using a constitutive relation for plasticity in cladding cavities, see section 2.6. A stability criterion comes directly from the application of the yield criterion eq. (2.50). The derivation is outside the scope of these lecture notes and it is also necessary to replace p_c for a parameter f^* which permits cavity coalescence to be effectively modelled (Tvergaard 1981, 1982):

$$f^* = p_c \qquad \text{when } p_c < 0.15$$

$$f^* = p_c + \frac{5}{12}\left(\frac{p_c - 0.15}{0.1}\right). \tag{5.36}$$

Failure occurs at a similar strain to that predicted by eq. (5.34) and is not sensitive to work hardening coefficient for the range of values normally encountered. This approach has been successfully employed by Ford and Matthews (1989) to explain the reduction in UTS and ductility in stainless steels containing radiation damage produced cavities.

Channel fracture is seen in materials that have been hardened by fine precipitate distributions and by radiation damage. It is related to slip channelling in heavily work hardened materials and can be interpreted as a very local dynamic recovery. Fine dispersion of obstacles, such as carbides in stainless steels, γ′ in nickel alloys and small point defect loops in irradiated metals (Fish and Hunter 1976), are very effective in preventing dislocation motion. If the load is high enough eventually dislocations can penetrate the obstacles by cutting through them. The effect is localised because once

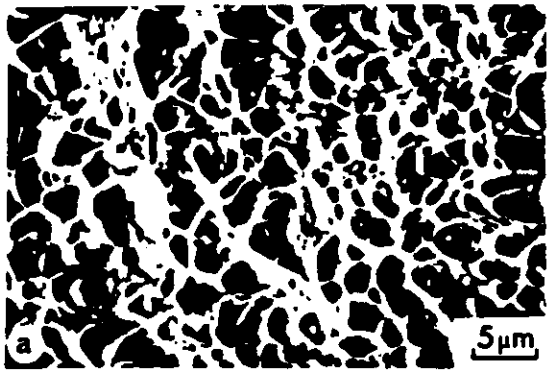

Ductile dimple fracture in austenitic stainless steel (fractured at 23°C).

Cleavage fracture in ferritic steel weld metal (fractured at -196°C).

Channel fracture in ferritic steel neutron irradiated to 1×10^{24} n/m^2 and fractured at -196°C.

(Scanning electron micrographs courtesy E A Little)

Fig. 5.12.

one obstacle is cut the load on adjacent obstacles increases and they soon follow. Slip can then continue to occur along the path cleared by the first dislocations. This very localised slip can then lead to failure by shearing-off of the material along the channels. This failure mechanism is restricted to lower temperatures, where dislocation climb is not important and the obstacles cannot coarsen by Ostwald ripening. In applying failure criterion a stress limit for channel fracture has to be determined experimentally. If the bulk yield stress is less than this the channel fracture is inhibited. The effective strain to failure by this process is very small.

5.4 Creep Fracture

Creep fracture, as opposed to ductile creep rupture, is a process that is mostly concerned with the growth of cavities on the grain boundaries or the nucleation and growth of intergranular cracks. For temperatures high enough to support creep, creep rupture usually dominates the time to failure even if some creep fracture process is responsible for the final parting of the material (see section 5.1). At low stresses the ductility during creep is much reduced and the failure time is significantly reduced if the ductility falls below 10%. This type of behaviour used to be known as creep damage and elaborate phenomenological theories were constructed to describe this and permit fitting to experimental observations (e.g. see Odqvist 1973). I prefer a microstructural approach and there has been a growth in this approach to creep fracture in recent years. By doing this we hopefully can predict problems in materials with particular structures and design materials for applications.

Creep interactions with intragranular cavities and inclusions do not easily lead to failure because the plastic instabilities are reached at very high strain, see eq. (5.16) and Fig. 5.6. The exception is when the volume concentration cavities or incoherent precipitates exceeds 20% when failure by creep in the ligaments between the cavities is almost immediate. Ductile transgranular failure under creep conditions is almost always due to the increase in the section as the area is reduced in tertiary creep. At the failure site the material starts to yield and local plastic instabilities can develop.

The subject of cavity nucleation and growth on grain boundaries has too many aspects for an adequate treatment here. A good introduction to the subject can be found in Beere (1982). A number of possible nucleation mechanisms have been suggested. During neutron irradiation embrittlement occurs during creep from cavities nucleated on helium bubbles associated from grain boundaries. Most of this helium comes from (n,α) reactions with boron, which segregates to the grain boundaries. In other

applications cavity nucleation is associated with deformation. Grain boundary sliding is frequently though to be responsible. Any obstacle to grain sliding will result in a local stress concentration which could open up a cavity. The junctions between three grains and precipitates on the boundaries are obvious possible sites. To nucleate a cavity the shear rates on the boundary have to be much greater than the bulk creep rate in the material. In order to grow the cavity nucleus has to satisfy the Hyam-Sumner condition, eq. (2.22) and (2.33) modified to account for the grain boundary dihedral angle and the hydrostatic stress replaced by the tensile stress normal to the boundary:

$$\sigma_n > \frac{4}{3}\frac{\gamma_s}{r_c}\sin(\phi/2) \qquad (5.37)$$

The growth of cavities, once nucleated is controlled by surface diffusion, grain boundary diffusion and creep deformation. In the absence of diffusion, creep will grow the cavity at a rate (Edward and Ashby 1979):

$$\frac{dr_c}{dt} = \frac{c^2}{2r_c} B\sigma_n \left[\frac{1}{(1-r_c^2/c^2)^n} - 1\right]. \qquad (5.38)$$

This expression gives a larger creep rate than that given by Beere (1980), but the reduction in supporting area at the grain boundary is accounted for. Eq. (5.37) is derived from a model of the growth of the cavity in a cell of radius c which is constrained by the adjacent material which is cavity free. The failure time is given by integrating (5.37) to get (with some approximation):

$$t_f = t_i + \frac{1}{n\dot{\varepsilon}_s}\ln\left\{\frac{1-(3/4)^n}{n\, r_{ci}^2/c^2}\right\} \qquad (5.39)$$

where t_i is the time to nucleate a cavity of critical size r_{ci}. This expression was derived without taking into account the reduction of area of the section during deformation which would decrease the time to failure under a dead load. This can be done by incorporating t_f from eq. (5.38) into a damage fraction rule eq. (5.17) and taking $\dot{\varepsilon}_s$ as the bulk strain rate of the material on the assumption that the cavities do not contribute significantly to the final strain of the material. When we do this and if we can neglect the time to nucleate the cavities a failure time is obtained of:

$$t_f = \left(1 - \frac{n r_{ci}^2/c^2}{1-(3/4)^n}\right)\frac{1}{n\dot{\varepsilon}_{so}}. \qquad (5.40)$$

Unless the cavity nuclei are large there is little effect on the Hoff time to failure (5.8). Cavity growth by creep is therefore a process that occurs during testing creep and has little effect on the failure time and the uniform strain to failure.

The most important role of grain boundary cavity growth is at lower stresses when bulk creep rates are low. The growth is mainly by grain boundary diffusion although surface diffusion and creep are important in determining the final growth rate. We have already seen in section 2.3 how cavities can grow purely by the transport of vacancies along the grain boundaries. One important consequence of this process is the redistribution of stress on the grain boundary. In Fig. 5.13 we show the stress distribution normal to the grain boundary as a function of distance from the cavity for cavity spacing of $2c = 10r_c$. On first applying the load the elastic response of the material produces a stress concentration at the junction of the cavity with the grain boundary. Once grain boundary diffusion has redistributed the stress, the stress concentration is eliminated and the maximum stress is found in the region between the bubbles. The reason for this redistribution is that for dynamic equilibrium vacancies must be formed uniformly over the boundary. This constraint and the concentration gradient necessary to drive the vacancies to the cavity requires the stress to decrease as the cavity is approached. Grain boundary diffusion in this way decreases the likelihood that such cavities can form crack nuclei.

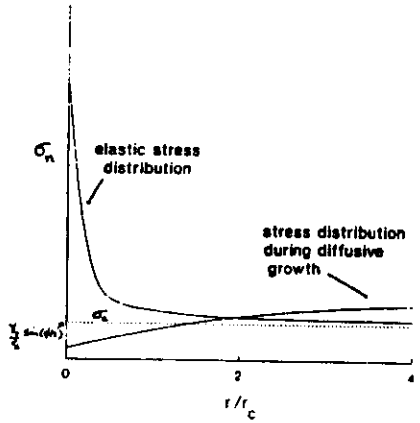

Fig.5.13

Eq. (2.32) assumes that surface diffusion is rapid so that the radius of curvature over the cavity is constant and that grain boundaries are perfect sources of vacancies. The first assumption is frequently not fully justified for many engineering materials where surface and grain boundary diffusion rates are comparable for the temperature ranges of interest. Restriction of the surface diffusion rate means that as material is removed from the tip of the cavity by grain boundary diffusion the surface of the cavity

can only redistribute over a small distance comparable with the cavity width. The surface curvature will be strongest at the interface with the boundary and will progressively decrease away from the tip. This results in the cavity being extended along the boundary in a crack-like shape, see Fig. 5.14. In the limit that surface diffusion is much less than grain boundary diffusion the cavity growth rate is controlled by surface diffusion:

$$\frac{dr_c}{dt} = \frac{\delta_s D_s \gamma_s \Omega}{8c^3 kT[1 - r_c^2/c^2]^3} \left[\frac{\sigma_a c}{\gamma_s \sin(\phi/4)}\right]^3 . \tag{5.41}$$

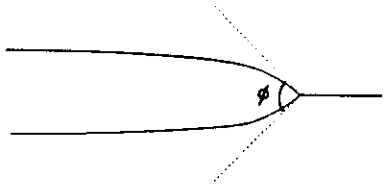

Fig.5.14

This limit also applies for cases of rapid cavity growth even when surface diffusion is comparable with grain boundary diffusion.

The other assumption is that vacancies are freely produced on the grain boundaries. The main restriction to this is for the effect of precipitates on the boundaries that are not cavity nuclei. A stress concentration develops near the precipitates as vacancies are generated on the boundary. Cavity growth can then only proceed if the material around the precipitates can deform to relieve the stress. This constraint places an upper limit on diffusion controlled cavity growth rate of (Beere 1980):

$$\frac{dr_c}{dt} = \frac{\pi}{8}\frac{c^2}{r_c^2}\frac{\lambda B \sigma_a^n}{(1 - r_c^2/c^2)^n} \tag{5.42}$$

where λ is the spacing precipitates on the boundary. Cavitation becomes much easier at higher temperatures when not only are diffusive processes faster but precipitates coarsen and solubilities increase.

The strain associated with cavity growth is usually small; the component in the direction of the applied stress at failure is given by:

$$\varepsilon_c = 4\alpha c/9d_b \tag{5.43}$$

where α is the coefficient defined for eq. (2.31).

In structures with cracks undergoing creep deformation it is commonly observed that the cracks extend at stresses below the critical fracture toughness. The crack growth rate is often correlated with the stress intensity factor:

$$\frac{da}{dt} \alpha K_I^p \tag{5.44}$$

where the index p is found to be close to that for creep (e.g. see Dimelfi and Nix 1977). As creep is normally expected to blunt crack tips and inhibits brittle fracture, it is thought that the crack growth is due to the growth and coalescence of grain boundary cavities by creep near the crack tip. A related approach is used in the CEGB's R5 design rule for high temperature assessment (Ainsworth 1982 and Milne and Goodall 1988). The crack growth rate is correlated against a parameter c where

$$C^* = \dot{\sigma}_{ref}\,\dot{\varepsilon}_{ref} R , \tag{5.45}$$

R being the effective crack length (Miller 1987).

The generation of helium from radiation damage has a large effect on the creep rupture properties of austenitic steels and high nickel alloys. The effect is not so pronounced in bcc metals. In the higher temperature range (>1/2 Tm) the reduction in creep life is due to the growth of cavities nucleated in helium bubbles (e.g. see Baker et al 1987 and Bullough and Jenkins (1987). For low temperatures there is still a strong effect at levels of He where bubble formation is not possible (Shaarfe and Marshall 1983). The reduction in creep rupture life and ductility for 316 steel is shown in Fig. 5.15. Grain boundary cracking is responsible for the failure and it is thought that helium can reduce the effective surface energy of the material for fracture. The basic cracking mechanism for cracking is probably that originally suggested by Stroh (1954), where dislocations piling up against a grain boundary can nucleate a wedge crack. The dislocations form a super-dislocation which either open the crack if the fracture energy is low enough or propagate deformation into adjacent grains, see section 1.2 (Hall 1951 and Petch 1953). The magnitude of the stress concentration on the boundary is inversely proportional to the square root of the grain size. Large grained material is found to be more sensitive to this type of cracking.

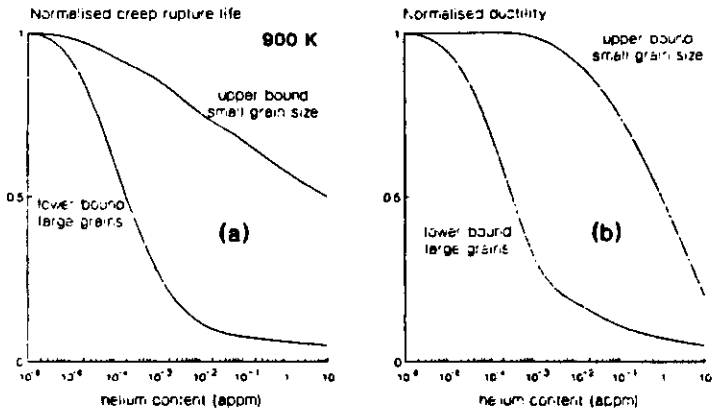

Fig.5.15

5.5 Fatigue

Perhaps the most important mechanism for the growth of cracks during operation is fatigue. Almost all industrial plant and engineering structures have operating cycles that result in variable loading either directly or from thermal fluctuations. In order to nucleate fatigue cracks the material must suffer some plastic strain on each cycle. Once nucleated this is not necessary. In a nominally defect free structure an empirical observation is that the number of cycles to failure is related to the amplitude of the imposed strains by (Coffin 1954 and Mason 1954):

$$N_f = C_1 / \Delta\gamma_p^q \,, \tag{5.46}$$

where C_1 and q are constants and $\Delta\gamma_p$ is the size of the plastic strain on each cycle. This relationship mainly governs the nucleation stage for large plastic strains. A wide range of materials, in non-corrosive atmospheres and relatively low temperatures, obey eq. (5.54) with C~1 and q~2. However, this relationship represents an upper bond to the fatigue life as environmental effects (corrosion and creep) reduce the number of cycles to failure.

Fatigue crack nucleation is known to occur at surfaces and is thought to be the result of slip bands creating ledges. A dislocation source operating near a surface can lose dislocations out the material, which will produce an increment in the length of the

ledge on each cycle. Stress concentrations at the ledge could nucleate a crack. Reversible slip could also produce a crack when gas atoms are adsorbed on to the surface. The adsorbed gas atoms could prevent the perfect reversal and instead produce a region of imperfect cohesion on the slip band (Thompson, Wadsworth and Lonat 1956). More severe environmental effects remove the need for any nucleation phase, e.g. when there is intergranular corrosion.

Once a fatigue crack is nucleated its growth rate is found to be related to the variation in the crack stress intensity factor on each cycle ΔK_I by the Paris law (Paris and Erdogen 1963):

$$\frac{da}{dN} = C_2 \Delta K_I^p \tag{5.47}$$

where C_2 and p are constants. This relationship holds for very wide ranges of stress intensity factor, but for very small values of ΔK_I there is a threshold below which fatigue does not occur and there is of course an upper limit imposed by K_{IC}. These limits to the Paris equation are in terms of the maximum value of K_I during the cycle. It is necessary to introduce another parameter R which is the ratio of the minimum to maximum value of K_I during the cycle. An improved version of the Paris equation is then given by (Pearson 1972):

$$\frac{da}{dN} = C_2 \frac{[\Delta K_I - K_{thr}(1-R)]^p}{[1-R-(\Delta K_I/K_{IC})]^{1/2}} \tag{5.48}$$

where K_{thr} is the threshold value of K_I to produce fatigue crack growth. The fatigue crack growth behaviour is shown schematically in Fig. 5.16 for different values of R.

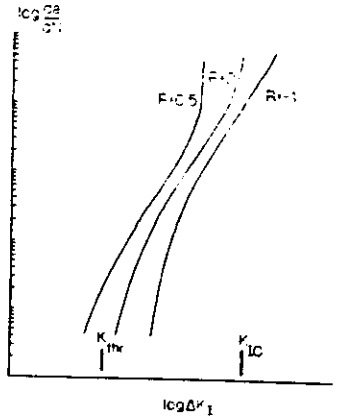

Fig.5.16

Fatigue crack growth is driven by the plastic blunting of the crack tip, which produces crack advance on reversal or reduction of the load. Alternatively the crack growth can be described by the partly irreversible emission of dislocations from the crack tip or from dislocation sources near the crack eq. (5.21) which would give a value of p in eq. (5.47) of 2. In practice p is found to occur between

2 and 6. The deviation from the expected value may come from creep or environmental effects but there may also be some sensitivity of p to the work hardening index of the material. Austenitic stainless steels obey eq. (5.48) with p = 2 to a good approximation, but an even better correlation is found if $\sqrt{\Delta J}$ is used insteady of ΔK_I (Sadananda and Shaninian 1979).

Fatigue crack growth is very sensitive to creep effects. At temperatures where creep occurs the fatigue crack growth rate increases with increasing temperature and decreases with increasing frequency of cycling. For such conditions introducing a hold on the tensile part of the loading cycle will produce a further increase in the crack growth with each cycle (Wareing, Tomkins and Bretherton 1983). Fatigue is generally a transgranular fracture phenomenon but when creep effects become important the cracking becomes intergranular in nature. During fatigue cycling, particularly in the plastic loading range, cavities are easily nucleated on grain boundary inclusions. The growth and absorption of these cavities by the growing crack is the main mechanism for creep-fatigue interaction effects.

5.6 Environmental Effects

By environmental effects we mean chemical effects produced by the surrounding atmosphere or liquid medium in which a structure operates or those from impurities transported by the fluid to the structure. The environments may be oxidating from water, steam or air, or reducing from hydrogen or liquid metals. The main contaminants in water may lead to caustic conditions or acid conditions from various salts. The subject is vast and complicted and here I will only give a brief indication of the problem, dealing with general chracteristics.

Let us look first of all at corrosion, where there is little effect on corrosion rate from the loading, but there are large implications on the propensity to fail. The most direct effect of corrosion is the reduction of the load bearing section of the structure. Corrosion may occur by dissolution of the structural material relatively uniformally. This type of corrosion is rare and most oxidative processes leave an oxide scale, which may adhere to the structure or if it is of low density spall off. In some cases an adherent oxide scale may even strengthen a structure, which is the case when zircaloy cladding tubes react with steam (Hindle, Haste and Harrison 1987). The rate of penetration of a structure by corrosion is a very complex and difficult subject depending both on the nature of the environment and the details of the chemical and microstructural state of the material. In particular the presence of a scale and its

integrity will determine how easily the components of the reaction can come together. Sometimes pitting corrosion can occur under a scale where the electrochemical state of the material is different. Such corrosion pits have little effect on the strength of the structure and are not important unless they penetrate a pressurised component.

In some cases corrosion proceeds by intergranular penetration particularly when reactive inclusions are on the grain boundaries. Oxygen or other reactive elements can also penetrate via grain boundary diffusion and cause sensitisation of the boundary to cracking by precipitating hard inclusions. Frequently one component of an alloy is more reactive and is removed preferentially at grain boundaries. In stainless steels this is chromium which readily reacts with oxygen, nitrogen and carbon. Intergranular corrosion is a way in which cracks are nucleated in structures. Cracks can also grow during operation of a structure in corrosive environments. In dissolution type corrosion this can lead to the extension of the crack by removal of material at the crack tip if the electrochemical environment enhances corrosion at this point, but it can also lead to blunting the crack in other circumstances. An important crack extension mechanism is oxide jacking where oxidative corrosion in a crack produces a bulky corrosion product which forces the crack apart, presenting new surface for attack. This mechanisms is also important in increasing crack growth rates during fatigue in oxidising atmospheres.

These intragranular corrosion processes are frequently sensitive to an applied stress producing the phenomenon of *stress corrosion cracking*. In some cases the material has first to have a crack nucleated by some other process, e.g. from fatigue or the application of a load above some critical value. Most engineering alloys are sensitive to stress corrosion cracking in some environments, examples include: for brass - ammonia and mercurous salts; for carbon steels - nitrates and other salts; and for low alloy steels - causic environments (Cowen and Thorley 1983). In the nuclear industry an important example of stress corrosion cracking is from the fission product iodine which embrittles the zircalloy cladding tubes of BWR and PWR fuel rods (Garlick and Gravenor 1981). The sensitivity to stress corrosion cracking is often determined by minor chemical constituents of alloys which segregate to the grain boundaries, such as P and S. These elements are also important in the related problem of hydrogen embrittlement of steels with bcc structures hydrogen is highly mobile in many metals and in hydrogren embrittlement the hydrogen is drawn to the crack tip by its stress field, where it locally reduces the effective surface energy for fracture (Hirth 1980). Hydrogren embrittlement can also take place in other materials by the formation

of brittle hydrides on the grain boundaries (Birnbaum 1979) and this is also important for zircalloy cladding tubes in water reactors (Pickman 1975).

Perhaps the most dramatic example of environmental embrittlement is liquid metal embrittlement. Certain combinations of metals with liquid metals can reduce a normally ductile material to one where brittle cleavage fracture can occur with essentially zero strain. The classic example of this is Al and its alloys in contact with liquium gallium. Ferrous alloys, with both austenitic and ferritic structures, are reported to exhibit liquid metal embrittlement with a bewildering range of liquid metals and mixtures including: Bi, Hg, Ga, Cd, Sn, Sb, Cu, Li, Zn and Pb but luckily not Na (Old 1980). Zircalloy is also embrittled by cadmium. The degree of embrittlement varies with each combination and is dependent also on the metallurgical state of the steel. Liquid metal embrittlement in its broadest sense is probably a combination of dissolution corrosion, corrosion from dissolved oxygen or stress corrosion cracking. There is however a sub-class of true liquid metal embrittlement which is distinct, is characterised by failure, some critical stress and gives prompt failure with no ductility if the critical stress is below the yield point. The embrittlement takes place over a temperature range defined by the melting point of the liquid metal and by a brittle-ductile transition temperature, above which the yield stress of the material restores ductility. The embrittlement is thought to be due to a reduction in the surface energy for fracture at the crack tip.

Of concern to the performance of nuclear fuel is the question as to whether liquid metal embrittlement can occur in cladding tubes from contact with fission products. The most abundant fission product in metallic form is Cs and this only produces mild embrittlement in steels and zircalloy (Old 1980). However, mixtures of Te and Cs with ratios 1:1 produce severe embrittlement in austenitic stainless steels and high nickel alloys, but not in ferritic steels (Adamson et al 1986). This may explain reduced ductility of irradiated fast reactor cladding tubes, but as Cs is produced in much greater quantities than Te some process for concentrating Te is required.

In the related problems stress corrosion cracking, hydrogen embrittlement and liquid metal embrittlement the susceptibility of a material is related to its hardness or strength. Optimised engineering alloys are frequently more likely to show these effects than simpler alloys and pure metals.